UCL
Université
catholique
de Louvain

miro
molecular imaging, radiotherapy & oncology

IREC
Institut de Recherche Expérimentale et Clinique

Integration of functional imaging and tumor motion in intensity modulated radiation therapy for non-small cell lung cancer

Marie Wanet

Février 2016

Thèse présentée en vue de l'obtention du grade
de docteur en sciences médicales

Secteur des sciences de la santé

Université catholique de Louvain
Secteur des sciences de la santé

Institut de Recherche Expérimentale et Clinique (IREC)
Laboratoire : Molecular Imaging, Radiotherapy and Oncology (MIRO)

Promoteur : Professeur Xavier Geets

UCL
Université
catholique
de Louvain

Born in Namur, Belgium, in 1982, Marie Wanet is a radiation oncologist in CHU Namur since August 2015. She was graduated as medical doctor from UCL in 2007. She started her training as radiation oncologist in the oncology department of Jolimont hospital and then in the radiotherapy department of Cliniques universitaires Saint-Luc in Brussels. She began her PhD in Molecular Imaging and Radiation Oncology laboratory in 2009, for studying the integration of functional imaging and tumor motion in non-small cell lung cancer. She is co-author of five articles published in international scientific journals, including three as first author. She pursued and finished her training in 2015 in the radiation oncology department of CHU Namur.

Conventional treatment of locally advanced non-small cell lung cancer patients with concomitant chemo-radiation achieves poor tumor local control rates and strongly affects the patient outcome. Although it appears essential to implement dose intensification strategies, this remains challenging due to the proximity of highly radiosensitive organs, which may result in unacceptable toxicities. A potential solution would be to escalate the dose in restricted areas within the tumor identified as potentially radio-resistant, by functional imaging (FDG-PET), and using high conformal radiation treatment delivery and optimized tumor motion management. This concept mainly requires an accurate definition of the target volumes in order to spare healthy tissues. In this context, we validated a gradient-based segmentation method for primary lung tumor definition on FDG-PET imaging by comparison with surgical specimens. Then, in a clinical trial, we assessed how an individualized and non-uniform escalated dose based on FDG-PET images would affect the tumor local control and the radio-induced toxicities. Finally, we investigated the tumor motion caused by breathing and studied the feasibility of the mid-position strategy in helical radiation treatment for lung tumors.

La radio-chimiothérapie concomitante est le traitement de choix pour les patients atteints de cancer bronchique localement avancé non à petites cellules. Cependant, le taux de récidive locale après un tel traitement reste élevé et affecte négativement le pronostic de ces patients. Bien que les stratégies d'intensification de dose paraissent essentielles, celles-ci sont limitées par la proximité des organes sains. Par conséquent, une augmentation de la dose sur une partie restreinte de la tumeur, identifiée par l'imagerie fonctionnelle FDG-PET, associée à une prise en charge optimale du mouvement tumoral, pourrait améliorer le contrôle tumoral local tout en limitant les toxicités. Cette approche nécessite une délimitation rigoureuse des volumes tumoraux afin d'épargner les tissus sains. C'est dans ce contexte que ce travail, scindé en trois phases, s'inscrit. Nous avons d'abord validé une méthode de délimitation automatique des tumeurs pulmonaires basée sur les gradients d'intensité dans les images FDG-PET par comparaison avec les pièces chirurgicales de lobectomie. Ensuite, dans le cadre d'une étude clinique, nous avons évalué l'impact d'une augmentation individualisée de la dose guidée par l'imagerie FDG-PET sur le contrôle tumoral local et sur les toxicités radio-induites. Enfin, nous avons étudié le mouvement tumoral lié à la respiration et intégré une stratégie, nommée mid-position, dans la planification du traitement des tumeurs pulmonaires, délivré de manière hélicoïdale.

UNIVERSITE CATHOLIQUE DE LOUVAIN

Institut de Recherche Expérimentale et Clinique (IREC)

Molecular Imaging, Radiotherapy and Oncology (MIRO)

Integration of functional imaging and tumor motion in intensity modulated radiation therapy for non-small cell lung cancer

Marie WANET

Thesis presented in fulfillment of the requirements for the degree of
" Docteur en Sciences Médicales "
Orientation " Radiothérapie Oncologique "

2016

Promoter: Xavier Geets

A mon Bon-papa

PhD Committee

Promoter:

Prof. Xavier Geets
Radiation Oncology Department
Molecular Imaging, Radiotherapy and Oncology
Université Catholique de Louvain

President of the jury:

Prof. Frédéric Lecouvet
Radiology Department
Cliniques Universitaires Saint Luc
Université Catholique de Louvain

Members:

Prof. François-Xavier Hanin
Nuclear Medicine Department
Cliniques Universitaires Saint Luc
Université Catholique de Louvain

Prof. Birgit Weynand
Pathology Department
Katholieke Universiteit Leuven

Dr Edmond Sterpin
Molecular Imaging, Radiotherapy and Oncology
Université Catholique de Louvain
Laboratory of experimental radiotherapy
Katholieke Universiteit Leuven

Prof. Thierry Pieters
Pneumology Department
Cliniques Universitaires Saint Luc
Université Catholique de Louvain

Prof. Vincent Gregoire
Radiation Oncology Department
Molecular Imaging, Radiotherapy and Oncology
Université Catholique de Louvain

Invited members:

Prof. Dirk De Ruysscher
Radiation Oncology Department
MAASTRO clinic
The Netherlands

Prof. Pierre Vera
Nuclear Medicine Department
Centre Henri Becquerel
Rouen, France

Remerciements – Acknowledgements

Je remercie avant tout mon promoteur, Xavier Geets, de m'avoir proposé d'entreprendre ce projet de recherche à ses côtés. En effet, en commençant ma formation en radiothérapie, rien ne me prédestinait à prendre la direction de la recherche scientifique. C'est donc après mûres réflexions que j'ai accepté ce nouveau challenge qui m'était offert. Il m'a fait confiance, m'a supervisée tout au long de mon parcours et m'a appris énormément tant sur le plan scientifique, que clinique et humain.

Je remercie également tous les membres de mon comité d'accompagnement pour leurs commentaires constructifs lors des différentes épreuves qui m'ont permis d'améliorer l'état de mes recherches année après année. Merci au Professeur Birgit Weynand pour sa disponibilité ainsi que son aide efficace et indispensable dans l'étude de mes pièces chirurgicales de lobectomie. Merci à Edmond pour sa collaboration, ses réflexions toujours plus pertinentes et l'obligatoire pédagogie qu'il a dû employer pour me faire comprendre certains concepts physiques, pas toujours évidents à saisir pour une novice en la matière. Merci à François-Xavier (ainsi qu'à l'équipe de médecine nucléaire) pour la disponibilité de la caméra PET/CT et pour son aide dans le domaine de la médecine nucléaire, dans l'étude d'escalade de dose et dans l'interprétation des résultats des imageries. Merci aux Professeurs Thierry Pieters et Frédéric Lecouvet pour leur soutien scientifique. Enfin, merci au Professeur Grégoire, de m'avoir accueillie au sein de son laboratoire et de m'avoir autorisée une formation scientifique pointue et continue par le biais de participation à de nombreux congrès, formations et séminaires.

Je remercie particulièrement les deux membres invités de mon jury, les Professeurs Dirk De Ruysscher et Pierre Vera d'avoir pu libérer de leur temps précieux pour la lecture de mon manuscrit. Merci aussi pour leur participation active à la défense privée de ma thèse. Leurs remarques et questions pertinentes m'ont amenée à de nouvelles réflexions, tant dans le domaine de mes recherches que pour ma pratique clinique future.

Ce projet n'aurait pas vu le jour sans le financement indispensable du FNRS. Je tiens à remercier, plus particulièrement, toutes les personnes, qui me sont certes inconnues, mais qui, chaque année, se mobilisent au profit du cancer par le biais des médias et du Télévie.

Il me paraît indispensable de remercier les patients qui ont accepté de participer aux différentes études et, en particulier, ceux qui ont donné leur accord pour être traités selon l'étude clinique d'escalade de dose. Bien que la majorité d'entre eux soit encore en vie, certains sont malheureusement décédés, des suites de leur maladie ou de toxicités sévères liées à la radiothérapie. Un contact privilégié avec chacun d'entre eux m'a permis de garder un lien intime avec la pratique clinique et de vivre des moments intenses, partageant souvent avec le patient et sa famille des moments parfois drôles, souvent émouvants.

Ces quatre années et demi au sein du laboratoire MIRO m'ont permis non seulement d'approcher la science, la physique, la médecine nucléaire et l'informatique, tout en côtoyant la radiothérapie clinique, mais aussi de rencontrer une équipe formidable. Malgré un environnement majoritairement « testostéroné », je me suis rapidement fait une place au sein du bureau des ingénieurs/physiciens. Merci à John, Sam, Guillaume, Fiona et Kevin pour les agréables moments passés ensemble, dans une ambiance studieuse ou détendue, régulièrement entrecoupée de moments de repos et d'échange (des épisodes de « Bref » en passant par quelques bons sketchs anglais ou francophones, au partage de musique, de films, des dernières news de l'actualité ou de photos de vacances). Merci à John pour ses conseils avisés, sa collaboration, sa patience et sa pédagogie, sa disponibilité (malgré son agenda surchargé) et les multiples relectures d'articles et de ce manuscrit de thèse. Merci à Sam pour son aide sur mes différentes études et ses encouragements dans les moments difficiles. Merci à Guillaume et Kevin pour leurs conseils face à mes petits tracas informatiques et leur soutien.

Merci aussi à l'équipe féminine, qui s'est étoffée au fil des mois : Séverine, Vanesa, Sarah, Anne et Myriam. Leur soutien moral et leur aide tant sur le plan scientifique que logistique furent salutaires. Merci également à Anne pour son aide précieuse dans les acquisitions PET et les analyses d'images, ainsi que pour la relecture de ce manuscrit de thèse.

Je n'oublierai pas non plus l'aide inestimable de Guillaume, Jonathan et Edmond dans l'implémentation de nouvelles techniques, de nouveaux softwares et leur collaboration à cette recherche. Merci enfin à tous les autres membres du labo de lui permettre d'exister. Et que serait d'ailleurs le laboratoire MIRO sans ses pauses de midi remplies de discussions et de débats plus intéressants les uns que les autres et sans les activités extra-scientifiques entreprises régulièrement ? Merci à tous !

Je tiens vivement à remercier toute l'équipe clinique du -4 et le Professeur Scalliet qui m'a encouragée dans cette voie. Un merci spécial à Antoine qui m'a assistée tout au

long de mes recherches, notamment dans la réalisation des plans de traitement, dans mon apprentissage de la planification et bien plus encore. Son soutien fut toujours présent, même dans les moments pénibles. Merci également à l'équipe technique qui m'a aidée à résoudre bien des soucis souvent d'ordre informatique et logistique. Merci à Maxime de m'avoir, en plus de son aide professionnelle, donné goût au voyage par ses rêves partagés de bout du monde.

La pratique clinique, enrichie de ces 4 ans et demi de recherche, est indispensable à la formation du radiothérapeute. En ce sens, je tiens à remercier l'ensemble de mes maîtres de stage et les équipes qui m'ont accueillie au sein de leur service.

Je remercie en particulier l'équipe médicale et para-médicale du SORMN de Sainte Elisabeth pour leur accueil au pied levé après la fin de mon contrat FNRS, pour leur enseignement et leur soutien durant l'année et demi de dur labeur combinant clinique et recherche.

Un grand merci également à mes amis proches pour m'avoir soutenue malgré mon isolement social durant cette dernière année. En particulier, merci à Steph pour son soutien incessant tout au long de mon parcours, depuis la première candidature jusqu'à l'aboutissement de cette thèse. Merci aussi à Aline, Ariane, Maud, Cath, Nath et leur famille pour leur soutien et leur compréhension.

Enfin, sans le soutien de ma famille, tout ce travail ne serait pas aussi abouti. Mille mercis à ma maman et mon papa qui ont toujours été là, dans les bons moments comme dans les plus difficiles. A chaque obstacle ou chaque échec, ils ont été présents pour me relever. Ils ont assuré plus qu'ils n'auraient dû tant au niveau du soutien moral que de la logistique et de l'intendance. Je ne leur en serai jamais assez reconnaissante.

Un immense merci à ma petite sœur, Anne-So, à Julien, à ma mamy, au reste de ma famille et bien sûr aussi à ma belle-famille, Yolande, Jacques, Delphine, Quentin et Juliette qui m'ont suivie et soutenue pas à pas ces dernières années. Un double merci à Quentin qui a permis une avancée considérable de ce manuscrit par sa mise en page claire et réussie.

Merci à mon rayon de soleil, Emma, d'avoir accepté les longues absences de sa maman durant ces derniers mois. Merci de m'avoir rappelé de temps à autre à l'ordre, de me faire revenir sur terre pour réfléchir aux priorités et me ramener à l'essentiel.

Merci aussi à mon futur petit loulou qui a enduré stress, angoisse et montées d'adrénaline pendant ces neuf derniers mois, censés être les plus calmes et les plus rassurants d'une vie. Je lui promets de me rattraper dans les prochaines semaines et prochaines années.

Et surtout, merci à Pierre, pour tout ce qu'il a enduré et supporté ces deux dernières années. Merci de m'avoir laissé le temps de réaliser et parfaire ce travail au détriment de notre vie de famille. Merci de ton aide, ta confiance, ton soutien moral, ton écoute, ton amour. Je t'en suis éternellement reconnaissante.

List of abbreviations

2D	two-dimensional
3D	three-dimensional
3D-CRT	three-dimensional conformal radiotherapy
4D	four-dimensional
ABC	active breathing control
ART	adaptive radiation therapy
BL	baseline
CB-CT	cone-beam computerized tomography
CRT	chemo-radiotherapy
CT	computerized tomography
CTLA-4	cytotoxic T-lymphocytes-associated protein 4
CTV	clinical target volume
D	delineation
DNA	deoxyribonucleic acid
DLCO	diffusing capacity of the lung for carbon monoxide
DPBN	dose painting by numbers
DVH	dose-volume histogram
EGFR	epidermal growth factor
EORTC	European organisation for research and treatment of cancer
EPID	electronic portal imaging device
FDG-PET	18-fluoro-deoxyglucose positron emission tomography
FEV1	forced expiratory volume in 1 second
FSU	functional subunit
FWHM	full width at half maximum
G	gram
GLUT-1	glucose transporter 1
GTV	gross tumor volume
ICRU	international commission on radiation units and measurements
IGRT	image-guided radiation therapy
IMRT	intensity-modulated radiation therapy
ITV	internal target volume
kBq	kilobecquerel
LA	locally advanced
LBM	lean body mass
LC	local control
LOR	line of response
LW	lung window
MC	monte carlo
MED	mean esophageal dose
MidP	mid-position
mL	milliliter
MLC	multi-leaf collimator

MLD	mean lung dose
MV-CT	megavoltage computerized tomography
MW	mediastinal window
NSCLC	non-small cell lung cancer
NTCP	normal tissue complication probability
OAR	organ at risk
OS	overall survival
OTT	overall treatment time
P	penumbra
PBS	pencil beam scanning
PD-1	programmed cell death one
PD-L1	programmed death-ligand one
PERCIST	PET response criteria in solid tumors
PET	positron emission tomography
PET/CT	combined positron emission tomography and computerized tomography
PFS	progression free survival
PL	particle therapy
PRV	planning organ at risk volume
PSF	point spread function
PT	particle therapy
PTV	planning target volume
PVE	partial volume effect
RECIST	response evaluation criteria in solid tumors
ROI	region of interest
RT	radiation therapy
RTOG	radiation therapy oncology group
SBR	source to background ratio
SBRT	stereotactic body radiation therapy
SD	standard deviation
SIB	simultaneous integrated boost
SNR	signal to noise ratio
SUL	standardized uptake lean mass
SUV	standardized uptake value
SWOG	southwest oncology group
TCP	tumor control probability
TKI	tyrosine kinase inhibitor
TM	tumor motion
TNM	TNM classification of malignant tumors
TPS	treatment planning system
TTD	tumor total dose
TV	target volume
VEGF	vascular endothelial growth factor
VOI	volume of interest

Table of content

Chapter 1

Background

Contents

General introduction

1. Epidemiology

In Belgium, lung cancer is the second most frequent malignancy in males and the third in females [1], with 6783 and 2349 new cases diagnosed in 2012, respectively. It is the leading cause of cancer death in males and the second in females. More than half of the patients die within the first year after diagnosis [2]. Currently, lung cancer remains a major health issue due to its high incidence and its extremely poor prognosis.

Radiotherapy (RT) holds an important place in the treatment of non-small cell lung cancer (NSCLC) patients. About two third of patients will receive a radiation treatment at least once during the course of their pulmonary illness [3].

Due to the limited symptoms, lung cancer is mostly diagnosed at locally advanced stages (stage II-III, see TNM table in appendix A) and in these inoperable cases, the 5-year overall survival is as low as 5-15%. Concurrent chemo-radiotherapy (CRT) is the standard treatment for inoperable or locally advanced (LA) NSCLC. However, local recurrence (i.e. at the primary tumor site) still occurs in about one third of patients even with conventional schemes [4-7].

2. Radiobiology

Currently, the conventional treatment of LA stage NSCLC includes a cisplatin-based chemotherapy delivered concomitantly with definitive thoracic radiotherapy with a dose of 60 Gy in 2 Gy fractions once daily [6-8]. One of the general principles of radiotherapy relies on the quantitative description of the relationship between the delivered dose and the cell death rate. The sigmoid dose-response curve, originating from theoretical, experimental, and clinical data, predicts the tumor control probability (TCP) for a given dose. Based on this, it seems obvious to increase the dose to the tumor in order to limit local recurrence. However, dose escalation is rapidly limited by the organs at risk (OARs) surrounding the tumor. This is depicted by the therapeutic index, which is the ratio between the TCP and the normal tissue complication probability (NTCP). This ratio can be enhanced in a number of ways, using biological and/or physical factors, shifting either the TCP curve to the left (radio sensitization) or the NTCP curve towards the right (radioprotection), to gain in terms of tumor control while keeping toxicities as low as possible (Figure 1.1).

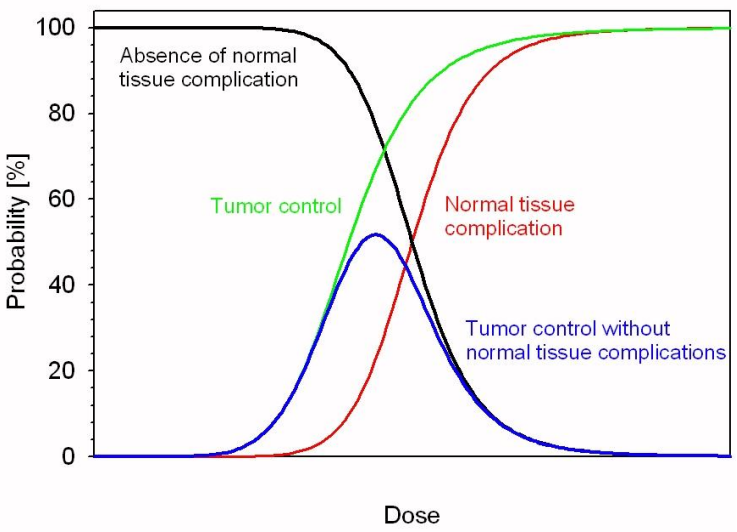

Figure 1.1 *The principle of the therapeutic ratio with the green curve representing the tumor control probability (TCP) and the red curve illustrating the probability of normal tissue complication (NTCP). In an ideal radiation treatment, the TCP is maximized while the NTCP is minimized. However, the TCP curve is shallower than the NTCP curve. Consequently, it is essential to use biological and/or physical factors, in order to shift either the TCP curve to the left (radio sensitization) or the NTCP curve towards the right (radioprotection), to gain in term of tumor control while keeping toxicities as low as possible. From dkfz.de.*

Martel et al. have estimated that for NSCLC patients, the dose required to achieve a significant probability of tumor control (> 50%) might be as high as 84 Gy for longer local progression free survival (> 30 months) with standard fractionation [9]. Many studies have thus focused on dose escalation and on the various ways to improve the therapeutic index.

Chemotherapy has been proposed since years in association with radiotherapy. The radiobiological benefit of concomitant CRT would stem from the inhibition of tumor cell proliferation by drugs during the radiation inter-fraction interval rather than from other identified mechanisms of interaction, i.e. modulation of deoxyribonucleic acid (DNA) and chromosome damage and repair, cell-cycle synchronization, enhanced induction of apoptosis and re-oxygenation. Several randomized trials associating RT and chemotherapy have been conducted and a recent meta-analysis has demonstrated the superiority of the concomitant CRT over the sequential one in locally advanced NSCLC [7]. The 5-year overall survival (OS) increases from about 10% in the sequential arm to 15% in the concomitant arm. Interestingly, this survival gain has been mainly attributed to an improvement in local tumor control.

The overall treatment time (OTT) over which the RT is given is also an important determinant of outcome. Machtay et al. have demonstrated that prolonged treatment time is significantly associated with poorer survival, even in concomitant CRT [10]. Therefore, accelerated fractionation, which is defined as an increase of the average dose per week above 10 Gy, given in conventional fractionation, can be used. Shortening the OTT may overcome tumor rapid repopulation, which takes place after 3 to 4 weeks of radiotherapy, and corresponds to clonogenic doubling times of 3 to 3.5 days [11]. Although early normal tissue reactions are expected to increase when using such a scheme, late normal-tissue damage is expected to remain constant, assuming that recovery from sub-lethal radiation damage between fractions is complete.

Altered fractionation schemes that deviate from the classical 2 Gy per fraction, 5 days a week, have also been tested. Hyper-fractionation is the use of a reduced dose per fraction being delivered several times per day during a classical OTT. The therapeutic advantage stems from the difference in fractionation sensitivity between tumor cells and late-responding tissues. In clinical practice, the tumor total dose (TTD) is often escalated compared to classic treatment, improving tumor control rates without increasing the risk of late complications.

The CHART trial combined both strategies, comparing continuous hyper-fractionated and accelerated RT (total tumor dose of 54 Gy, 36 fractions, thrice a day, in 12 consecutive days) versus conventional RT (60 Gy, 2 Gy per fraction) and demonstrated the gain of accelerating and hyper-fractionating the treatment in terms of survival and local tumor control [12]. Despite the lower total dose, the 2-year survival was increased from 21% in the conventional arm to 30% in the CHART arm. Exploratory analysis revealed that this was a consequence of improved local tumor control.

Hypo-fractionation is the term used for doses per fraction higher than 2 Gy with a reduced total number of fractions. Moderate hypo-fractionation with doses per fraction up to approximately 3.5 Gy is more and more used for curative radiation therapy. Although the TTD often needs to be decreased to avoid severe late normal tissue toxicities, the TCP remains quite similar thanks to the shorter OTT. There is growing interest in moderate hypo-fractionation for dose escalation clinical trials. Indeed, this scheme is convenient for the patient and helps to spare resources.

A refinement of these concepts is the prescription of an individualized dose according to normal tissue dose constraints, in association with either acceleration or hyper- or hypo-fractionation of the treatment. The MAASTRO clinic developed such a strategy by delivering the highest achievable radiation dose to a patient based on localization, tumor size, and dose-limiting OARs, sequentially or concomitantly with

chemotherapy. Planning results were particularly promising in term of TCP (up to 30% higher) while first clinical results demonstrated the feasibility of an individualized hyper-fractionated and accelerated scheme [13-16]. Another clinical study confirmed the gain in survival for stage III NSCLC patients, particularly for concomitant CRT with an Individualized Isotoxic Accelerated RT (INDAR) [17]. However, INDAR is obviously more expensive and less convenient than once-daily fractionation. Individualized, accelerated, and moderately hypo-fractionated RT should be investigated in clinical trials as dose escalation with such a scheme could potentially lead to late toxicities, even though better local control and survival can be achieved.

3. Concepts of volumes in radiotherapy

A successful RT relies on subsequent steps in the patient preparation and treatment planning. It is by nature a localized treatment and requires first accurate diagnosis imaging and invasive procedures (e.g. bronchoscopy, EBUS/EUS, mediastinoscopy) to define the exact location and extent of the tumor. After a complete staging determining the indication of a RT, the radiation therapy team plans the treatment in a process called simulation, including a careful immobilization of the patient (thermoplastic thorax mask), a thorough imaging planning as three-dimensional (3D) and four-dimensional (4D) computed tomography (CT) and marks ensuring the reliably alignment and position for each treatment session. Then, the most crucial step of the planning is the exact definition of target and non-target volumes, as discussed below. Eventually, dosimetrists or physicists determine the optimal beam energy and arrangements to best conform the tumor, preserving the OARs.

In order to provide a standardized terminology, the International Commission on Radiation Units and Measurements (ICRU) published some recommendations about volumes in radiotherapy [18] (Figure 1.2).

The Gross Tumor Volume (GTV) is the gross demonstrable extent and location of the tumor defined using clinical examination and/or multimodality imaging.

The Clinical Target Volume (CTV) is a volume of tissue that contains a demonstrable GTV and/or subclinical malignant disease with a certain probability of occurrence considered relevant for therapy. The notion of subclinical malignant disease includes the microscopic tumor spread at the boundary of the primary-tumor GTV, the possible regional infiltration into lymph nodes, and the potential metastatic involvement of other organs (e.g. brain), despite their normal appearance on clinical and radiological examinations. The selection of the tissues that bear risk for microscopic infiltration outside of the GTV is a probabilistic assessment integrating the biological and clinical

behavior of the various tumor entities and the knowledge of the surrounding anatomy, including structures that are barriers to tissue infiltration (e.g., muscular fascia, bone cortex), or—on the contrary—structures that are easy conduits for tumor dissemination (e.g., fatty space).

The Internal Target Volume (ITV) might be useful only in clinical situations in which uncertainty concerning the CTV location dominates setup uncertainties and/or when they are independent. An internal margin must thus be added to the CTV to compensate for expected physiologic movements and the variations in size, shape and position of the CTV during therapy related to anatomic reference points. The ITV, encompassing the CTV and internal margin, is considered as an optional tool in helping to delineate the PTV.

The Planning Target Volume (PTV) is a geometrical concept introduced for treatment planning and evaluation. It is the recommended tool to shape absorbed-dose distributions to ensure that the prescribed absorbed dose will actually be delivered to all parts of the CTV with a clinically acceptable probability, despite geometrical uncertainties such as organ motion and setup variations. It is also used for absorbed-dose prescription and reporting.

The Organs at risk (OARs) or critical normal structures, i.e. non-target tissues, are structures sensitive to irradiation, included, at least partially, in the irradiated volume. They might influence the treatment planning in the aim of limiting toxicities.

The Planning organ at Risk Volume (PRV) is a geometrical concept, i.e. a margin applied around serial OARs to compensate for uncertainties and variations in the position of the OARs during treatment, using a similar principle as for the PTV.

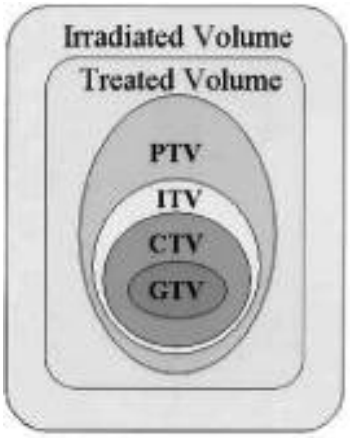

Figure 1.2 *ICRU 62. From Purdy et al., Semin. Radiat. Oncol., 2004.*

Thoracic radiation therapy limitations

1. Organs at risk

1.1. Generalities

In lung cancer, the main OARs are healthy lungs, spinal cord, esophagus, brachial plexus, heart, large vessels, and main bronchi.

Despite the technical improvements in treatment planning and delivery, all target volumes (TVs) necessarily include a substantial amount of normal tissue. Whereas the Clinical and Planning Target Volumes (CTV and PTV) encompass almost exclusively normal parenchymal cells, even the Gross Tumor Volume (GTV) encloses blood vessels and normal connective tissue. Healthy tissues within the TVs are thus unavoidably exposed to the tumor prescribed dose while the remaining normal tissue (i.e. outside the TVs) receives less but potentially significant dose, depending on physical parameters used in treatment planning and delivering.

Organs comprise a number of functional subunits (FSUs), i.e. units of cells that can be regenerated from a single surviving clonogenic cell. The clinical damages depend on the arrangement of the FSU, either in parallel or in series like in an electrical circuit, within the exposed organ. In parallel organized tissue (e.g. lungs), a critical number of FSU must be damaged before loss of function becomes manifest. Consequently, potential toxicities depend on the dose distribution throughout the whole organ rather than the maximum dose to a small area. In contrast, in serial organs (e.g. spinal cord), failure of only one FSU can cause loss of function of the entire organ. The risk of complications is strongly influenced by “hot spots” rather than by dose distribution within the organ.

Generally, toxicities are described as early or late according to the latency time, respectively less or more than 90 days, of symptoms appearance after the start of the treatment. Early radiation effects, which develop in turnover tissues, are dominated by vascular and inflammatory changes as well as by hypoplasia. The latency time of early effects is largely independent of dose, while severity and duration are dose-dependent. In contrast, late radiation effects involve an interactive response of parenchymal cells, vascular endothelium, fibroblasts and macrophages in association with cytokine cascade, which lead to parenchymal damage and loss of function within the irradiated organ. The latency time of late reactions is inversely dependent on dose.

For years, many studies have addressed the issue of radio-induced toxicities after RT for NSCLC and have tried to define some reproducible predictors of acute and late effects related organs. Some of them are presented in the following sections.

1.2. Lungs

In lungs, early pneumonitis is usually observed at 4-6 weeks after the end of RT, while fibrosis develops after several months to years. Rodrigues et al. demonstrated that the ideal parameter for estimation of the NTCP for pneumonitis from dose-volume histogram (DVH) has not been identified yet [19]. Nonetheless, some parameters, such as the percentage of total lung volume irradiated with defined doses (i.e. 5Gy, 10Gy, 13Gy or 20Gy) [15, 20-25] are currently used while the mean lung dose (MLD), which does not include any critical-volume parameter, appears to be correlated well with the incidence of pneumonitis [26]. The European Organization for Research and Treatment of Cancer (EORTC) recommends keeping V_{20Gy} below 35-37% and MLD lower than 20-23 Gy [27]. Some authors have also suggested to adapt lung constraints according to pulmonary function, i.e. the forced expiratory volume in one second (FEV1) and the diffusing capacity (DLCO) [15].

1.3. Spinal cord

Acute radio-induced myelopathy, revealed by the Lhermitte sign, occurs approximately 10 to 16 weeks after RT and is probably due to transient demyelination lesions. Its evolution is favorable with regression of symptoms after a few months to more than a year. It may occur at doses as low as 35 Gy in 2 Gy per fraction, i.e. well below usual admitted tolerance, particularly when long segments of cord are irradiated. On the contrary, the late myelopathy develops months to years after the irradiation. This complication is rare but extremely severe and is associated with a poor prognosis (i.e. sensitive, motor and sphincter disorders). Two main syndromes are described. The first, occurring 6-18 months after RT, is mostly limited to demyelination and necrosis of the white matter, whereas the second, occurring 1 to more than 4 years after RT, is mostly a vasculopathy. The main risk factors are the TTD as well as the dose per fraction received by the spinal cord. Surprisingly, spinal cord still presents a volume effect for irradiation of very short lengths (<1cm) while it is less pronounced for lengths above 2cm, i.e. the spinal cord tolerates a high radiation dose as long as few millimeters are irradiated. This suggests the migration of surviving clonogenic cells to the edge of the irradiated field, explaining also the partial repair of RT-induced subclinical damage after several years. The clinically accepted maximum tolerance dose for spinal cord is approximately 50 Gy, given in 2 Gy per fraction, even if it is probably too conservative. Indeed, using conventional

fractionation, the estimated risk of myelopathy is <1% and <10% at 54 Gy and 61 Gy, respectively [28].

1.4. Esophagus

The symptoms of severe esophagitis (≥ grade3) typically occur 4-8 weeks from the start of RT. Late esophageal damage, i.e. stricture and dysphagia, develops 3-8 months after the end of RT. Concurrent chemotherapy or hyper-fractionation increases the rate of severe acute esophagitis up to 30% [29, 30]. The most robust dosimetric parameter might be the mean esophagus dose (MED), with less than 15% esophagitis of grade ≥ 3 for MED below 28 Gy [29]. In addition, consistent data demonstrated that esophagitis of grade ≥ 2 increased to more than 30% as V_{70} exceeds 20%, V_{50} exceeds 40% and V_{35} exceeds 50% [29, 31]. Any hot spot should also be avoided, especially in the era of IMRT. Nonetheless, exceeded esophagus constraints should not prevent the patient from receiving a curative intent CRT because esophagitis of grade 3 or 4 usually heals rapidly without late effects (<1%) [27].

1.5. Heart

Radiation damage to the heart can involve the pericardium, myocardium, valves, and coronary vessels. The latency of RT-associated cardiac effects ranges from months (pericarditis and arrhythmia) to decades (coronary artery disease or myocardial infarction). The risk of cardiac events is probably related to both dose and irradiated volume. Pericarditis is the most common cardiac effect and it is generally asymptomatic although approximately in 20% of cases it develops into chronic and/or constrictive pericarditis. Radiation-induced cardiomyopathy, such as congestive heart failure, is increased by the additional exposure to anthracycline-based chemotherapy. Late damage to the pericardium and myocardium is characterized by diffuse interstitial fibrosis, perivascular fibrosis and loss of cardiomyocytes. Perfusion myocardium defects are detected as early as 6-24 months after RT and their incidence is strongly correlated with the volume of the left ventricle exposed in the RT field. Most perfusion defects are encompassed within an isodose line of 45Gy in the RT plan [32, 33]. Importantly, even though endothelial dysfunction is the primary pathological cause of the radio-induced coronary artery disease, other cardio-vascular factors such as age, smoking and hyperlipidemia appear to act as accelerating factors [33, 34]. Radiation can also impair aortic and mitral valves but most of the time, lesions are asymptomatic. The heart conduction system is the least commonly involved. One of its serious manifestations is complete atrio-ventricular block with required pacemaker implantation.

Most of the data concerning cardiac toxicities come from RT in breast cancer or lymphoma. In the field of lung cancer, where an increased rate of heart disease has been observed [34], dose-volume data are scarce and arise only from retrospective analysis. Especially, RTOG 0617 and IDEAL CRT trial demonstrated some evidence of negative association between overall survival and heart volume receiving more than 5 Gy (V_{5Gy}) and heart volume receiving doses of 65-75 Gy or left ventricule volumes receiving 1-5 Gy, respectively [35, 36]. Nonetheless, further studies are required to better understand the radiation effects on heart structures and to define reliable predictors of toxicities.

1.6. Tracheo-bronchial tree and large vessels

Tracheo-bronchial tree and large vessels are considered less radiosensitive than lung parenchyma. Even though no constraint has been applied to these organs in conventional treatment, bronchial stenosis or fistula with hemoptysis are becoming novel and often threatening recognized side effects. These mediastinal organs are particularly dose limiting in centrally located tumors treated with intensified dose strategies (stereotactic body radiation therapy or dose escalation). Several authors suggest a dose-relationship for radiation induced stenosis and fistula [37-39]. High-dose RT appears to cause a fibrosing mediastinitis with extrinsic compression of airways, which develops as early as 2 months and up to several years after RT. The EORTC recommends keeping doses to the central bronchi below 80Gy in conventional concurrent CRT [27].

1.7. Brachial plexus

Brachial plexus is a dose-limiting OAR for apex-located tumor. Symptoms of radiation-induced brachial plexopathy are mainly pain together with sensitive and motor disorders; they appear usually 1 to 4 years after treatment, even if some of them can be diagnosed up to 20 years after treatment. Physiopathology reveals demyelination damages, microvasculature alteration, and fibrosis of surrounding tissues and of nervous structures themselves. The brachial plexus is considered as a serial organ, very sensitive to high doses per fraction. Based on old patient series and techniques, its classically tolerated dose is approximately 60 Gy [40]. However, Hall et al. have demonstrated that, in head and neck cancer radiation treatment, brachial plexus receives doses considerably higher than 60 Gy [41]. Actually, brachial plexus tolerance is difficult to assess due to uncertainties in location and organ delineation, as well as to the lack of DVH parameter data, especially for NSCLC treatment.

2. Tumor motion and other geometric uncertainties

Geometrical uncertainties are inherent in any radiation treatment. Many factors can impact the precision of the radiation dose delivered. As previously discussed, radiotherapy includes several steps from the initial consultation and simulation to the daily treatment delivery. Each step involves some degree of potential error, usually on the order of a millimeter. But larger error can occur when most errors are in the same direction. This can affect the adequate coverage of the tumor, resulting in cold spots with potentially poorer LC or in unexpected dose and hot spots in surrounding normal tissue. Quantifying these uncertainties is a particular subject of concern in lung cancer, where the tumor moves during the breathing. Rigorous margins have thus to be chosen to ensure correct target dose coverage.

2.1. Description of geometrical errors

Geometrical uncertainties may jeopardize the radiation treatment. With IMRT, the impact of these uncertainties could be more severe compared to conventional treatment due to the better dose conformation. These potential geometric uncertainties and variations have to be assessed in order to measure their impact on dose to the CTV and to the OARs.

They can be categorized in two groups:

(1) The treatment execution error, random error or day-to-day variation, is different for each fraction but constant within a fraction. It is estimated by averaging one or more measurements made during a single fraction. Its uncertainty is computed by taking the standard deviation (SD) of this error over many fractions (σ). The sources of random uncertainties are setup error and organ motion on the treatment machine, poor reproducibility of the treatment machine, and errors in daily correction procedure [42].

(2) The treatment preparation error, or systematic error, is different for each patient, but identical for all fractions of one patient. This error is estimated by averaging measurements made during multiple fractions of a single patient treatment. Its uncertainty is estimated by computing the SD of this error for many patients (Σ). The sources of systematic uncertainties are “frozen” setup error and organ motion on the planning CT image, artifacts on planning CT related to physiological motion, errors in CTV and OARs delineation, multi-modality registration errors, poor reproducibility of the planning procedure, and differences in patient anatomy between imaging and treatment [42].

Tumor motion, baseline shift, and setup errors include both random and systematic components.

Breathing consisting in the muscular contraction and relaxation of the diaphragm and intercostal muscles generates thoracic and abdominal motion. In the case of lung cancer, the parenchymal tumor moves with amplitude up to 2 cm, especially for tumors located in the lower lobe and for cranio-caudal motion direction [43, 44]. The trajectory of the tumor is usually not rectilinear and possible hysteresis can make it look like a loop. Moreover, motion does not only affect the primary lung tumor. Mediastinal and hilar lymph nodes, together with upper abdominal organs, also undergo the effects of motion. Consequently, respiratory motion can introduce significant uncertainties [45, 46] in the entire process of RT from imaging and treatment planning to daily treatment delivery.

The baseline shift is an inter- and intra-fraction variation of the average tumor position relative to the bony structures (Figure 1.3 and 1.4). The physiologic process causing baseline variations are not well understood. Its potential shift seems to correlate with motion amplitude, suggesting it might be due to diaphragm motion, difference in stomach filling, stress status or heartbeat characteristics [47].

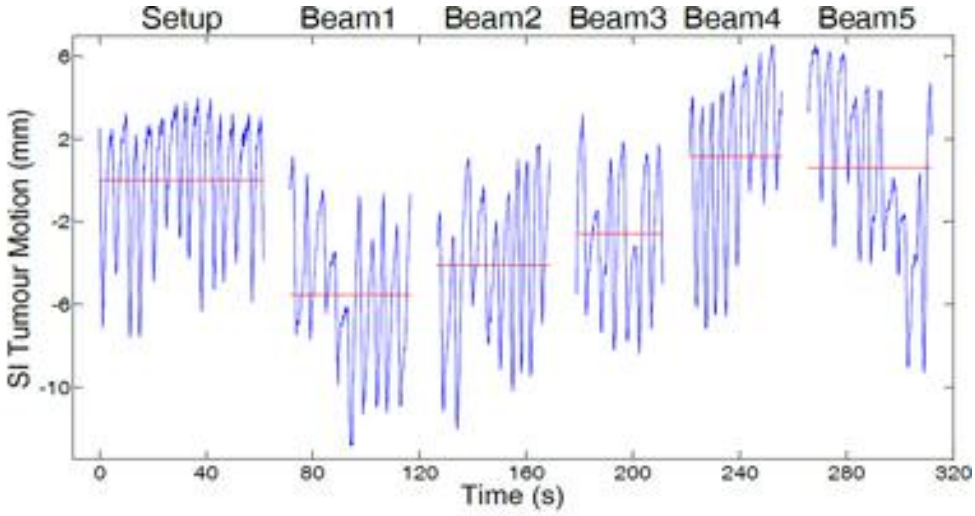

Figure 1.3 *Intra-fraction baseline variation. The graph shows the average tumor position (red line) in the superior-inferior direction in function of time, notably between the different sequential beams of a radiation treatment. From Sydney.edu.*

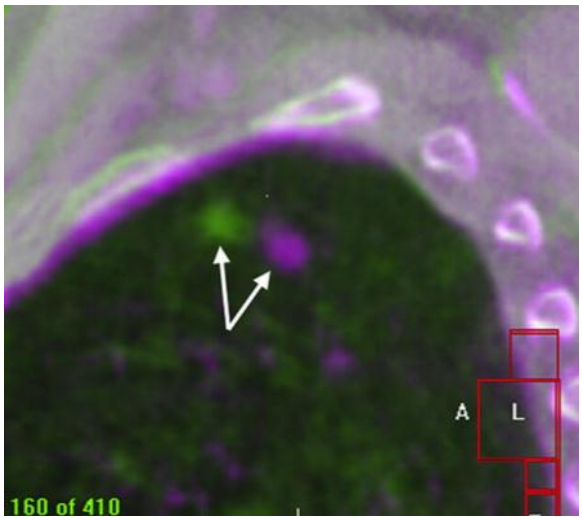

Figure 1.4 *Illustration of the inter-fraction baseline shift. The tumor has moved between fractions with respect to the bony anatomy. From Van Rooijen C. et al., IJROBP, 2012.*

The setup error corresponds to variations in patient positioning and alignment of the therapeutic beams during the treatment planning through all treatment sessions. The setup uncertainties depend on the patient-immobilization devices, the application of quality-assurance programs, the skill and experience of the technologists or nurses, and the use of image-guidance systems or other uncertainty-reduction techniques.

The delineation step is by far the largest source of error (Figure 1.5). It depends on the radiation oncologist experience and appreciation, the tumor location (peripheral versus central), the planning CT image quality, the window level used for contouring, etc. Several studies have demonstrated the high rate of inter- and intra-observer variability in GTV delineation for NSCLC tumors [48-55].

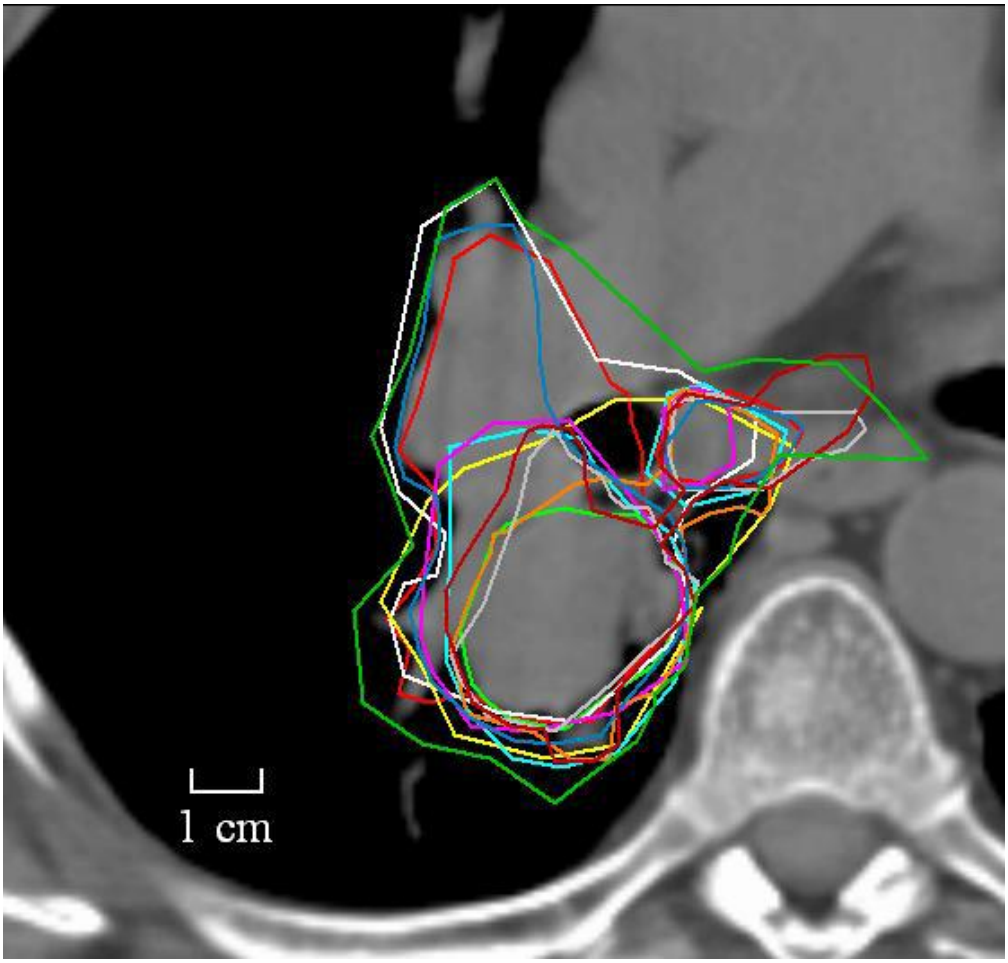

Figure 1.5 *Inter-observer variability in lung tumor delineation. From Steenbakkers et al., IJROBP, 2006.*

2.2. Effects of errors on the dose

The treatment execution deviations lead to a blurring of the dose distribution (Figure 1.6) while treatment preparation deviations lead to an unknown shift or sometimes more complex distortion of the cumulative dose distribution relative to the CTV (Figure 1.7).

Systematic errors have more impact on dose distribution than random errors. Consequently, margins accounting for systematic errors are much larger than random error margins [42].

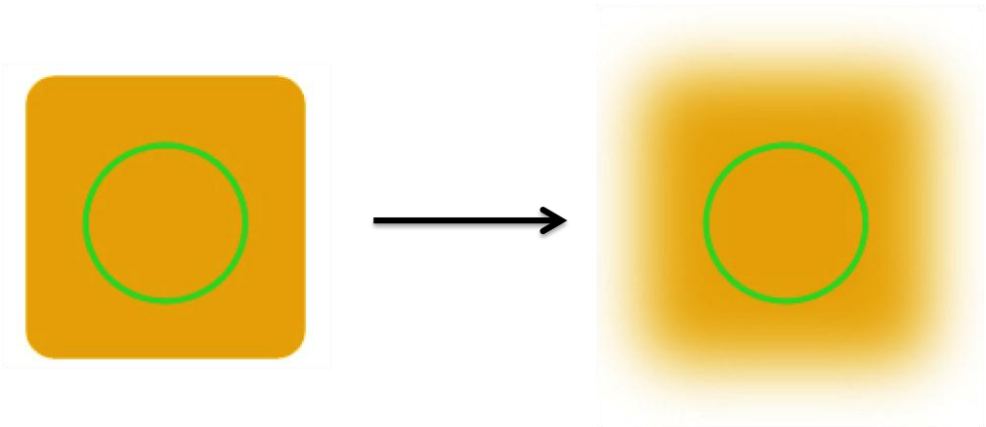

Figure 1.6 *Effect of treatment execution errors.*

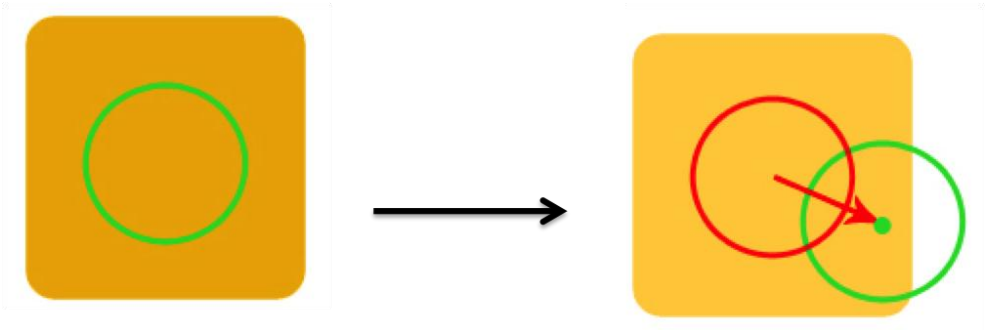

Figure 1.7 *Effect of treatment preparation errors.*

2.3. CTV to PTV margin recipe

The definition of safety margins around the visible tumor (GTV) and the microscopic invasion (CTV) is mandatory to include uncertainties and avoid deviation from the prescribed dose in the CTV. Van Herk et al. have proposed the dose-population histogram concept, which describes the probability for a patient in a population to receive a certain cumulative CTV dose [42]. Population-based margins concept stems from the fact that, even with Image Guided Radiation Therapy (IGRT) or even if they can be quantified, there will always remain uncertainties that cannot be corrected for individual patients, e.g. definition of TVs, unfeasibility of daily planning for dealing with tumor/anatomy changes or deformations.

The PTV margin is affected by each aforementioned error, i.e. variations in CTV position, size, shape and variations between patient and beam positioning, as well as by dosimetric uncertainties (i.e. penetration of the beam).

Consequently, Van Herk et al. analytically computed probability distributions of the minimum cumulative CTV dose and then derived a margin rule [42]:

$$M_{PTV} = 2.5\sqrt{(\Sigma_{TM}^2 + \Sigma_{BL}^2 + \Sigma_{SETUP}^2 + \Sigma_D^2)} + 1.64\sqrt{(\sigma_{TM}^2 + \sigma_{BL}^2 + \sigma_{SETUP}^2 + \sigma_p^2)} - 1.64\,\sigma_p$$

where Σ and σ denote the standard deviations of the systematic and random errors, respectively. Subscripts *TM*, *BL*, *SETUP*, *D* and *p* refer to tumor motion, baseline shift, patient setup variability, delineation uncertainty, and penumbra width, respectively. The coefficients in the formula ensure that the CTV receives at least 95% of the prescribed dose for 90% of patients. The coefficient of the systematic errors determines the confidence level or the percentage of patient population properly treated with a given prescription dose. A confidence level of 90% is generally considered as acceptable. On the other hand, the coefficient of the random errors determines the minimal isodose covering correctly the CTV. As a minimum CTV dose of 100% of the nominal dose cannot be achieved and would require an infinite margin, one should define clinically acceptable probabilities for the clinical goal, and 95% seems a good compromise. In the formula, σ_p denotes the SD of the dose gradient or penumbra, for which Sonke et al. have suggested a value of 3.2 mm for a photon beam in the water and 6.4 mm in the lung [47].

The penumbra represents the region at the edges of a radiation beam, where the dose falls off rapidly, and is usually specified by the lateral width of isodose levels (e.g. 90%-20%) (Figure 1.8). Related to scattered beam from tissues and treatment head, it is influenced by many factors, such as field size, depth, transmission through the jaws of the machine and energy of the beam. The penumbra contributes to blurring the dose distribution and can be harnessed in the computation of margins for random errors [56].

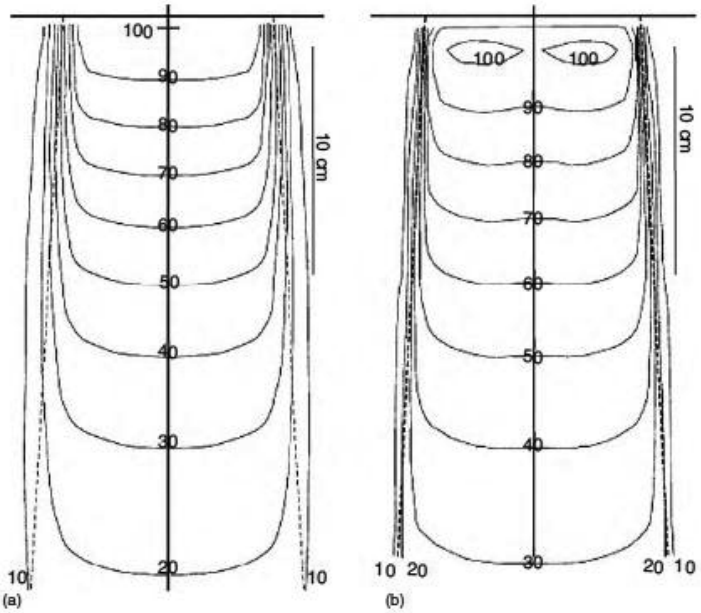

Figure 1.8 *Isodose lines in the central plane (a) from an 80 SSD cobalt-60 beam and (b) from a 6 MV linear accelerator. The penumbra is tighter for the 6 MV beam. From Handbook of radiotherapy physics, Theory and Practice, 2007.*

Importantly, as formalized in the equation above, the SDs of all treatment execution and preparation variations have to be squared before being summed because internal and external error sources are usually uncorrelated.

Noteworthy, some simplifications have been introduced in the recipe and adjustments should be made accordingly. Actually, it was assumed that the patient population was homogeneous, that RT included many fractions, that CTV was spherical and that probability distributions were normal. In addition, tumor rotations and shape variations have been ignored, isotropic errors were used for computation, the different sources of errors were assumed to be statistically independent and a shift invariant dose distribution was considered [42]. Notwithstanding, the validity of the margin recipe for clinical plans was demonstrated using Monte Carlo (MC) simulation methods [57].

The PTV is probably not the only tool to allow sufficient dose coverage of the CTV. Indeed, margin recipes are well established for rigid motion but issues still remain when it comes to rotations, deformations, changes in biology, delineation errors and non-uniform dose. The integration of TCP and NTCP model parameters as well as geometric uncertainties directly in the optimization process could lead to better treatment plan [58].

Improving the therapeutic index

1. Better defining the targets

As already mentioned, improving the therapeutic index involves intensification of the dose to increase the tumor control probability, while keeping toxicities as low as possible. However, this approach requires an accurate selection and definition of target volumes as a first step.

1.1. Multimodality imaging for gross tumor volume definition

1.1.1. CT imaging

The main role of imaging in RT planning is to provide an accurate and reproducible delineation of the true tumor volume. Nowadays, CT is the reference imaging modality for the treatment planning of NSCLC.

CT imaging is based on the fundamental principle that the differential attenuation of the X-ray beam by the various crossed tissues depends on the differences in tissue densities. Practically, the helical CT consists of an x-ray tube, a collimator and a receptor including several detectors. The X-ray tube rotates around the patient while the detectors measure the intensity of transmitted radiation (Figure 1.9). The transmitted intensity profiles obtained at different angles allow axial CT slices to be reconstructed.

CT is widely available, conveys essential anatomical information, has a high spatial resolution (about 0.5 mm) and also gives information about the electronic density of the tissues allowing dose calculation in RT planning. Nevertheless, it offers poor soft tissue contrast between the primary tumor and the surrounding normal tissues. It can present artifacts due to metallic material, breathing motion (i.e. in lung or upper abdomen) or beam hardening when traversing thick and/or bony structures like the spine/ribs. These limitations could affect the actual definition of target volumes.

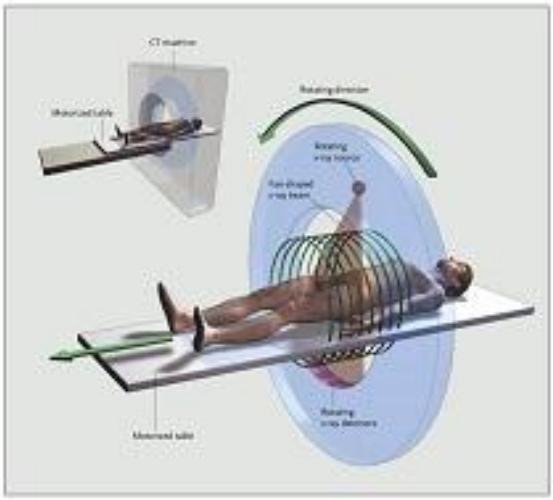

Figure 1.9 *Principle of computed tomography. The table moves continuously as the x-ray source and detectors rotate, producing a helical scan. From Brenner DJ et al., NEJM, 2007.*

1.1.2. FDG-PET imaging

In that regard, positron emission tomography with the radiotracer [^{18}F]-fluoro-deoxy-glucose (FDG-PET) used in combination with structural imaging, such as CT, can improve this task by providing then a combination of anatomical and functional information about tumors. Currently, FDG-PET is used for tumor staging, tumor response prediction before treatment, tumor response assessment after therapy, and detection of early recurrence in NSCLC. In addition, FDG-PET has some advantages over CT. First, it offers higher sensitivity and specificity than CT for the detection of primary tumors and mediastinal lymph nodes. Second, FDG-PET modifies significantly the size, location, and shape of the primary GTV, leading to the opportunity of adapting treatment planning or patient's management. Third, FDG-PET decreases dramatically the inter-observer variability of CT-based delineation, even when contouring protocols are available. Finally, with an appropriate radiotracer, PET allows potentially for the identification of tumor sub-volumes that are suspected of being radio-resistant, and could therefore beneficiate from dose escalation.

1.1.2.1. Principle of PET

The basis of PET is the injection of radiopharmaceuticals labeled with positron emitting radioisotopes allowing annihilation coincidence detection. The positron emitted from the nucleus of the radioisotope travels a short distance in a random direction before meeting with an electron from the tissue. Their annihilation produces two 511 keV photons, which are emitted in opposite directions at nearly 180° of each other. The almost simultaneous detection (in a short coincidence window) of two

annihilation photons by two opposite detectors defines a line of response (LOR) (Figure 1.10). The number of recorded coincidence events is proportional to the activity concentration. Parallel LORs from all angles are assembled into projections, which are then processed by iterative algorithms to reconstruct a 3D image that renders the distribution of the activity inside the patient.

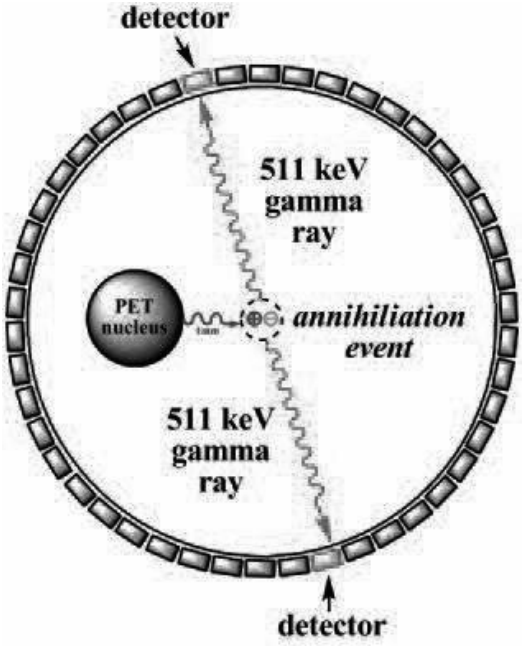

Figure 1.10 *Positron emission, annihilation and creation of a line of response. From ANSTO.gov.au.*

1.1.2.2. PET features and limitations

Accuracy of PET imaging depends on several physical factors. Some of them can be modeled in reconstruction; some others are taken into account by applying corrections on data prior to reconstruction. Imperfect corrections are potential limitations to image quality and jeopardize the interest of integrating PET into planning radiation treatment.

- Erroneous LOR assignments stem from both scattered and random coincidence events. A scattered coincidence is produced when one (or both) of the detected photons deviates from its trajectory by Compton scattering prior to its detection, whereas a random coincidence is the detection of two photons that are not arising from the same annihilation event. These

unwanted coincidences lead to image contrast degradation and incorrect quantitation and their estimation adds statistical noise to the signal (Figure 1.11).

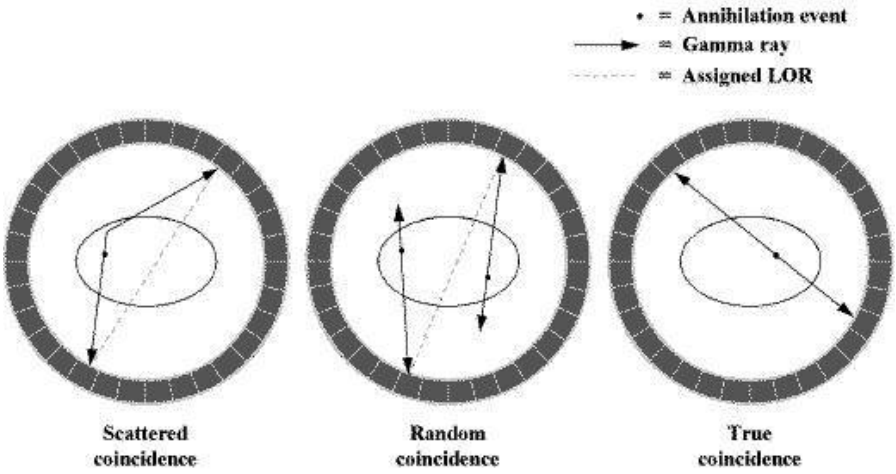

Figure 1.11 *Types of coincidences. From depts.washington.edu.*

- Attenuation is caused by the loss of true events, i.e. loss of coincidences. It is related to scattering and absorption of photons in the imaged subject him/herself. This results in an inaccurate estimation of the tracer distribution. Attenuation correction is usually performed using an additional transmission scan to measure attenuation factors for a PET alone device (leading to increased noise in the image) or using the attenuation map of the CT for a combined PET/CT system (with potential bias in the resulting image, i.e. different energy and acquisition time between both imaging modalities).

- Spatial resolution of PET images is by far lower that of CT images. It is estimated by measuring the point spread function (PSF), which describes the response of the imaging system to a point source, i.e. the signal intensity as a function of the distance. The PSF is distributed as a Gaussian function with the spatial resolution expressed as the full width at half maximum (FWHM) of this distribution (Figure 1.12). The spatial resolution of current PET systems ranges from 4 to 7 mm.

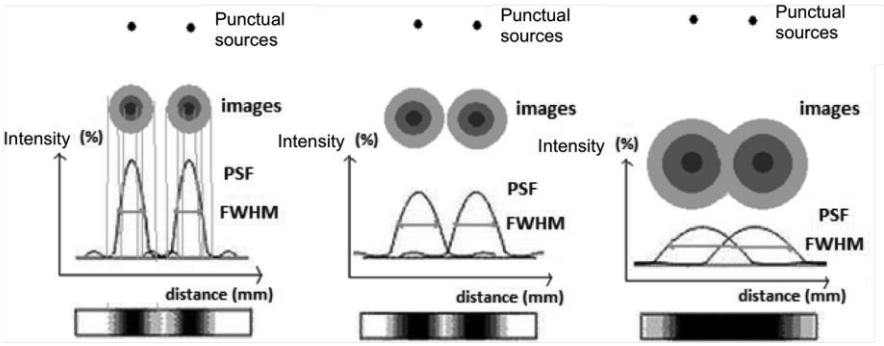

Figure 1.12 *The spatial resolution of a PET image is estimated by measuring the point spread function, which describe the response of an imaging system to a point source. The PSF is distributed as a Gaussian function with the spatial resolution expressed as the full width at half maximum of this distribution. As shown, the smaller the FWHM, the better is the spatial resolution.*

- The partial volume effect (PVE) results from the poor spatial resolution of the PET image, which leads to blurred images. A secondary cause is the sampling of the radiotracer distribution in a voxel grid, also called the tissue fraction effect, i.e. the pixels covering the edges of the source measure a mixture of both source and background signals (Figure 1.13). The PVE affects the quantification of the activity in objects smaller than twice or thrice the FWHM of the system. In this case, part of the object signal spills out into surrounding areas and the object looks larger and dimmer than it is actually.

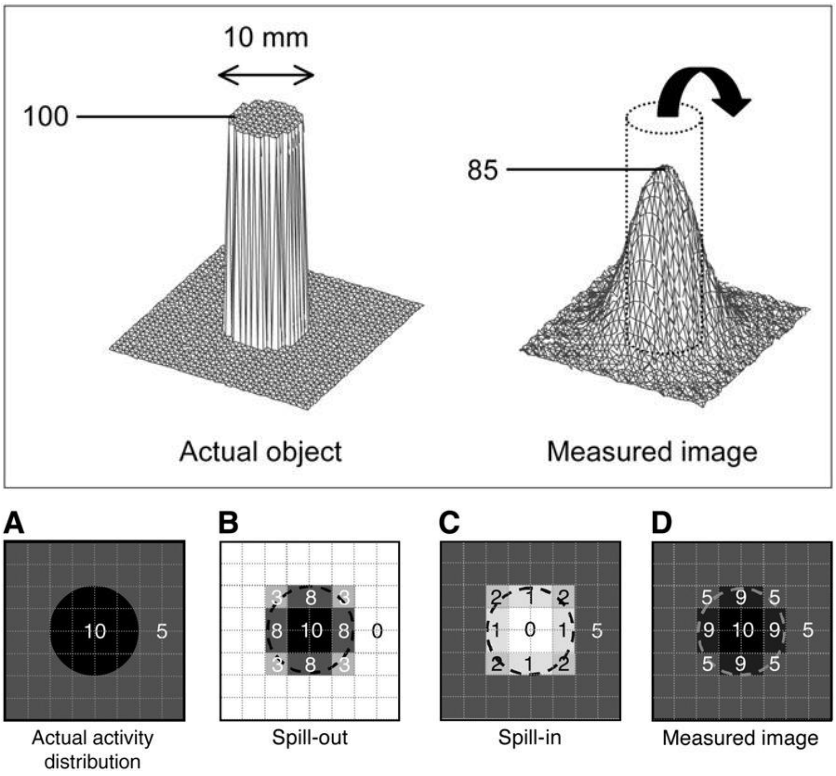

Figure 1.13 *The partial volume effect affects the quantification of the activity distribution in an object. Especially, the measured image (D) of the activity distribution (A) results from a mixture of spilling out (B) and spilling in (C). Consequently, the measured image looks larger and dimmer than it is actually. From Soret et al. JNM, 2007.*

- The statistical noise is the random variation in the pixel intensity of the reconstructed image. Increasing the injected tracer dose to the patient, the acquisition duration or the detection efficiency can reduce the image statistical noise. It can also be reduced by image filtering, but at the cost of a reduced spatial resolution. However, even with all optimized features, the number of detected events is much lower than in CT imaging and reconstructed PET images suffer from high level of noise.

- In combined PET/CT systems, breathing can generate artifacts since acquisition duration between PET and CT is different. As a result, structures located in the lower chest and the upper abdomen are acquired in a mean respiratory position during PET imaging or as a snapshot of a particular breathing position during CT.

1.1.2.3. Physiologic distribution of [^{18}F]-FDG tracer

In the field of oncology and radiation therapy planning, FDG is the most widely used tracer. [^{18}F]-FDG is an analogue of glucose with the positron-emitting radioactive isotope fluorine-18 substituted for the normal hydroxyl group at the 2' position in the glucose molecule (Figure 1.14). After intravenous injection, FDG is distributed in the body like glucose. It is incorporated into the tumor cell via a glucose transport protein (i.e. mainly GLUT-1) and is phosphorylated by hexokinase. However, FDG cannot be further metabolized and is consequently trapped in cells. Tumor cells show an increased anaerobic glycolysis resulting in an up regulation of GLUT-1 and hexokinase, which together with physiologic trapping leads to an accumulation of FDG. This accumulation is affected by tumor blood flow, activity of glucose transporters and hexokinase, and by cellular glucose consumption. As a result, FDG is not a specific tracer of tumor cells detection, as it can also be detected in inflammatory cells, in normal brain tissue, muscles, myocardium, musculature of the bowel, brown fat tissue and, in urinary tract, when it is excreted.

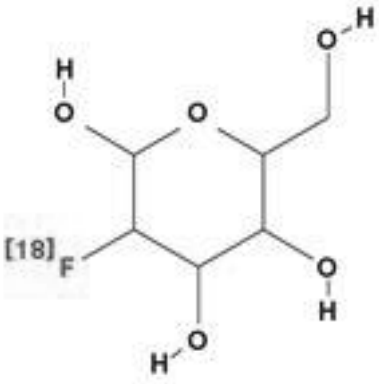

Figure 1.14 *A radioactive label called fluorine 18 (^{18}F) is produced in a cyclotron. The ^{18}F replaces a hydroxyl group in the glucose molecule resulting in fluorodeoxyglucose.*

1.1.2.4. Standardized uptake value

In clinical practice, the standardized uptake value (SUV) is commonly used for semi-quantitative evaluation of the FDG uptake in tumors. It is calculated as follow:

$$SUV = \frac{tissue\ radioactivity\ concentration\ (kBq/mL)}{injected\ activity\ (kBq)/\ body\ weight\ (g)}$$

Nonetheless, this semi-quantitative index suffers from major simplifications. First, the temporal evolution of the FDG uptake and the unmetabolized FDG are neglected.

Second, it is assumed that normal tissue uses a quantity of FDG proportional to the patient weight, i.e. no distinction between lean body mass and body fat. Finally, the formula neglects glycaemia level and ignores the metabolic difference between glucose and FDG.

Actually, the SUV provides an uptake index (i.e. not a measure of the glucose metabolic rate) and depends on many physiological, technical, and physical factors.

The SUV can be significantly affected among other things by image noise, low image resolution, reconstruction algorithm, attenuation correction, the kind of PET scanner used, time point of acquisition, lean body mass, blood glucose concentration, and user biased region of interest (ROI) selection.

Consequently, standardization of SUV is mandatory to compare measures performed in different centers. Protocols describing all aspects of the examination have been proposed, like patient preparation, tracer administration, dose standardization, image reconstruction and processing, guidelines for data analysis and standard quality control process [59].

FDG-PET/CT is being used increasingly to evaluate tumor response in addition to diagnosis and staging of tumors. The FDG uptake can be assessed visually or using a (semi) quantitative assessment, such as SUV (i.e. normalized to body weight) or SUL (i.e. SUV normalized to lean body mass (LBM)). Because large changes in body weight may occur during the course of the treatment, SUL should preferably be calculated alongside SUV, as follows:

$$SUL = \frac{tissue\ radioactivity\ concentration\ (kBq/mL)}{injected\ activity\ (kBq)/\ lean\ body\ mass\ (g)}$$

where LBM is calculated according to the formula of James et al. [60], i.e.

$$LBM\ (male)(kg) = 1.1\ x\ BW - 128\ x \left(\frac{BW}{Height}\right)^2$$

and

$$LBM\ (female)(kg) = 1.07\ x\ BW - 148\ x \left(\frac{BW}{Height}\right)^2$$

where BW is the body weight expressed in kilogram, while height is expressed in centimeter.

In the context of the evaluation of response to therapy, the extent and intensity of the FDG uptake have to be documented and compared to prior measurements. The EORTC firstly suggests the use of SUV_{max} as criteria for assessing tumor response [61]. Although SUV_{max} is widely used in clinical practice, easy to measure and less sensitive to PVE, it is strongly affected by statistical fluctuations since it is based on only one pixel. As a result, Wahl et al. proposed the so-called PERCIST criteria, using a 3D peak spherical volume of interest (VOI) of 1 cm^3, centered on the pixel with the maximum value, i.e. SUL_{peak} [62]. Reporting relative change in SUV or SUL during therapy represents the most robust parameter, classifying response into complete or partial metabolic response, and stable or progressive disease.

1.1.2.5. Integration of PET in RT planning

As already mentioned, conventional concomitant CRT for LA stages NSCLC achieves poor tumor local control rates. Available data support the dose intensification strategies. However, increasing the radiation dose in the whole target volume might potentially impair the surrounding healthy tissues. In that regard, functional imaging could help us to determine some sub-volumes suspected to be radio-resistant, which would require an additional radiation dose to obtain tumoricidal effect.

The NKI and MAASTRO groups have demonstrated that FDG-PET can provide sensitive and accurate molecular information to guide selective boosting.

Firstly, a high pre-treatment FDG uptake within the tumor correlates with poor tumor local control and survival [63-66]. Secondly, the high FDG uptake within the tumor remains at the same location during a course of RT or CRT [14]. Thirdly, the stable FDG uptake within the tumor is identifiable based on only one pre-treatment FDG-PET/CT [64, 67, 68]. Finally, high FDG uptake voxels in the pre-treatment FDG-PET have a higher probability to contain residual metabolic disease after therapy. As a consequence, these areas could probably beneficiate from dose escalation [69].

Although FDG-PET imaging seems to be a promising tool for guiding selective boosting, its integration in RT planning remains technically complex especially for the accurate definition of the tumor boundaries. Currently, several delineation methods have been suggested, relying mainly on either manual contouring [70-75] or automatic threshold-based segmentation [49, 74-94]. However, the main pitfalls for PET delineation stem certainly from the rather low resolution and signal-to-noise ratio of the images. Manual delineation is hindered by image blur, which can lead to inaccurate TV delineation. On the other hand, automatic threshold-based segmentation suffers from the fact that the optimal threshold depends on the size, the shape, and contrast to the background of the target, which are not known a priori or

difficult to estimate. In addition, theory shows that a threshold value can recover the true target boundary only if the target is spherical, the target and background activity are uniform, and the PSF isotropic and constant through the whole field of view; this is not the case in the reality. To overcome the inherent limitations of these approaches, a segmentation method that exploits the image gradient information has been developed in our lab. The gradient-based segmentation includes two main steps. First, a pre-processing step reduces statistical noise and resolution blur in order to sharpen the image gradient (Figure 1.15). Afterwards, the watershed transform algorithm detects the gradient magnitude peaks and generates the object contour (Figure 1.16). This method has been validated on both phantoms and head and neck cancer patients [95]. In NSCLC, the validation of this gradient-based segmentation technique on pathological specimens was still lacking.

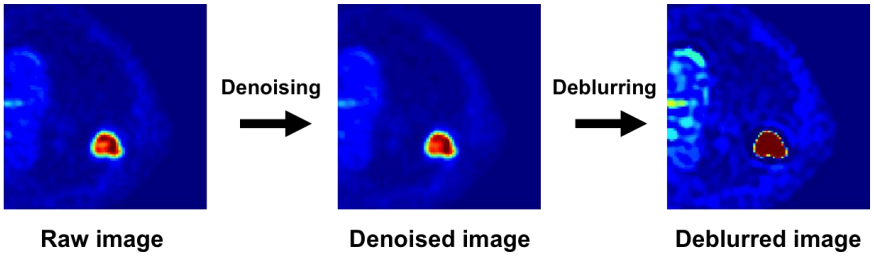

Figure 1.15 *The image processing reduces statistical noise and resolution blur in order to sharpen the image gradient.*

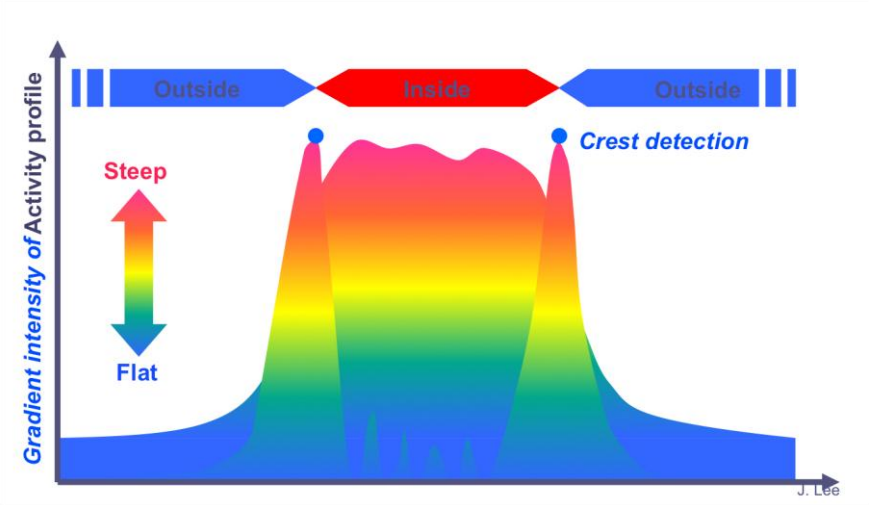

Figure 1.16 *The watershed transform algorithm detects the gradient magnitude peaks and generates the object contour (J. Lee).*

2. Better defining and preserving OARs

Usually, a classical predefined dose is prescribed for all LA NSCLC patients, i.e. 60 to 66 Gy in 2 Gy per fraction once daily. This standard scheme leads to poor tumor local control and survival in a number of patients, who could tolerate higher dose without increasing toxicities. The MAASTRO clinic has suggested prescribing the dose based on normal tissue constraints instead of a classic predefined prescription. This individualized isotoxic strategy has been shown feasible [13-15, 96] and increases the fundamental therapeutic ratio. Moreover, prediction models for radiation-induced acute dysphagia and dyspnea have been proposed to assist in treatment decision-making [97, 98].

Although some OARs constraints are well defined, data are lacking or equivocal for some of them. In addition, analyzed data arise from 3D-CRT and classical fractionation. Few studies report risk of toxicity from hypo-fractionation schemes and no dose-volume based analyses have been published. We also need standardization to obtain coherent recommendations. First, OARs delineation is critical in daily practice as well as in clinical trials. Currently available atlases from RTOG, EORTC and SWOG may guide to define the OARs with less variation and generate more reliable and consistent dosimetric data [99]. Second, uniformity is required when using dosimetric parameters. Confusedly, the mean lung dose is defined on the basis of either the whole lungs volume or the lungs volume minus the GTV, minus the CTV or minus the PTV, which can lead to large variability in the assessment of lungs tolerance. Third, toxicity assessment should be based on only one standard international grading system. Finally, recommended and common dosimetric parameters as well as early and late toxicities should be registered and shared for the constitution of large international and multicenter database.

The current recommended or used dosimetric parameters for each organ are presented in Table 1.1.

OARs	Constraints		Values	Authors
Lungs	MLD	FEV1/DLCO>50%	<19Gy	Van Baardwijk et al.
		FEV1/DLCO40-50%	<15Gy	Van Baardwijk et al.
		FEV1/DLCO <40%	<10Gy	Van Baardwijk et al.
			<20-23Gy	EORTC and QUANTEC
			<20Gy	RTOG 0617, MAASTRO
	V_{20Gy}		<35-37%	EORTC
			< 37%	RTOG 0617
			<30%	QUANTEC
Esophagus	MED		<28Gy	EORTC and QUANTEC
			<34Gy	RTOG 0617
	V_{70Gy}		<20%	QUANTEC
	V_{50Gy}		<40%	QUANTEC
	V_{35Gy}		<50%	QUANTEC
			<80%	MAASTRO
Heart	$D_{100\%}$		<30Gy	QUANTEC
	$D_{33\%}$		<60Gy	RTOG 0617 - Emami et al.
	$D_{66\%}$		<45Gy	RTOG 0617 - Emami et al.
	$D_{100\%}$		<40Gy	RTOG 0617 - Emami et al.
	D_{mean}		<46 Gy	MAASTRO
Pericardium	D_{mean}		<26Gy	QUANTEC
	V_{30Gy}		<46%	QUANTEC
Spinal cord	D_{max}		<54Gy	EORTC
			<50.5Gy	RTOG 0617
			<52Gy	QUANTEC
			<53Gy	MAASTRO
	D_{1cc}		<50Gy	QUANTEC
Mediastinal organs	D_{max}		<80Gy	EORTC
	D_{max}		<96Gy	PET boost trial
	D_{max}		<76 Gy	MAASTRO and KULeuven
Brachial plexus	D_{max}		<60Gy	Emami et al.
	D_{max}		<66Gy	MAASTRO

Table 1.1 *OARs dosimetric parameters currently used.*

3. Better delivering the dose

3.1. From 2D conventional RT to Intensity Modulated RT (IMRT)

Since a few decades, technological innovations have greatly improved treatment delivery and outcome. Historically, two-dimension (2D) conventional radiotherapy was limited to generate dose distributions in a single or a few planes of the patient's target volume, leading to unsatisfactory and heterogeneous dose distributions to both TVs and normal tissues. Rectangular shaped radiation fields encompassing the presumed tumor location were roughly defined using skin or bony landmarks according to planar radiographs.

Several advances in the field of image data acquisition, computer science and development of new machines and accelerators have led to high precision radiation techniques, such as 3D conformal radiotherapy (3D-CRT). Computerized treatment planning and 3D CT acquisition of the patient's anatomy allowed to precisely define the tumor and created shaped dose distribution that closely conform to the target volume while minimizing the dose to critical normal tissue. In 3D-CRT, multiple beams are usually used to better conform the tumor but the radiation intensity remains uniform within each beam, even if intensity profile can be slightly modified by using wedges or compensators to offset contour irregularities and produce more uniform composite dose distribution.

In the 90's, the refinement of 3D-CRT has ultimately led to Intensity Modulated Radiation Therapy (IMRT) (Figure 1.17). IMRT refers to a radiation therapy technique in which non-uniform fluence is delivered to the patient from some different angles in order to optimize the composite dose distribution, i.e. to deliver a high dose to the TVs and a low dose to OARs with a sharped dose fall off. A Multi Leaf Collimator (MLC) geometrically shapes the field, where intensity is modulated, allowing to create homogeneous concave dose distributions for complex shaped TVs or when an OAR is closely juxtaposed. The optimal fluence profiles are determined through inverse planning, where number, energy and direction of treatment beams are chosen, adjusted and optimized to satisfy predefined dose criteria to TVs and dose constraints to OARs. An additional advantage of IMRT over 3D-CRT is its ability to intentionally generate inhomogeneous dose distributions within TVs, inhomogeneities that are notably required in Simultaneous Integrated Boost (SIB) or dose painting strategies.

Since its emergence, IMRT has spread to most radiotherapy departments with rapid implementation for a wide range of indications.

Although from a planning point of view, IMRT clearly has the potential to improve dose delivery in NSCLC, especially for centrally located tumors, reports on its clinical

use and comparison with 3D-CRT remain scarce. Several issues including the effect of tumor and organ motion, the risk of pneumonitis and/or secondary malignancy resulting from low radiation doses, and the optimal planning algorithm remain unanswered and require further analysis. However, based on available data, IMRT seems promising with a clear impact on volumes irradiated at high dose and dosimetric parameters allowing a potential way for dose escalation. In addition, survival and progression free survival are at least similar to 3D-CRT technique [21, 100-107].

TomoTherapy, similar to helical CT, delivers intensity modulated, rotational radiation therapy using a fan-beam. It allows treatment delivery by continuous gantry rotation and treatment couch translation. In addition to full IMRT technique, the advantage is its ability to provide accurate verification of the delivery using megavoltage CT (MV-CT) images.

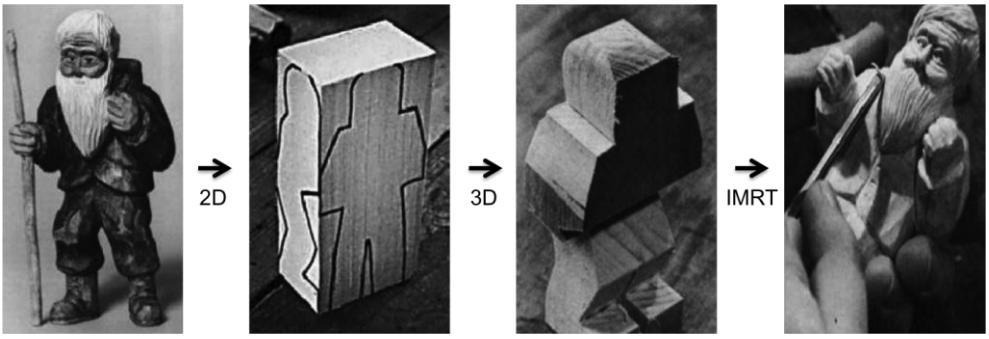

Figure 1.17 *Two-dimensional RT consists of radiation beams delivered to the patient from one or several directions, e.g. parallel opposed beams antero-posterior, postero-anterior or lateral beams. This results in rectangular shaped radiation fields encompassing the presumed tumor location. Using a three-dimensional representation of the patient anatomy, 3D-CRT sculpts the radiation beams to the shape of the tumor. Intensity modulated radiation therapy delivers radiation beams from different angles. At each of these angles, the intensity of the radiation is varied and the beam shape is changed to closely conform to the target volume while minimizing the dose to critical normal tissue.*

3.2. A step forward with Image-Guided RT (IGRT)

The accurate knowledge of the TVs and OARs location is of utmost importance for the correct dose delivery. This is even more important in the era of IMRT because dose distribution is more conformal than in 3D-CRT. Image Guided Radiation Therapy (IGRT) is defined as an external beam radiation therapy with positional verification using imaging prior to treatment delivery. However, guiding the placement of the treatment field is not a new concept. Treatment field was firstly verified using surface

and skin marks, and then portal images using gamma-ray (i.e. gammagraphy) were used. Currently, the acquisition of electronic portal imaging (EPID) with two orthogonal radiographs allows patient setup verification based on bony landmarks before the session. In contrast, the acquisition of a cone-beam CT (CB-CT) or MV-CT allows patient alignment based on soft tissue visualization (i.e. tumor and/or bony based matching) before the session. The adjustment of the patient and beam position can be performed either online, i.e. before or during the treatment process, or offline, i.e. after determination of the best patient position through accumulated data gathered during first treatment sessions. IGRT is especially indicated in case of moving target, complex positioning, potential tumor shrinkage or expansion, tumor shape or anatomy changes and is thus mandatory for hypo-fractionated RT, dose painting strategies and adaptive RT. Finally, the exact knowledge of the tumor location allows clinicians to reduce safety margins, thus reducing the volume of tissue irradiated, and/or potentially to escalate the dose.

4. Better integrating tumor motion

4.1. Tumor motion: an issue in thoracic RT

As already mentioned, the breathing leads to organs, lung primary tumor and mediastinal lymph nodes motion. This is a complex and asynchronous motion, including translation, rotation and deformation of the image voxels, which introduces errors in the entire process of RT from imaging and treatment planning to daily treatment delivery.

As a consequence, it appears essential to integrate it in the RT processes either in treatment planning and/or in treatment delivery according to the chosen method.

4.2. Three-dimensional CT (3D-CT) and the conventional PTV margin

Careful acquisition of images of the patient anatomy is the prerequisite for a correct RT planning. For years, free-breathing 3D-CT has been the reference imaging modality for treatment planning of NSCLC patients. However, it is merely a snapshot of the tumor and of the whole patient anatomy at some point of the respiratory cycle. As a result, it suffers from geometric distortions of the tumor volume by interplay effect between advancing image plane and internal organ motion, leading to blurring, duplication, overlapping and truncature artifacts (Figure 1.18). Moreover, 3D-CT does not provide any information on the actual tumor position and shape, on the amplitude range, on the complex trajectory (i.e. hysteresis) or on the baseline position of the tumor. In order to include uncertainties related to intra- and inter-fraction tumor

motion and patient setup in RT planning, a generic and isotropic PTV margin based on population statistics has to be applied around the CTV.

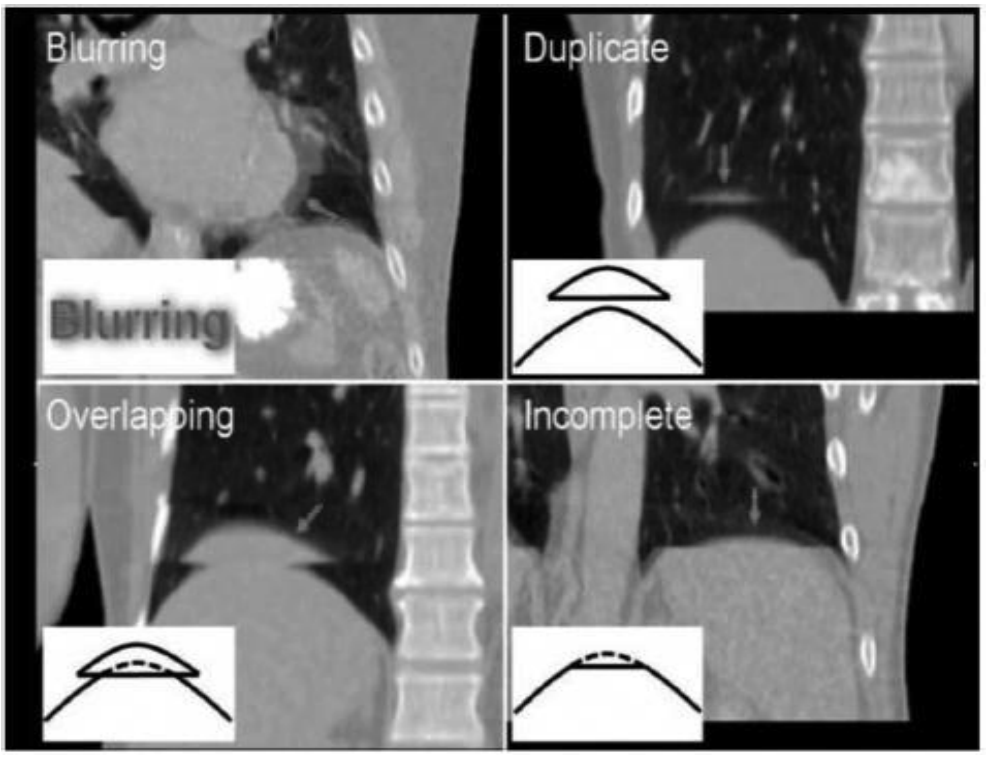

Figure 1.18 *CT imaging performed in free breathing can suffer from geometric distortions. From Yamamoto et al., IJROBP, 2008.*

4.3. Time-resolved four-dimensional CT (4D-CT): a definite innovation

4D-CT scanning techniques have been developed to reduce geometric uncertainties inherent to 3D-CT images. 4D-CT consists in the synchronization of a low-pitch CT data acquisition with the respiratory signal, which is generated either from a pneumatic elongation belt, from magnetic sensors or from infrared markers placed on the patient chest or epigastric area. From this dataset, breathing CT images can be prospectively or retrospectively sorted according to either phase or amplitude of the respiratory signal (Figure 1.19). 4D-CT allows a precise and individual quantification of tumor and organ motion. In particular, the radiation oncologist can assess the various positions, the amplitude, the baseline and the trajectory of the tumor. Nonetheless, the patient breathing during the planning 4D-CT might not be

representative of the breathing during treatment and the correlation between internal tumor motion and the external recorded signal could became unreliable, i.e. in case of irregular breathing or baseline shifts. The reproducibility of the breathing pattern is critical and can be increased by using audio and video coaching during the planning imaging as well as during each treatment session. It has been shown that using audio coaching decreases the respiratory rate variability whereas video coaching reduces amplitude and baseline shift uncertainties [108]. In addition, a CT imaging is required prior to each treatment session to validate and/or adapt the correlation between the external respiratory signal and the internal tumor motion. In that regard, setup correction protocols should consider imaging features in order to perform correct matching between planning CT and daily CB-CT or MV-CT, i.e. a bony-based or tumor-based matching [109].

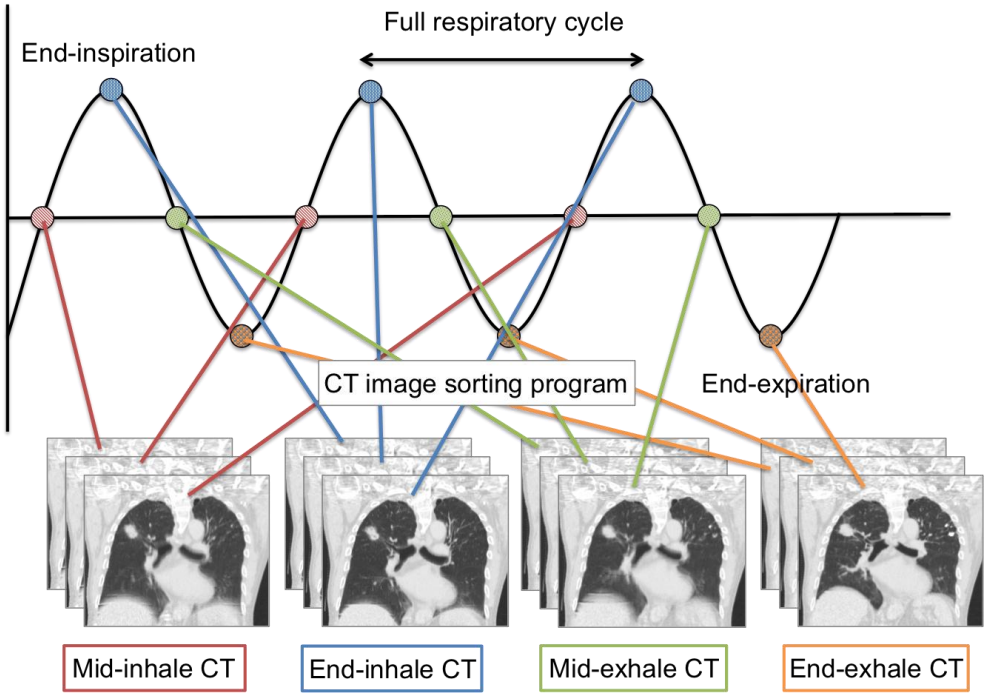

Figure 1.19 *Schematic overview of the 4D-CT image sorting principle.*

4.4. Integration of 4D data into treatment planning

Various approaches to incorporate 4D-CT data in treatment planning have been reported, including respiratory synchronized techniques and margin based strategies.

4.4.1. Respiratory synchronized techniques

In these techniques, the breathing pattern is obtained from an external or internal signal, which is correlated to the internal tumor motion. Integrating information on tumor motion into the treatment planning process allows to minimize tumor motion contribution in the PTV margin. However, it generally involves advance equipment, education and training in the use of complex technology, and the implementation of a dedicated quality assurance program.

4.4.1.1. Breath-hold

The deep inspiration breath-hold consists in an attempt for the patient to reproducibly and deeply inhale during imaging session and treatment delivery. In contrast, the Active Breathing Control (ABC) assists the patient breath-hold by using a valved spirometer blocking at a predefined relative lung volume level and airflow direction, i.e. moderate or deep breath-hold. These techniques aim at decreasing tumor motion and potentially shifts a significant volume of lung tissue outside the treatment field [110]. However, the poor patient compliance can lead to a lower reproducibility and the reduction of lung density might overestimate the dosimetric coverage if an inappropriate dose calculation algorithm is used [111].

4.4.1.2. Abdominal compression

An abdominal compression plate can be used to limit diaphragmatic motion and force a shallow breathing. Although amplitude tumor motion should be reduced, it has been demonstrated that this gain is limited to lower lobe tumors [112]. For other tumor locations, the abdominal compression provides only a minor benefit or even induces unwanted effects such as larger or erratic tumor motion and resulting margins. This technique may also be unsuitable for obese patients or those with poor respiratory function.

4.4.1.3. Gating

In gating technique, the patient breathes freely but the tumor is irradiated within a predefined portion of the patient breathing cycle, i.e. the gating window. Radiation is generally delivered during exhalation because exhalation takes longer than inhalation and corresponds to the most stable part of the cycle, thus improving the reproducibility. As a result, delineation of TVs and treatment planning are performed

on a particular frame of the 4D-CT corresponding to the end exhalation phase. During treatment, patient breathing is recorded either externally (e.g. infrared or skin markers, pressure belt) or internally (e.g. fiducials, fluoroscopy) to determine when the beam should be on and off. In an idealized gated approach, margin from CTV to PTV could be very small, as systematic errors due to breathing are significantly reduced and the margin becomes insensitive to patient-specific motion [113]. Nonetheless, a real gated treatment requires an online monitoring of the tumor position and assumes precise and real time tumor localization as well as prompt linear accelerator reaction to the gating signal, all conditions that are difficult to meet. Moreover, imprecise correlation between actual tumor motion and its surrogate can lead to uncertainties and poor treatment outcome if margins are too tight. Finally, a gated treatment requires additional equipment in the treatment room and increases the session duration. However, the application of guided voluntary breath-hold at a predefined position in the breathing cycle by using visual feedback and audio assistance and/or an increase in dose rate could significantly reduce this time [114, 115].

4.4.1.4. Tracking

The tracking technique is the real-time delivery of radiation with simultaneous tracking of the tumor, usually by using internal or external surrogate. This requires a dedicated device which is able to identify the tumor in real time, to anticipate the tumor motion, i.e. compensate for system lag (< 0.5 seconds [116]), to reposition beam in real time and to adapt dosimetry for changing target and critical structure locations. Basically, using ionizing or non-ionizing (e.g. electromagnetic transponders) imaging modalities, implanted fiducials or target position surrogates are localized. After image acquisition, data are processed and the beam has to be realigned either by moving the beam (i.e. MLC tracking, gimbaled linac head or robot-mounted linac) or by moving the patient (i.e. repositioning of the couch). Finally, a "time-resolved dosimetry" is required to assess the target coverage and OARs sparing. In an idealized tracking system, safety margins are significantly reduced and the delivery treatment time is faster than in gated treatment. However, uncertainties can accumulate through each step of the process, especially in the determination of the tumor position (i.e. accurate tumor prediction models) or in the relationship between the target and its surrogate (i.e. efficiency of MLC or gimbals tracking [115, 117, 118]), potentially resulting in considerable and unexpected safety margins.

4.4.2. Margin based strategies

These strategies aim at covering the entire tumor trajectory derived from 4D information, such as the ITV technique or take advantage of the geometrical time-weighted mean tumor position derived from the mid-position CT, extended with appropriate margin.

4.4.2.1. Internal Target Volume (ITV) strategy

The ITV encompasses all tumor positions during the breathing cycle. Therefore, the ITV concept aims to provide 100% dose coverage to the CTV during the whole cycle, i.e. considering tumor motion as a systematic error. This method tends to overestimate the safety margins as the tumor spends only a fraction of time at each position of the breathing cycle, and thus may lead to unnecessary irradiation of healthy tissues. Nevertheless, ITV approach is widely used because it is easy to determine, either automatically using non-rigid registration or manually on all phases of the 4D-CT.

4.4.2.2. Mid-position (MidP) strategy

The MidP represents the exact time-weighted average position of the tumor and all other internal structures during the breathing cycle (Figure 1.20). This average position can be automatically generated using 4D-CT data and non-rigid registration applied to each phase of the 4D-CT [119, 120]. As a result, the systematic error due to hysteresis is eliminated and motion is integrated in the Van Herk probabilistic margin recipe as a random error. In that regard, correct dose coverage can be obtained, even if the tumor is not fully within the PTV during a small part of the breathing cycle, thanks to the wide penumbra in lung parenchyma [121, 122]. The MidP concept presents several advantages. First, it can be applied to both primary tumor and regional lymph nodes. Second, it achieves smaller PTV margin than the ITV approach (and similar margin compared to gated treatment), resulting in smaller irradiated volume. Finally, it affects only the target volumes definition, and leaves all other aspects of planning unchanged; MidP is a simple method requiring no additional equipment in the treatment room, or complex 4D features in the treatment planning station (TPS) [113]. However, it uses a 4D-CT scan whose phases are non-rigidly registered. Unfortunately, no commercial implementation of MidP exists at the moment, which hinders adoption in clinical routine.

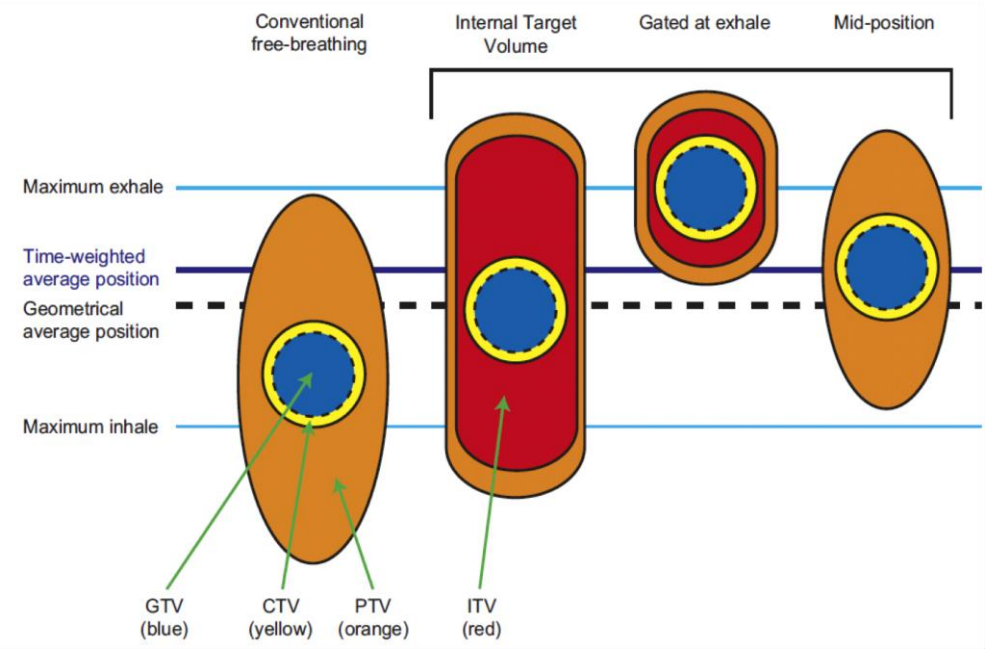

Figure 1.20 *Schematic overview of the margin based strategies for moving tumors treatment. From Wolthaus et al., Med Phys, 2008.*

Chapter 2

Aim of the thesis

Contents

Conventional treatment of LA-NSCLC patients with concomitant chemo-radiation achieves poor tumor local control rates and strongly affects the patient's outcome with an overall survival rate at 5 years of approximately 15%. It has been demonstrated that improved loco-regional tumor control strongly influences survival of NSCLC patients. Moreover, given the relationship between local tumor control and dose, it appears essential to implement dose intensification strategies. However, this remains challenging due to the proximity of highly radiosensitive organs, which may result in unacceptable toxicities. In that regard, escalating the dose uniformly over the whole tumor is arduous as demonstrated by the RTOG 0617 trial, which has failed to show any survival gain from dose intensification (74 Gy versus 60 Gy). A potential solution would be to escalate the dose in restricted areas within the tumor using high conformal RT delivery and optimized tumor motion management. In this context, functional imaging could allow the identification of potentially radio-resistant sub regions within the tumor, notably using FDG-PET, as a surrogate of tumor burden. This imaging technique benefits from a wide and long-term clinical experience and provides higher sensitivity and specificity than CT for the detection of primary tumor and mediastinal lymph nodes. Moreover, it offers a good signal to background ratio and is able to modify the size, location, and shape of the primary GTV for NSCLC, leading to the opportunity to adapt the treatment planning or patient's management. Finally, FDG-PET decreases the inter- and intra- observer variability of CT-based target volumes delineation.

Target volumes definition: concept and validation with pathology (Chapter 3)

The FDG-PET based selective boosting concept mainly requires an accurate selection and rigorous definition of the target volumes in order to spare as much as possible the healthy tissues. Although promising, the integration of FDG-PET in the treatment planning remains technically complex, especially for the accurate definition of the tumor boundaries. Currently, PET-based delineation methods rely on either manual contouring or automatic threshold-based segmentation. To overcome the inherent limitations of these approaches, a segmentation method that exploits the image gradient information has been developed in our laboratory. This algorithm has been first validated on phantoms and then on head and neck cancer patients. In NSCLC, the pathological validation of this gradient-based segmentation technique is still lacking. As a result, we designed a first study aiming at validating FDG-PET imaging as an accurate tool to define the tumor and identify tumor sub-volumes considered as radio-resistant. We validated a gradient-based segmentation method for GTV

delineation on FDG-PET images in NSCLC with surgical specimen, in comparison with threshold-based approaches and CT images.

Dose escalation based on FDG-PET (Chapter 4)

Besides the ability of FDG-PET to accurately define the actual GTV, it provides sensitive and accurate molecular information to guide a selective boosting. As already mentioned, a high pre-treatment FDG uptake within the tumor correlates with poor tumor local control and survival [63-65]. This high uptake is identifiable from one pre-treatment FDG-PET/CT and it remains at the same location during the course of RT [14, 67]. Moreover, a dose prescription based on OARs constraints instead of a fixed prescribed dose has been shown feasible with promising results in terms of toxicity and outcome [13-15, 96]. Based on these assertions and on the validation of a gradient-based method for the GTV definition on PET imaging with the surgical specimen, we designed a clinical trial to assess how an individualized escalated dose based on FDG-PET images would affect the tumor local control and the chemo-radio-induced toxicities.

Validation of the mid-position concept (Chapter 5)

Our third study investigated the tumor motion caused by breathing, which is another key issue in thoracic radiotherapy. It can be accounted for in the treatment plan by drawing an ITV that encompasses all tumor positions during the breathing cycle. Nonetheless, this widely used technique turns out to be overly conservative in terms of dose coverage and impedes dose escalation. In contrast, the mid-position (MidP) corresponds to the time-weighted average position of the tumor during the respiratory cycle. The knowledge of the average position is completed with the definition of specific margins to account for both motion and other geometrical uncertainties, according to the formalism of the margin recipe developed by M. Van Herk in NKI Amsterdam. Currently, MidP has never been implemented for helical TomoTherapy of moving lung tumors, nor compared to ITV for this treatment modality. In this context, we designed a study to assess the potential gain of MidP over ITV in terms of margin and PTV reduction, as well as in term of OARs dosimetric advantage. Finally, using a 4D Monte Carlo model, we assessed the plan quality and more particularly, the potential impact of intra-fraction motion and treatment delivery mechanics on tumor dose coverage when margins are reduced.

Chapter 3

Target volumes definition: Concept and validation with pathology

Gradient-based delineation of the primary GTV
on FDG-PET in non-small cell lung cancer:
A comparison with threshold-based approaches,
CT and surgical specimens

Marie Wanet, John Aldo Lee, Birgit Weynand, Marc De Bast, Alain Poncelet,
Valérie Lacroix, Emmanuel Coche, Vincent Grégoire, Xavier Geets

Radiotherapy and Oncology 2011; 98(1): 117-125

Contents

Introduction

Radiotherapy is one of the most important treatment modalities for locally advanced or unresectable non-small cell lung cancer (NSCLC). However, conventional radiation regimens still lead to high local recurrence rates that strongly affect the patient's outcome. Although dose intensification strategies, such as concomitant chemo-radiation, altered and dose-escalated schemes have been shown to improve the tumor local control and survival [13, 15, 123-125], their clinical implementations remain problematic. The proximity between the target volumes (TVs) and highly radiosensitive organs, such as the lungs, spinal cord, esophagus and heart, might result in unacceptable short- and long-term toxicities when dose intensification is considered. Therefore the recent development of additional techniques such as intensity modulated radiotherapy (IMRT), image guided radiotherapy (IGRT) and stereotactic radiation therapy (SRT) offers new perspectives by providing high precision in radiation dose delivery. They require however a thorough selection and delineation of the TVs, particularly the gross tumor volume (GTV), to avoid inadequate dosage of these TVs and/or organs at risk (OARs).

Nowadays, computed tomography (CT) is the reference imaging modality for the treatment planning of NSCLC. It is widely available, conveys essential anatomical information, and also indicates the electronic density of the tissues used for dose calculation. Nevertheless, it offers poor soft tissue contrast between the primary tumor and the surrounding normal tissues in cases of lung parenchyma changes (i.e. fibrosis, atelectasis, pleural effusion, poststenotic pneumonia), contiguity between the primary tumor and mediastinal nodes, and tumor located close to the mediastinum or chest wall. Alternatively, positron emission tomography with 18F-fluorodeoxyglucose (FDG-PET) is a functional imaging modality that provides higher sensitivity and specificity than CT for the detection of primary tumor and mediastinal nodes [126]. In radiation therapy, FDG-PET has already been shown to significantly modify the size, location, and shape of the primary GTV for NSCLC, leading to the opportunity to adapt the treatment planning or patient's management [70, 76-80, 127-129]. Likewise, FDG-PET dramatically decreases the inter-observer variability of CT-based delineation, even when contouring protocols are available [48-55, 72, 73, 81, 82, 130, 131]. Finally, with an appropriate tracer, PET allows the identification of tumor sub-volumes that are suspected of being radioresistant, in which case a targeted dose escalation [14, 64, 68, 69, 132, 133] could improve tumor control probability and overall survival [65, 134].

Although promising, the integration of FDG-PET in the treatment planning remains technically complex, especially for the accurate definition of the tumor boundaries

[135]. At the moment, several delineation methods were suggested relying mainly on either manual contouring [70, 72-75, 130] or automatic threshold-based segmentation [49, 74-94, 136]. To overcome the inherent limitations of these approaches, a segmentation method that exploit the image gradient information has been developed in our lab and validated on both phantoms and head neck patients with pathology specimens [95]. In NSCLC, the pathological validation of this gradient-based segmentation technique is still lacking. The few studies conducted in this field only concerned conventional threshold-based segmentation approaches, and suffered from important methodological issues, such as image acquisition in free breathing mode, or the lack of true volumetric assessment of tumors with the surgical specimen [85, 87, 88, 90, 136-138]. In this context, the present study aimed to compare the GTV delineation on CT and FDG-PET by using this novel segmentation method as well as the classical techniques described in the literature and to validate the results with surgical specimen in NSCLC. The originality of the study lays in its methodology, which addresses tumor motion by using gated imaging acquisitions, relies on an innovative segmentation technique, and compares the delineated volumes in a 3D mode to pathology specimens.

Materials and methods

1. Patient Selection

Ten patients (mean age 66 years; range 54-85) with histologically proven NSCLC stage I-II were prospectively enrolled in this study between October 2008 and February 2010. From these 10 patients, 6 had squamous cell carcinoma (SCC) and 4 had an adenocarcinoma (ADC). All patients were exclusively treated by lobectomy, excluding thus atypic resections and pneumonectomy. One patient had pre-operative chemotherapy. The patients and their primary tumor characteristics are summarized in Table 3.1. This study was approved by the local Ethical Committee, and informed consent was obtained from all patients.

Table 3.1 *Patient and primary tumor characteristics*

Patient No	Gender	Age (years)	Tumor localization	Tumor type	Histologic grade	cTNM**	Stage**	pTNM	Change in lung
1	Female	85	LU	ADC	2	T2aN0M0	Ib	T2aN0M0	No
2	Male	66	RM	SCC	NA	T1aN0M0	Ia	T1aN0M0	No
3	Male	59	RU	SCC	2	T1bN0M0	Ia	T0N0M0	No
4	Male	66	RU	ADC	2	T1bN0M0	Ia	T1aN0M0	No
5	Female	54	LU	ADC	2	T2aN0M0	Ib	T2aN0M0	Yes†
6	Male	62	LU	SCC	2	T2aN0M0	Ib	T2aNoM0	No
7	Male	69	LL	SCC	2	T1aN0M0	Ia	T1bN0M0	No
8	Male	64	LU	ADC	3	T1aN1M0	IIa	T1aN2M0	No
9	Male	73	LL	ADC	2	T1bN0M0	Ia	T1bN2M0	No
10	Female	62	RL	ADC	2	T2aN0M0	Ib	T1aN0M0	Yes*

Note: LU: left upper, RM: right middle, RU: right upper, LL: left lower, ADC: adenocarcinoma, SCC: squamous cell carcinoma.
**Atelectasis, †BOOP (Bronchiolitis Obliterans Organizing Pneumonia), ** 7th Edition IASLC TNM Staging Classification.*

2. Image acquisition

All patients successively underwent a contrast-enhanced (CE) CT, a 4D respiratory-correlated CT, and a respiratory-gated FDG-PET on a combined PET-CT camera (Gemini TF, Philips Medical system, Cleveland, OH, USA). The image acquisitions were performed the day before surgery during a single session. The total acquisition time for all scans was approximately 35 minutes. For all acquisitions, the patients were immobilized in a forearm support (Posiboard-2, Med Tec, Cablon Medical system, The Netherlands) in a supine, head first and arms overhead position.

The CE-CT acquisition started 35 seconds after an injection of 70 ml of iodinated contrast intravenously at a rate of 2.0 ml/sec (Iottexol, Omnipaque 350, HealthCare, Diegem, BE). The image acquisition was performed using a slice thickness of 2.0 mm, a reconstruction interval of 2 mm and a pitch of 0.94. The tube voltage and current were set at 120 kV and 200 mAs, respectively. Axial images were reconstructed using a matrix of 512 x 512 pixels, corresponding to a voxel size of 0.48 x 0.48 x 2 mm^3 in the x, y and z directions, respectively. The longitudinal field of view (FOV) typically covered the entire pulmonary region, from the supraclavicular fossa to the upper abdomen, and the axial FOV was set at 500 mm. The image data sets were transferred to the treatment planning system (Elekta CMS Computerized Medical Systems Software - Focal v4.40).

The 4D respiratory-correlated CT had the same parameters as the CE-CT, except for the low pitch value of 0.08 and the axial FOV of 600 mm. The respiratory signal was

generated from a pneumatic elongation belt placed on the epigastric area (Medspira/Mayo Clinic Breath Hold™, Interactive Breath-Hold Control System, Mayo Clinic Medical Devices, USA). From this dataset, 10 phase-binned breathing images were retrospectively reconstructed, covering thus the entire breathing cycle.

For gated FDG-PET, the patients were fasted for at least 6 hours and normal blood glucose levels were confirmed before tracer injection. Images were obtained between 60-120 minutes after injection of an average dose of 8.1 mCi (range 5.7-9.8 mCi) of FDG. The acquisition of the breathing signal was performed with the same respiratory device as the 4D-CT. After correction for decay, random, scatter, and attenuation, images were reconstructed with the iterative algorithm 3D LOR-OSEM (line of response ordered-subset expectation maximization) using only 20% of the breathing cycle's duration centered on the end of the expiratory phase, with a transverse FOV of 180 mm (one bed position centered on the primary tumor). The acquisition time was multiplied by 5 to compensate for the gating procedure and to avoid loss of statistics. The attenuation correction was performed by means of the averaged images of the 4D respiratory-correlated CT. The images were first reconstructed with a matrix of 288 x 288 x 90 voxels and a voxel size of 2 x 2 x 2 mm. The same acquired data was also used to reconstruct images with a matrix of 144 x 144 x 45 voxels and a voxel size of 4 x 4 x 4 mm. The resolution of the PET images measured in the center of the FOV with a punctual source led to a full width at half maximum (FWHM) of approximately 7.7 mm.

3. Processing of the Surgical Specimen

The surgical specimen was processed according to the method described in [86] for laryngeal tumors, which was adapted to the peculiarities of NSCLC.

The first step consisted in collecting the fresh lobe just after lobectomy in the operating room. Next, the lobe was immediately inflated with liquid gelatin (Gelatin 15%, BDH Prolabo, Leuven, BE) until being uniformly filled. The surgical specimen was then slightly cooled with ice to solidify the gelatin and placed inside a polystyrene box containing four parallel and equally spaced wooden sticks, longitudinally placed between the corners. The box was then filled with gelatin, frozen at -20°C for at least four hours, and thereafter at -80°C for two days. CT images of the frozen specimen were acquired on the Gemini TF PET-CT camera, with a slice thickness of 2 mm. Next, the box was cut with a carpentry band saw (EBS 3601; Elu, Köln, Germany) into transverse parallel slices of an average thickness of 4 mm. Afterwards, both sides of each slice were digitized with a flatbed scanner, and images were stored in tag image file format (TIFF) with a resolution of 150 x 150 pixels per inch. The digitized slices

were semi-automatically aligned using the wood rods as markers (home-made software), and eventually stacked to assemble the 3D volume of the surgical specimen.

The CT images of the whole box served to adjust the slice thickness of the 3D assembly, in order to compensate for the loss of material caused by the saw teeth. In practice, the CT image and the 3D assembly were manually registered. The rigid-body registration parameters and the slice thickness of the 3D assembly were alternately and iteratively updated until a good visual agreement was found. On average, the loss of material was evaluated at 0.6 mm per slice. Corrections of the resolution in the Z direction were thus applied to ensure the best fit between both imaging modalities. The slice thickness of the 3D assembly ranged from 2.28 to 2.35 mm, with an average of 2.3 mm.

Eventually, this methodology yielded a three-dimensional image of the surgical specimen that was used for further comparisons with conventional CT and PET imaging modalities.

4. Delineation of GTV (Figures 3.1 and 3.2)

The primary GTVs were delineated on each transverse section of all considered imaging modalities by two operators (MW and XG).

The GTVs on CT images (GTV_{CT}) were manually outlined on the planning workstation without knowledge of the FDG-PET results. Two fixed-display window settings were used: the lung window (width, 1700 HU; center, -300 HU) (GTV_{CTLW}) and the mediastinal window (width, 600 HU; center 40 HU) (GTV_{CTMW}). In complex cases, the delineation of GTVs was done with the help of an experienced radiologist in the field of thoracic oncology (EC).

The GTVs on FDG-PET imaging (GTV_{PET}) were automatically segmented on the two sets of reconstructed images with voxel sizes of 2 mm (GTV_{PET2}) and 4 mm (GTV_{PET4}) using four different methods with homemade software (IMREviewer). Firstly, we applied the gradient-based method on denoised and deblurred PET images ($GTV_{PETW\&C}$), as described in [95]. Then, we used the fixed thresholds of the maximal standardized uptake value (SUV) at 40% ($GTV_{PET40\%}$) and 50% ($GTV_{PET50\%}$). Finally, we applied the adaptive thresholding method based on the source to background ratio (GTV_{PETSBR}) [83, 86].

The GTVs on the surgical specimen (GTV_{macro}) were defined from the visualization of gross tumor infiltration on each digitized slice with the help of an experienced pathologist (BW).

5. Image co-registration (Figures 3.1 and 3.2)

All images obtained from CT, FDG-PET and surgical specimens were transferred to the IMREviewer software. PET and CT images were rigidly registered with those from the surgical specimen using manual translations and rotations in x, y and z directions until visual agreement was obtained. In this regard, it is noteworthy that the lobe as it appeared on the specimen images had a slightly different shape than on the pre-lobectomy CE-CT images, because *in vivo* and *ex vivo* mechanical constraints were not the same. Consequently, the rigid registration between the CT imaging and the surgical specimen was globally adjusted for the specimen orientation but locally optimized in the vicinity of the tumor. All volume contours were transferred to the CT images for comparison.

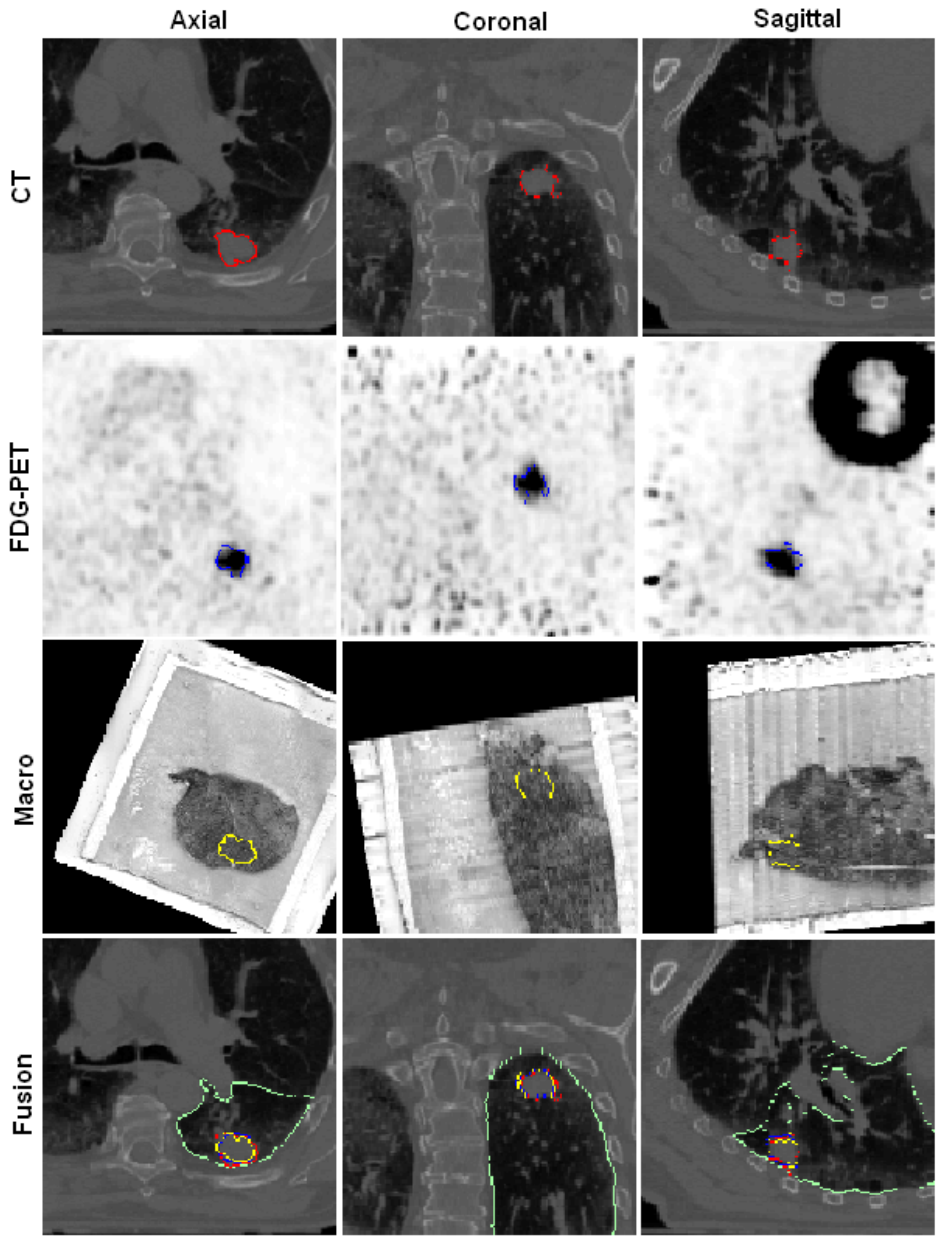

Figure 3.1 *Overview of the tumor delineation and image registration between CT, FDG-PET, and the macroscopic specimen of a well defined tumor. Volumes are displayed in transverse, coronal, and sagittal planes. The fusion represents the transfer of the three volumes on CT. The outlines show the GTVs delineated on each imaging modality: CT with the mediastinal window (red line), FDG-PET reconstructed with a voxel size of 2 mm³ using the gradient-based method (blue line), macroscopy (yellow line), and the lung contour (green line). GTVs do not significantly differ between the various imaging modalities.*

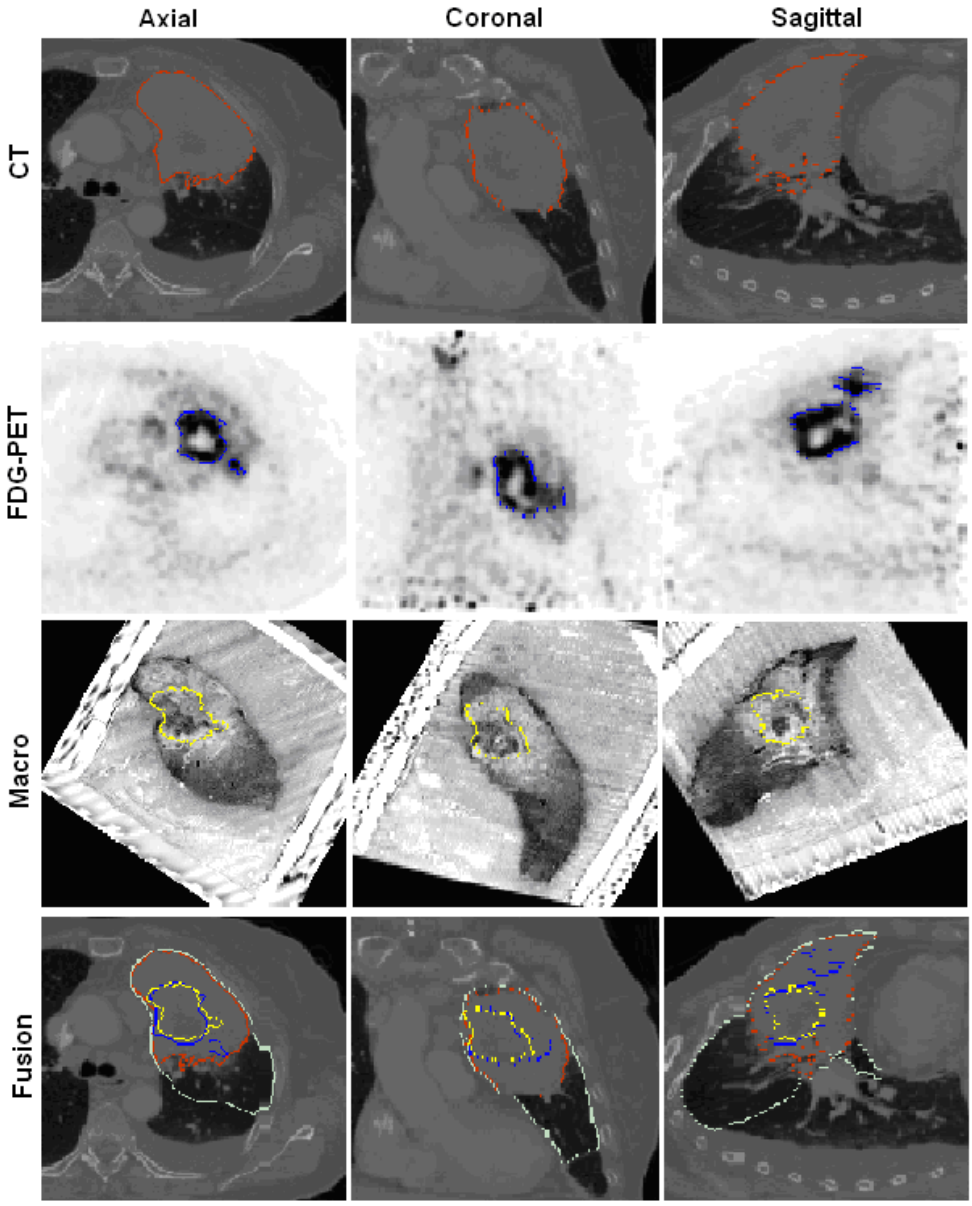

Figure 3.2 *Overview of the registration between CT, FDG-PET and the macroscopic specimen of a poorly defined tumor surrounded by BOOP. In comparison with Figure 3.1, CT largely overestimates the true tumor volume as defined on the macroscopic specimen, while FDG-PET provides a more accurate estimation of this later one.*

6. Statistical Analysis

GTVs delineated on macroscopic, CT and FDG-PET images with the different segmentation methods were quantitatively analyzed for all patients.

The analysis was twofold. A first volumetric analysis was conducted with the raw volumes expressed in ml. The second analysis considered a logarithmic transformation to reduce the magnitude of both skewness and kurtosis of the volume distributions. The main purpose of this transformation is to obtain nearly Gaussian distributions, as most statistical tests rely on this assumption. The identity ln(a) – ln(b) = ln(a/b) shows that comparing logarithmic transformed values equals considering the logarithm of their ratio. The analysis focused on $\ln(GTV_X) - \ln(GTV_{macro})$, where GTV_X can be any of the considered GTVs and GTV_{macro} is the ground truth. Zero indicates a perfect volume equality (ratio equal to 1). A positive value means that the technique overestimates the macroscopy, and a negative value results from an underestimation. In both analyses, the mean value and standard deviation were calculated. The impact of the imaging modality and the segmentation method on tumor volume assessment was estimated by ANOVA. In addition, the groups were compared with a pairwise Student *t*-test.

The same two analyses were also repeated after excluding a patient subgroup. Out of the ten patients, two had noticeable changes to the lung parenchyma surrounding the tumor. One had an extensive BOOP (Bronchiolitis Obliterans Organizing Pneumonia) and the second a basal atelectasis. We called this subgroup “poorly defined tumors” (PDT). As these modifications of parenchyma might significantly affect the delineation on CT, they were secondarily excluded for the sub-analysis.

While until here only volumes were considered, a matching analysis was also performed and the Dice’s similarity index (DSI) was calculated to estimate the discrepancies between the different GTVs. The DSI indicates the overlapping ratio between the GTV_{macro} and the various GTVs obtained at imaging. A DSI equal to one, means a perfect match between both volumes whereas a DSI equal to zero, means two disjoined volumes.

All the statistical calculations were performed with NCSS software 2004© (Number Cruncher Statistical System, Kaysville, UT, USA), *p*-values < 0.05 were considered statistically significant and all tests were two-sided.

Results

The GTVs delineated with the considered imaging modalities are reported in Table 3.2. The mean and standard deviations of the raw GTVs are provided as well. As detailed in the statistical analysis section, they were computed after logarithmic transformation of the volumes in order to process data distributions that were closer to normality. Means and standard deviations of transformed volumes are illustrated in Figure 3.3 with error bars (mean +/- 1 SD).

Table 3.2 *Raw GTVs (ml) measured on the different imaging modalities, along with averages and standard deviations.*

Patient No	Macro	CT		PET 2mm				PET 4mm			
		LW	MW	PET W&C	PET SBR	PET 40%	PET 50%	PET W&C	PET SBR	PET 40%	PET 50%
1	13.8	26.0	22.0	7.4	9.9	10.4	7.3	9.7	10.1	12.9	9.0
2	1.7	2.5	1.6	2.3	2.4	2.4	1.8	2.7	3.2	3.2	3.0
3	3.6	8.0	6.1	2.4	2.9	3.1	1.9	2.8	5.0	7.5	4.2
4	1.1	3.4	1.0	3.0	6.2	8.0	4.0	3.4	6.3	8.6	6.0
5	29.5	288.9	267.0	48.5	51.8	51.9	31.5	58.5	66.8	78.2	54.7
6	45.5	51.0	43.1	42.3	25.9	26.6	12.9	50.0	47.3	51.3	35.3
7	7.3	10.8	7.1	8.4	9.0	8.9	7.1	N/A	N/A	N/A	N/A
8	1.8	2.6	1.6	1.5	1.3	1.4	0.9	1.8	2.1	2.6	1.8
9	5.1	8.2	5.9	5.8	5.0	4.9	3.1	4.0	6.8	7.2	5.1
10	3.5	26.7	20.1	5.9	7.3	7.3	5.5	4.7	7.3	7.8	6.1
Mean for all patients	11.3	42.8	37.6	12.7	12.2	12.5	7.6	15.3	17.2	19.9	13.9
SD for all patients	14.8	87.8	81.7	17.4	15.6	15.6	9.1	22.3	23.2	26.5	18.4
Mean without PDF	10.0	14.0	11.0	9.1	7.8	8.2	4.9	10.6	11.5	13.3	9.2
SD without PDF	15.0	16.8	14.6	13.7	7.9	8.1	4.0	17.6	16.0	17.1	11.73

Abbreviations: N/A: Non available; Patient No: patient number; PDF: poorly defined tumors.

With all patients taken into consideration, CT led to a large overestimation of the true tumor volume as defined on the macroscopic specimen, both with the mediastinal and lung windows (ANOVA, $p<0.001$), although the paired analysis only revealed a significant difference for the latter one (Student *t*-test, $p=0.10$ and $p<0.005$, respectively). On the other hand, GTVs delineated on FDG-PET did not differ from GTV_{macro}, except for $GTV_{PET4\text{-}SBR}$ and $GTV_{PET4\text{-}40\%}$ that were significantly larger (Student *t*-test, $p<0.05$). $GTV_{PET2\text{-}50\%}$ was the only volume that was on average smaller than GTV_{macro}, but this difference was not statistically significant (Student *t*-test, $p=0.46$). Interestingly, moving from PET images with $2mm^3$ voxels to $4mm^3$ voxels resulted in larger GTVs on average, independently of the segmentation method used (ANOVA, $p<0.001$). For this reason, only data corresponding to PET images with 2 mm^3 voxels

are shown in Figure 3.3. As one can see, FDG-PET globally outperformed CT and showed the smallest SD. The gradient-based method achieved the best results, with the lowest average error and smallest standard deviation (0.14 ± 0.49). This confirms the robustness of this approach on a case-by-case basis, compared to usual threshold-based techniques.

Removing the 2 patients who presented parenchyma densifications surrounding the tumor from the data altered the analysis results. Here, CT achieved a close estimation of the macroscopy, particularly when the mediastinal window was selected, with average raw volumes of 10, 14, and 11 ml for GTV_{macro}, GTV_{CTLW} and GTV_{CTMW}, respectively. The logarithmic transformation led to means and standard deviations that are equal to 0.11 ± 0.25 and 0.54 ± 0.32 for CT with mediastinal and lung windows, respectively. Hence, mediastinal window showed a reduction of overestimation compared to the lung window (Student *t*-test, p=0.002 and p=0.28 for CT_{LW} and CT_{MW}, respectively) and also reached the smallest standard deviation among all imaging modalities. For FDG-PET, the results did not differ from those observed for the whole group, the best results being provided again by the gradient-based method ($GTV_{PETW\&C}$).

Regarding the matching analysis, there was no statistical difference between the different imaging modalities and delineation methods (ANOVA, p=0.59). The average DSI values were comparable with 0.58 and 0.62 for the CT_{LW} and CT_{MW} respectively, 0.68, 0.66, 0.66 and 0.63 for the $PET_{W\&C}$, PET_{SBR}, $PET_{40\%}$ and $PET_{50\%}$ with a 2 mm voxel, respectively, and 0.66, 0.64, 0.62 and 0.65 when images with a 4 mm voxel size were used.

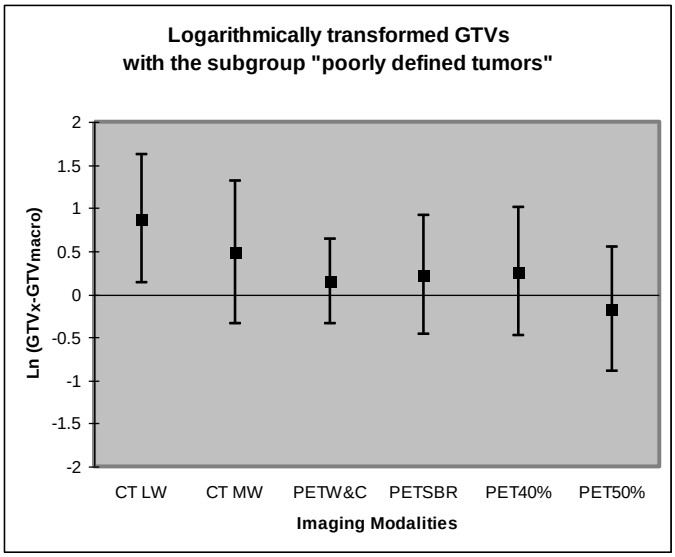

(a)

(b)

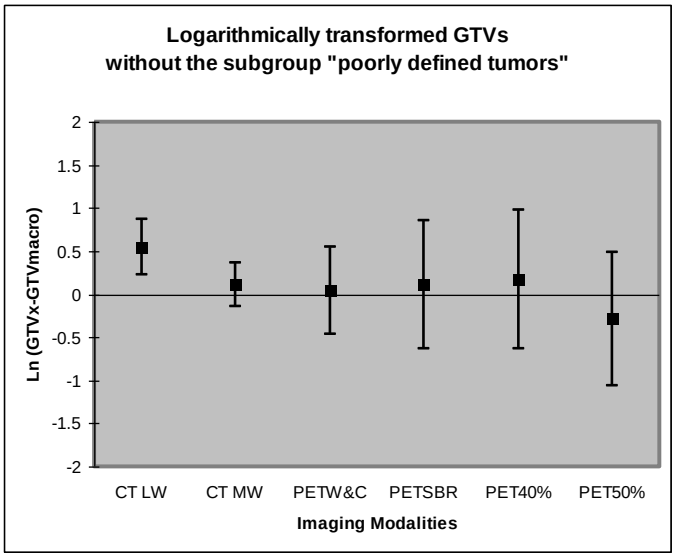

Figure 3.3 *Comparison between the mean volumes determined on each imaging modality for all patients (a) and for the subgroup excluding the "poorly defined tumors" (b). Volumes are presented as mean ± 1SD of logarithmic differences between the various GTV and* GTV_{macro}*. Differences and SD tending towards zero means that the imaging modality and delineation technique are reliable and robust to assess the macroscopy. Regarding the whole group of patients (left panel (a)), FDG-PET segmented by the gradient-based method (PETW&C) provided the closest and more robust estimation of the pathology. When only considering the "well defined tumors" (right panel (b)), CT reached an accurate estimation of the macroscopic specimen, which was even better when the mediastinal window was selected.*

Discussion

Overall, we showed that FDG-PET outperformed CT for the delineation of primary tumor volumes in NSCLC, as previously observed in HNSCC patients [86]. We also confirmed the superiority of the gradient-based segmentation, compared to usual threshold-based delineation, both in terms of raw volumes and logarithmically transformed ones. However, the added value of FDG-PET was more pronounced in cases of tumors surrounded by densifications of the lung parenchyma (atelectasis, BOOP). In other cases, the high natural contrast between the tumor and air allowed an estimation of the tumor volume on CT accurate enough for clinical use, even more if the mediastinal window was selected.

In comparison with previously published studies addressing the pathological validation of PET-based contouring in NSCLC, methodological aspects were performed in highly controlled conditions. Firstly, the validity of the pathologic specimen as "gold standard" relies on the accuracy of the whole procedure. In this respect, our work is based on the method previously developed and validated by Daisne *et al.* in laryngeal carcinomas [86]. The major advantages of this approach are that (i) the freezing procedure causes very limited tissue retraction compared to other fixation techniques, and (ii) the registration between CT and digitized images of the surgical specimen prevented from any distortion related to the slicing procedure. This leads to a reliable three-dimensional representation of the pathologic specimen. Interestingly, a three-dimensional assessment has been shown to provide a better estimation of the true tumor volume than measurements of one, two, or three sectional diameters [51, 85, 88, 90, 136, 137], since the relationship between the volume and the diameter along any direction is not linear except for strictly spherical objects [48]. To our best knowledge, only Stroom *et al*. performed a volumetric analysis between usual imaging and pathology findings [87].

Secondly, our study was the first to deal with the tumor motion during the images acquisition. In lung tumors, the long acquisition time required for PET imaging generates additional motion blur within images, with apparent loss of image contrast, increase of tumor size and decrease in activity [139, 140]. These artifacts caused by respiratory motion degrade the qualitative and quantitative accuracy for diagnosis purposes. In addition, they can also strongly affect the tumor delineation procedure, whatever the segmentation method used. This issue can largely be addressed by using 4D PET-CT acquisition, as described in [141]. In our study, PET images were reconstructed at the end-expiratory phase of the breathing cycle, which is the most stable [43, 142-144]. This guaranteed the most accurate target delineation by avoiding unwanted motion-induced blur. In order to keep acquisition statistics and

the signal to noise ratio (SNR) to reasonable levels, the acquisition time was prolonged accordingly.

Regarding PET image, the gradient-based method has been used in this study as a robust alternative to the threshold-based approaches. Indeed, the simple method that selects a fixed threshold of activity failed to provide an accurate estimation of the tumor volume. In summary, thresholds of 40% of the maximal activity led to an overestimation of the macroscopy, while a value of 50% underestimated it, with considerable variations on an individual basis for both approaches (Table 3.2, Figures 3.1 and 3.3). These findings confirm previously published data in NSCLC patients. Stroom *et al.* showed that a threshold of 42% overestimated the pathology [87]. Yu *et al.* determined that a cut-off of 31% ± 11% of the SUV_{max} provided the best estimate, which corresponded to a range from 15% to 55% according to individual patients [136]. Wu *et al*. used several fixed thresholds varying from 20 to 55%, and found that the value of 50% best correlated with the pathology, but CT remained superior to PET for this task [85]. In addition, some studies pointed out that the threshold for accurately recover the actual volume, substantially differs with the size, shape, heterogeneity, and background uptake of the tumor, questioning thus the use of a single threshold [74, 75, 84, 91, 92, 145]. Consequently, the adaptive threshold relying on the SBR appeared to be a valuable alternative [83]. However, this method did not improve the accuracy of the PET segmentation compared to fixed thresholds, and tended to overestimate the pathological specimen in our results. This confirms the data from Schaefer *et al*., showing that the SBR-based method led to an overestimation up to 28% of the PET over the CT-based GTV [94]. In contrast, Van Baardwijk *et al*. observed a slight underestimation of the macroscopic specimen when using this technique, although a good correlation was obtained [90].

Compared to thresholding approaches, the gradient-based method better deals with the inherent shortcomings of PET images, such as their low SNR and resolution. The method includes specific preprocessing steps to reduce statistical noise and resolution blur, which both preclude the accurate detection of the tumor boundaries. Denoising and deblurring sharpen the image gradient in a principled way, making it easier to detect peaks of gradient magnitude with algorithms such as the watershed transform [95]. This method was first validated in our center on phantom and HNSCC patient materials, and was shown to outperform the SBR method in a laryngectomy series [95]. Our data confirm the superiority of this approach also in NSCLC, since it provided a closer estimation of the pathological specimen than the threshold-based techniques, not only on average but also on case-by-case basis. The last observation is clinically important, as any misestimation of the target volume for a given patient might jeopardize the treatment outcome. Consequently, we believe that the gradient-

based method should be used as the reference segmentation method in the field of PET-driven delineation in NSCLC patients.

Although CT has been long-past considered as the reference imaging modality for the delineation of primary tumor in lung, it suffers from a low contrast resolution in cases of tumors associated with fibrosis, atelectasis, pleural effusion, post-stenotic pneumonia, or tumors located close to the mediastinum or chest wall. In such situations, consequential overestimations of the true volume can occur, as seen in the present study with the two patients suffering from BOOP and atelectasis, and large inter-observer variations have been reported due to image interpretation difficulties [48-50, 53-55, 81]. In the other cases, the air offers a high natural contrast in peripherally located tumors, and CT remains an appropriate modality imaging in these tumor locations. However, the window setting should be carefully selected before manual delineation, since these parameters are known to influence the image interpretation. In that regard, the radiotherapy group of the EORTC recommended some years ago the use of a lung window for the delineation of the primary lung tumor [146], based on previous phantom measurements [147, 148]. Although this recommendation is nowadays widely accepted and followed, most recent clinical studies have illustrated that its use typically led to an overestimation of the surgical specimen [85, 87, 88, 149]. In addition, data of Grills et al. showed that the volumes delineated with the mediastinal window were closer to the pathology findings compared to those defined with the lung one [149]. Obviously, the available clinical data based on patient material, including our own results, seems to indicate that the mediastinal window would be more appropriate. In this context, we recommend using mediastinal window for CT-based GTV delineation of primary NSCLC, even if the contradictory results from patient and phantom measurements preclude any definitive conclusion.

The collected data has potential limitations. Firstly, we assume that the surgical specimen is the ground truth. However, uncertainties persist about the volume of the macroscopic tumor despite each step of the procedure has been controlled carefully. Actually, we consider that the freezing procedure does not involve any consequential modification based on the assertion of Daisne *et al*. who observed very little or no tissue distortion after the same procedure on macroscopic laryngeal pieces [86]. Then, we estimated that the box slicing was performed regularly, although small deviations were observed. Finally, the 3D volume reconstruction of the digitized slices was processed by semi-automated tools that allowed for less variability.

Secondly, the lobe deformation might preclude the adequate assessment of GTV, and might impact the matching analysis. Albeit the lobe was filled with gelatin until it was

uniformly inflated as assessed by manual palpation and visual check, the lobe shape significantly differed from its *in vivo* status. However, we assumed that the GTV is a non-deformable rigid tissue, relying on previous investigations on the potential deformation of the lung lobe after surgery [87, 150]. This assumption excludes the use of any deformable registration algorithms, if artificially-induced volume and shape modifications of the tumor on the surgical specimen want to be avoided. Furthermore, such algorithms could encounter technical difficulties in case of different contrasted images, such as CT or PET and pathology images. However, optimizing rigid registration at the tumor level was a difficult task, and the resulting small translation gap between the various GTV may partially explain the relatively low DSI observed in our study.

Thirdly, since the tumors sample came from a surgical series, the size of our tumors set is relatively small with an average volume of 11.3 ml, which corresponds to a sphere of 28-mm diameter. We can assume that the partial volume effect (PVE) is relatively substantial since the sizes of some tumors are less than 3 times the FWHM considering individual patients. The PVE could explain the differences observed between the GTV_{PET} reconstructed with voxels size of 2 and 4 mm. In fact, the GTV_{PET4} seems to give a larger tumor than the GTV_{PET2} because of the relatively low spatial resolution of the imaging system and the tissue fraction effect. As a result, part of the tumor signal spills out into surrounding areas and the image is larger but dimmer compared to the actual tumor, hence overestimating it in size and underestimating it in intensity value. Basically, the parameters of image reconstruction should favor a high spatial resolution, in order to decrease the PVE [151].

Fourthly, the present study concerns surgical cases. Consequently, tumors have small sizes and peripheral location. The extrapolation of our data to central location or larger tumors seems feasible given that FDG-PET is more relevant in case of poorly defined tumors (i.e. tumors located next to the mediastinum or larger tumor inducing pneumonia or atelectasis). As a result, FDG-PET could be useful more often in radiotherapy intent NSCLC patients.

Finally, the small sample of patients decreases the power of the statistical tests. In consequence, some irrelevant tests could reach a level of significance for a larger cross-section and notably, would display some significant differences among the segmentation methods used.

In conclusion, in regard to these results, we suggest to use FDG-PET images segmented by a gradient-based technique for the delineation of the primary tumor in NSCLC, surely when they are poorly identifiable on conventional CT. For well-defined,

peripherally located tumors, the CT with mediastinal window remains a clinically acceptable alternative to FDG-PET.

Chapter 4

Dose escalation based on FDG-PET: A feasibility study

An individualized radiation dose escalation trial
in non-small cell lung cancer based on FDG-PET imaging.

Marie Wanet, Antoine Delor, François-Xavier Hanin, Benoît Ghaye, Aline Van Maanen, Vincent Remouchamps, Christian Clermont, Samuel Goossens, John Aldo Lee, Guillaume Janssens, Anne Bol, Xavier Geets

Submitted to Radiation Oncology journal in revised form, December 5th, 2015

Contents

Introduction

Concomitant chemo-radiation (CRT) for locally advanced (LA) stages non-small cell lung cancer (NSCLC) achieves poor tumor local control (LC) rates, which negatively affects the patient's outcome with a 5-year loco-regional failure rate of about 30% [7]. Available data show that increasing tumor LC improves survival, even in LA NSCLC [7, 152]. These evidences support dose intensification strategies [7, 153-157].

Escalating the dose uniformly over the whole tumor remains challenging, and may result in unacceptable toxicities due to the proximity of radiosensitive organs. Although the RTOG 0617 study failed to show any survival gain from dose intensification (74 Gy versus 60 Gy), pursuing validation of dose escalation makes sense, considering radiobiological evidence [23]. Indeed, several factors may explain this unexpected failure, like unadapted organs at risk (OAR) constraints in three-dimensional (3D) and IMRT planning and dose escalation on whole target volume (TV), causing late cardiac and pulmonary toxicity and death. The extended overall treatment time (OTT) in the 74 Gy arm [158] or less optimal target volume coverage in order to meet constraints could also explain the higher local failure rates.

In that regard, dose escalation schemes based on functional imaging might improve the therapeutic ratio. [^{18}F]-fluoro-deoxy-glucose positron emission tomography (FDG-PET) provides better soft tissue contrast between the tumor and normal tissues than computed tomography (CT), thereby improving the definition of the gross primary tumor volume (GTV) [159]. Furthermore, local recurrence or progression typically occurs within geometrically stable high FDG uptake regions of the primary tumor, providing a rationale to guide selective dose intensification [14, 63, 64, 67, 69, 160].

Moderate accelerated hypo-fractionation schedules might also improve the LC. Shortening the OTT reduces the effect of accelerated repopulation during the course of radiotherapy (RT) [10, 11, 13, 161]. Moreover, a dose prescription based on normal tissue constraints instead of a classic fixed prescription has been shown feasible, with promising results in terms of toxicity and outcome [13, 14, 16, 96]. This approach makes sense in case of moderate hypo-fractionation scheme, where particular attention is paid to radiosensitive organs to avoid late normal tissue injury.

Modern RT technologies like intensity modulated radiation therapy (IMRT) and image guided radiation therapy (IGRT) contribute to accurate delivery of selective boost doses to metabolically active regions in the tumor [162]. Nonetheless, if advanced delivery techniques allow steeper dose gradients, tumor motion management becomes even more critical in the process. The conventional Internal Target Volume (ITV) can adequately address this issue.

For all these reasons, we designed a clinical trial to assess the feasibility of an individualized and accelerated FDG-PET boost prescription delivered with IMRT in LA NSCLC patients. The study also aimed to assess the impact of this prescription on the tumor LC and chemo-radiation-induced early and late toxicities with a 2-year follow-up (FU).

Materials and methods

1. Patient selection

Thirteen patients with histologically proven stage II-III NSCLC were prospectively enrolled from November 2010 to February 2013. The diameter of their FDG-PET positive primary tumor had to exceed 3 cm, since smaller tumors have relatively better LC. Patients had no bulky lymph nodes (LN) involvement (average LN diameter of 13.3 ± 5.5mm). All patients were fit for sequential or concomitant CRT (i.e. ECOG-performance status ≤ 2). Patients with prior thoracic radiation or poor lung function (FEV_1 or DLCO <30% of predicted age-adjusted normal values) were not eligible. Patients were recruited from 2 different hospitals. The Local Ethical Committees approved the study and all patients gave their informed consent.

2. Image acquisition

Before irradiation (average 14.9 days), all patients underwent a contrast-enhanced computed tomography (CE-CT) in free breathing, a four-dimensional (4D)-CT and a 4D-FDG-PET on an EANM-accredited PET/CT camera (Gemini TF, Philips Medical System, Cleveland, OH, USA). Patients were immobilized with a customized thermoplastic mask (CIVCO Medical Solutions, Iowa, USA) in supine treatment position.

The CE-CT acquisition started 35 s after intravenous injection of 70 ml of iodinated contrast at a rate of 2.0 ml/s (Iohexol, Omnipaque 350, GE Healthcare, Diegem, BE). The acquisition typically covered the thoracic region from the supraclavicular fossa to the upper abdomen. CT images were reconstructed in 2 mm slice thickness, and transferred to the treatment planning system (Elekta Computerized Medical Systems Software – Focal v4.40).

The 4D-CT had the same parameters as the CE-CT, except for the lower pitch (0.08). Patients were audio-coached to regularize breathing [108]. The 4D-CT scans were binned retrospectively into 10 equally distributed temporal phases, for motion management purposes.

The 4D-FDG-PET images were acquired 60 to 120 min after injection of an average activity of 8.04 mCi of FDG in patients fasting for 6h and with normal glycaemia (<140 mg/dl). The scans were binned in 5 equally distributed temporal phases to create the 4D PET sequences. The acquisition duration was 15 min per bed position, to compensate for 4D gating and keep sufficient statistics. After correction for decay, random, scatter, and attenuation, images were reconstructed by iterative 3D LOR-OSEM, with a transverse field of view of 180 mm (one bed position) centered on the region of interest. Attenuation correction involved the averaged 4D-CT. The image matrix was 288 x 288 x 90 isotropic voxels (2 x 2 x 2 mm^3).

3. Definition of organs at risk and target volumes

3.1. CT images processing

The OARs, i.e. lungs, esophagus, spinal cord, bronchus, trachea, large vessels, heart and brachial plexus were manually delineated on the CE-CT. A 5 mm margin around serial organs was added to obtain the corresponding planning organ at risk volume (PRV).

The GTV on CT images included the primary tumor ($GTV_{T\text{-}CT}$) and the pathologic lymph nodes ($GTV_{N\text{-}CT}$), i.e. PET positive and/or histologically proven. $GTV_{T\text{-}CT}$ and $GTV_{N\text{-}CT}$ were manually delineated on the CE-CT using a mediastinal window (width, 600 HU; center, 40 HU), as shown in a previous study [159].

A 5 mm margin defined the clinical target volumes ($CTV_{T\text{-}CT}$ and $CTV_{N\text{-}CT}$) around both GTVs, to account for potential microscopic extensions. The CTVs were manually corrected for anatomical barriers, i.e. large vessels, bone, pleura and esophagus when organs were not clinically invaded on the available CT and PET-CT images.

Internal tumor motion due to breathing was estimated in the 4D-CT scan and an ITV was automatically generated [163].

The planning target volumes ($PTV_{T\text{-}CT}$ and $PTV_{N\text{-}CT}$) resulted from isotropic 5 mm expansions of both ITVs.

3.2. PET images processing

The metabolically active region within the primary tumor (GTV_{PET}) was automatically and accurately segmented on each temporal phase of the 4D-FDG-PET, using a validated gradient-based method [95, 159]. The union of these 5 $GTVs_{PET}$ defined the ITV_{PET}. No CTV margin was used. Finally, the PTV_{PET} was obtained by adding a 5 mm isotropic expansion to the ITV_{PET}.

All contours drawn on PET were transferred to the CE-CT images for planning.

4. Treatment planning

A total dose of 62.5 Gy was prescribed to $PTV_{T\text{-}CT}$ and $PTV_{N\text{-}CT}$ and delivered in 25 once-daily fractions of 2.5 Gy. The dose per fraction was then individually increased to the PTV_{PET} (maximum dose of 4.8 Gy per fraction), until a predefined dose constraint was reached for any organ [15, 16, 20, 22, 24, 29, 34, 153, 164-166]. This was performed using a simultaneous integrated boost (SIB) with either helical IMRT or an intensity-modulated arc therapy (IMAT) technique (11 and 2 patients, respectively). Treatment was delivered in an accelerated scheme of 5 weeks to minimize the effect of accelerated repopulation.

Treatment plans were made on either TomoTherapy V. 4.2.1 or Eclipse AAA v.10.0.28 Treatment Planning System (TPS). All TomoTherapy plans used a 2.5 cm field width, a pitch of 0.287 and a planned modulation factor of 2.0. RapidArc plans relied on MLC 120 HD and a calculation grid size of 0.25.

Treatment plan quality evaluation involved constraints to TVs and OARs. Acceptability criteria for TVs were: D_{50} equal to prescription for PTV_{CT} and PTV_{PET}, D_{95} above 95% of prescription, D_{99} above 90% of prescription and D_2 below 105% of prescription for the PTV_{PET}.

The physical dose constraints for the OARs [15, 16, 20, 22, 24, 29, 34, 153, 164-167], were normalized for the prescribed dose (i.e. 62.5 Gy given in 25 fractions) and equivalent doses in 2 Gy per fraction (EQD2) using the appropriate α/β ratios (i.e. $\alpha/\beta = 2$ for spinal cord and brachial plexus, and $\alpha/\beta = 3$ for lungs, esophagus, large vessels, bronchus, and heart) were calculated with the linear quadratic (LQ) model. Table 4.1 summarizes all OARs constraints.

Table 4.1 *Dose constraints for organs at risk.*

Organs at risk	α/β	Constraints		EQD2
Lungs – GTV	3	MLD	FEV_1/DLCO > 60%	< 19 Gy
			FEV_1/DLCO 40-60%	< 15 Gy
			FEV_1/DLCO < 40%	< 10 Gy
		$V_{20\ Gy}$		< 30%
		$V_{13\ Gy}$		< 40%
		$V_{10\ Gy}$		< 45%
		$V_{5\ Gy}$ total		< 65%
		$V_{5\ Gy}$ contralat		< 60%
Esophagus	3	$V_{40\ Gy}$		< 50%
		$V_{50\ Gy}$		< 30%
		$V_{70\ Gy}$		< 20%
		D_{mean}		< 34 Gy
Spinal cord	2	D_2		< 50 Gy
Brachial plexus	2	D_2		< 60 Gy
Large vessels	3	D_2		< 94 Gy
Bronchi	3	D_2		< 94 Gy
Whole heart	3	D_{mean}		< 46 Gy
		$V_{40\ Gy}$		< 50%

Abbreviations: MLD, mean lung dose; FEV1, forced expiratory volume in 1 second; DLCO: diffusing capacity for carbon monoxide; Dx, dose received by x percent of the organ at risk volume; VxGy, volume of the OAR receiving x Gy; EQD2, equivalent dose in 2 Gy fraction.

5. Treatment delivery and follow-up (FU)

RT started at day 22 (first day of cycle 2) of cisplatin/etoposide or cisplatin/vinorelbine chemotherapy regimen for concomitant scheme, and after 6 cycles of gemcitabine and cisplatin induction chemotherapy for sequential scheme (1 patient).

On-line verification was performed prior daily treatment using mega-voltage CT (MV-CT) or cone-beam CT (CB-CT) for set-up correction.

Each patient was seen before treatment (baseline consultation), weekly during RT, 2 weeks, 1 month, 2 months after RT, then every 6 months until 2 years. Consultations consisted of history, physical examination, and evaluation of potential toxicities.

6. Toxicities

Acute (i.e. less than 90 days after the start of RT) and late (i.e. more than 90 days after the start of RT) chemo-radiation induced toxicities were scored at each consultation according to common terminology criteria for adverse events (CTCAE) v.4.0.

7. Tumor response assessment

Tumor response was assessed with FDG-PET/CT at 2, 6, 12, and 24 months after RT. Measurements were blinded and performed by different experienced operators, depending on the image modality.

Local failure was defined as a recurrence in the primary tumor. Regional failure was defined as a mediastinal LN recurrence occurring either in field (i.e. initially involved nodes) or out of field. Distant failure was considered for recurrence in any distant LN or organs. All recurrences were stated based on the FDG-PET imaging and no proven histology was required.

Metabolic tumor response or recurrence was assessed using PET Response Criteria in Solid Tumors (PERCIST) [62, 168], which recommends using SUL_{peak}.

Moreover, tumor response was also assessed anatomically according to Response Evaluation Criteria in Solid Tumors (RECIST) [169] and metabolically with the classical maximum standardized uptake value (SUV_{max}) [61].

8. Statistical analysis

The various descriptive data (target volumes and doses) were presented with their mean and standard deviation.

Progression-free survival (PFS) and overall survival (OS) medians and 95% confidence interval (CI) were estimated using the Kaplan-Meier method.

PFS was defined as the time from the date of first RT to the earliest to the date of the event documented based on the PERCIST results. Patients with no recurrence (local, regional, or distant as appropriate) or alive at the time of analysis were censored at the date of last tumor assessment.

OS was defined as the time from the date of first RT until date of death. For patients alive at the date of analysis, time to death was censored at the time of last FU.

All statistics were computed with SAS 9.3 (Statistical Analysis System, NC, USA).

Results

1. Patient and tumor characteristics

Table 4.2 summarizes characteristics of patients and primary tumors. Mean age was 63.3 ± 8.9 years. Six patients had central tumors whereas 7 had peripheral tumors. Seven patients had adenocarcinoma while 6 had squamous cell carcinomas. Mean primary tumor diameter at baseline was 49.3 ± 15.0 mm. Mean PTV of the primary tumor at baseline was 262.4 ± 205.1 ml on CT and 108.6 ± 94.9 ml on PET. Mean SUL_{peak} of the primary tumor at baseline was 7.35 ± 2.70. Evolution of SUL_{peak}, SUV_{max} and longest diameter of the primary tumor are shown in Table 1 and Figure 1 of the appendix B.

Table 4.2 *Patient and primary tumor characteristics.*

Pat No	histology	cTNM	location	Age (years)	GTV_{CT} (ml)	GTV_{PET} (ml)	PTV_{CT} (ml)	PTV_{PET} (ml)	SUL_{peak} baseline	Dose (Gy)	Dose/# (Gy)
1	SCC	T3N3M0	RU – central	59	61.6	14.6	490.9	64.1	9.77	75	3.0
2	SCC	T4N2M0	LU – central	68	181.0	78.9	655.2	215.2	11.08	70	2.8
3	SCC	T4N2M0	RM – central	45	65.7	21.3	390.0	100.5	3.92	75	3.0
4	SCC	T3N2M0	LU – central	58	89.3	53.1	372.5	200.4	8.40	75	3.0
5	SCC	T3N2M0	RU – central	75	36.4	16.9	262.6	69.5	5.47	75	3.0
6	ADC	T4N2M0	LL – periph	69	174.1	80.6	587.8	300.2	9.62	65	2.6
7	ADC	T3N2M0	RU – periph	56	63.4	31.7	241.7	114.1	4.28	77.5	3.1
8	ADC	T3N2M0	RU – periph	59	277.2	193.3	661.2	342.4	7.35	65	2.6
9	ADC	T2aN2M0	RU – periph	69	8.1	4.4	84.3	42.8	5.07	120	4.8
10	ADC	T2bN1M0	RL – periph	72	34.0	23.4	185.1	78.4	10.14	75	3.0
11	SCC	T1bN2M0	RU – periph	66	7.3	5.65	62.3	25.6	9.87	100	4.0
12	ADC	T2N3M0	RU – periph	74	6.7	6.20	111.0	51.7	3.19	110	4.4
13	ADC	T3N3M0	RU – central	54	65.1	20.7	342.7	110.9	7.40	80	3.2

Abbreviation: Patient No, Patient number; SCC, squamous cell carcinoma; ADC, adenocarcinoma; RU, right upper; LU, left upper; LL, left lower; RL, right lower; RM, right middle; central, centrally located, based on RTOG criteria; periph, peripherally located, based on RTOG criteria; GTV_{CT}*, gross tumor volume on CT images;* GTV_{PET}*, Gross Tumor Volume on PET images;* PTV_{CT}*, Planning Target Volume on CT images;* PTV_{PET}*, Planning Target Volume on PET images;* SUL_{peak}*, lean body mass normalized SUV; Dose: prescribed dose to the PET positive area within the tumor.*

2. Dose escalation level

The mean prescribed dose to the PTV_{PET} reached 82.1 ± 17.9 Gy for all patients, with values of 89.2 ± 24.0 Gy, and 75.0 ± 3.2 Gy for peripheral and central tumors, respectively. The corresponding EQD2 with a α/β ratio equal to 10 (i.e. for tumor) were 90.8 Gy, 100.8 Gy, and 81.3 Gy, respectively. The main limiting organ was the lung (8 patients, 62%) although brachial plexus was also limiting for apex-located tumors (2 patients, 15.4%). Figure 4.1 shows two dose distribution profiles for a central and a peripheral tumor.

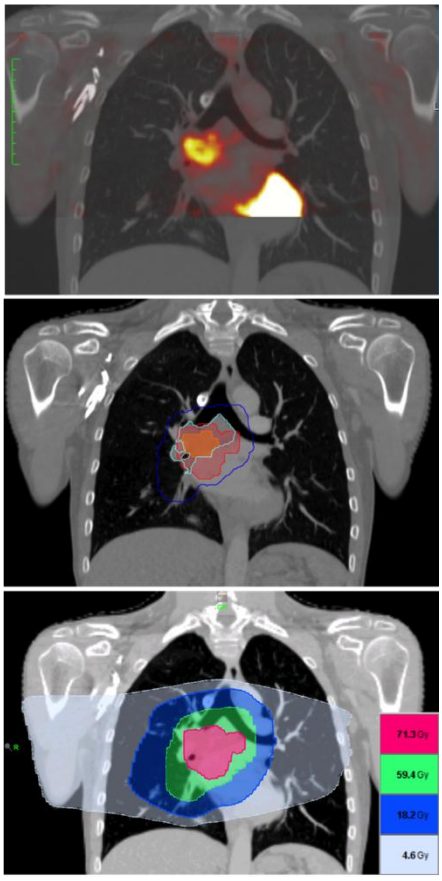

Figure 4.1a *Coronal plane of planning FDG-PET/CT in patient 3 presenting a squamous cell carcinoma of the right middle lung classified as cT4N2M0.*
Gross and planning target volumes are represented with GTV_{PET} in orange, PTV_{PET} in red, GTV_{CT} in light blue and PTV_{CT} in dark blue.
This centrally located tumor received a boost dose of 75 Gy on the metabolically active area (PTV_{PET}) while the remaining tumor received 62.5 Gy (PTV_{CT}). The isodose lines are represented with in red, the 71.3 Gy isodose (95% of 75 Gy), in green, the 59.4 Gy isodose (95% of 62.5 Gy), in blue, the 18.2 Gy isodose (corresponding to 20 Gy EQD2) and finally, in white, the 4.6 Gy isodose (corresponding to 5 Gy EQD2).

Figure 4.1b *Coronal plane of planning PET/CT in patient 11 presenting a squamous cell carcinoma of the upper right lung classified as cT1bN2M0.*
Gross and planning target volumes are represented with GTV_{PET} in orange, PTV_{PET} in red, $GTV_{T\text{-}CT}$ in light blue, $PTV_{T\text{-}CT}$ in dark blue, $GTV_{N\text{-}CT}$ in light green and $PTV_{N\text{-}CT}$ in dark green.
This peripherally located tumor received a boost dose of 100 Gy on the metabolically active area while the remaining tumor received 62.5 Gy. The isodose lines are represented with in red, the 95.0 Gy isodose (95% of 100 Gy), in green, the 59.4 Gy isodose (95% of 62.5 Gy), in blue, the 18.2 Gy isodose (corresponding to 20 Gy EQD2) and finally, in white, the 4.6 Gy isodose (corresponding to 5 Gy EQD2).

3. Toxicities

Acute and late toxicity rates are reported in Table 4.3.

All patients experienced acute grade 1 and 2 fatigue, cough, esophagitis and hematological toxicities while 9 patients (69.2%) presented grade 1 and 2 weight loss. Acute grade 3 toxicities included esophagitis (23.1%), dyspnea (23.1%), fatigue (30.8%), dermatitis (15.4%), anorexia (15.4%), and nausea (7.7%). No grade 4 acute non-hematological toxicity was reported. In all patients but one (patient 3), radio-induced symptoms had resolved within 2 months after treatment (6 months for respiratory symptoms).

Concerning late toxicities, 5 patients presented grade 1 pulmonary fibrosis (38.5%), 4 patients developed grade 2 pneumonitis (30.8%) but no late pulmonary toxicities of grade ≥ 3 occurred. One patient (7.7%) with a central tumor (patient 3) experienced grade 3 esophageal stenosis associated with a grade 4 dysphagia, a grade 4 pericarditis, as well as a bronchial fistula and a fatal grade 5 hemoptysis. An additional patient (P4) died from a grade 5 hemoptysis.

Two patients required unplanned hospitalization during or after the chemo-radiation treatment. Patient 3 (P3) was first hospitalized for a febrile neutropenia in the second week of radiation treatment. At the end of CRT, he was readmitted for hydration and parenteral alimentation in the context of a grade 3 acute esophagitis and dysphagia associated with tube feeding intolerance. Two weeks after the end of CRT, this patient presented with an aphagia due to an extrinsic compression of the esophagus by necrosis of mediastinal lymph nodes. A stent was placed. Five months later, he was admitted in intensive care unit for a pericarditis associated with a pericardial tamponade and hemoptysis treated by pericardial drainage and embolization, respectively. He died finally from a massive hemoptysis 8 months after the end of CRT. An additional patient (P11) was admitted for a febrile neutropenia in the last week of CRT.

Table 4.3 *Number of patients experiencing acute and late toxicities.*

	Maximum toxicity grade*	1	2	3	4	5
Acute	Fatigue	13	9	4	0	0
	Weight loss	9	4	0	0	0
	Anorexia	6	1	2	0	0
	Esophagitis/dysphagia	12	7	3	0	0
	Nausea	8	1	1	0	0
	Cough	11	3	0	0	0
	Dyspnea	12	6	3	0	0
	Pneumonitis	2	4	0	0	0
	Retrosternal thoracic pain§	9	4	3	0	0
	Hemoptysis	2	0	0	0	0
	Dermatitis	8	5	2	0	0
	Febrile neutropenia	0	0	2	0	0
	Anemia	12	8	0	0	0
	Leucocytopenia	7	8	1	2	0
	Lymphopenia	6	10	11	5	0
	Neutropenia	5	4	2	3	0
	Thrombopenia	7	2	1	1	0
Late	Esophageal stenosis ‡	0	0	1	0	0
	Dysphagia ‡	0	0	0	1	0
	Bronchial fistula ‡	0	0	1	0	0
	Pericarditis ‡	0	0	0	1	0
	Hemoptysis ‡	0	0	0	0	2
	Pulmonary fibrosis	5	0	0	0	0

** defined according to CTCAE v.4.0.*

§ due to esophagitis.

‡ P3 developed several late complications including dysphagia, esophageal stenosis, bronchial fistula, perdicarditis and a fatal hemoptysis.

4. Recurrence analysis

Median FU for living patients was 29.28 months (95%CI: 21.25-40.56). At the end of FU, 7 patients were still alive (53.8%) while 6 patients died (46.2%). Four distant progressions and 2 grade 5 toxicities (hemoptysis) led to 6 deaths.

Table 4.4 report patterns of relapse, whereas the appendix B provides all survival tables and figures as well as overall, local, regional and at distance PFS.

Local progression occurred in 2 patients (15.4%) at 6 and 12 months, respectively. In both cases, local recurrences were not isolated and happened simultaneously (1 patient) or after regional and distant recurrence (1 patient).

Regional recurrence occurred in 6 patients (46.2%). Four patients (30.8%) developed out-of-field regional recurrence while 1 patient (7.7%) had simultaneously an in-field and out-of-field regional recurrence and the last one (7.7%) experienced in-field recurrence. All but one were associated with either local (1 patient) or distant (4 patients) recurrence.

Distant recurrence occurred in 6 patients (46.2%), as cerebral, liver, distant LN or lung metastases.

Table 4.4 *Patterns of relapse.*

Recurrence	Number of patients (%)
No	6 (46)
Yes	7 (54)
Local tumor failure	2 (15)
Isolated	0 (0)
Non-isolated	2 (15)
Regional nodal failure	6 (46)
Isolated	1 (8)
Non-isolated	5 (38)
Distant failure	6 (46)
Isolated	3 (23)
Non-isolated	3 (23)

Discussion

Our study demonstrated the feasibility of individualized dose escalation based on FDG-PET in LA NSCLC patients. The boost on FDG-avid regions reached 82 Gy on average for all patients, with values of 89 Gy and 75 Gy for peripheral and central tumors, respectively. We showed with a minimum 2-year FU no isolated local recurrence in our cohort. Acute toxicities were mild and no late toxicity was recorded except two grade 5 toxicity for centrally located tumors. We also demonstrated that distant recurrence remains a critical issue.

All methodological aspects of the dose escalation trial were carefully programmed. Firstly, dose was escalated non-uniformly within the tumor, allowing for higher dose prescription, while keeping toxicities as low as possible (see Figure 4.1). Secondly, all patients but one received concurrent CRT in an accelerated way without treatment interruption and with perfect FU compliance. Thirdly, each treatment was planned and optimized meticulously with respect to OARs constraints in a step-by-step dose escalation fashion. Fourthly, treatments were delivered in helical IMRT or IMAT to obtain sharp dose distributions, and using SIB to keep identical OTT. Finally, 4D imaging was acquired in strict conditions for each patient and TVs were delineated accurately with methods validated on NSCLC patients [154, 159, 170].

In our cohort, P1 and P6 had non-isolated local recurrence at 6 and 12 months, respectively. Both patients had large (T3-T4) and poorly differentiated primary tumors with high FDG uptake at diagnosis, as well as poor response to the first course of chemotherapy. P1 received a boost on metabolically active areas of 75 Gy and P6, a dose of 65 Gy, which corresponded to low dose escalation levels limited by lung constraints.

Our local tumor control results compared favorably to those from conventional CRT, even though most multicenter randomized trials do not study tumor LC as a primary endpoint. In a radiation dose escalation studying LC, Kong et al. demonstrated that progression was initially observed at local site alone in 37% and at distant sites only in 46% [153].

Regarding regional recurrence, several studies have demonstrated that involved nodes irradiation (i.e. omitting elective nodal irradiation) is safe with less than 5% of isolated nodal failure [171-175]. De Ruysscher *et al.* showed that selective mediastinal node irradiation based on FDG-PET resulted in low isolated nodal failure rates, with only 1 patient (2%) developing isolated out-of-field regional recurrence and 2 patients (4.5%) presenting a non-isolated out-of-field regional recurrence [170]. However, the incidence of out-of-field regional failures was higher in our series

(38.5%), and mainly in the sub-clavicular area (3 out of 5 patients). Despite the potential role of incidental irradiation of uninvolded mediastinal areas close to the PTV, the sub-clavicular area does not beneficiate from this effect for these three patients. For the other patients, the LN recurrences were located far away from the RT field and these areas did not beneficiate from any incidental irradiation.

As in most trials, the main pattern of recurrence remains distant metastases, which raises the issue of systemic treatments. In that regard, systemic targeted therapies appear as a promising strategy and combination with RT could favorably affect the patient's outcome [176, 177], as shown in head and neck cancer.

Acute and late toxicity rates were comparable to conventional schemes except for two patients who died from a grade 5 hemoptysis. The first patient (P3) had a central tumor, classified cT4N2M0 by invasion of the esophagus and bronchial tree, and encasement of the pulmonary artery (grade 3 pulmonary artery involvement according to [178]). The prescription to the PTV_{PET} was 75 Gy (i.e. 90 Gy EQD2 with α/β ratio of 3 for OARs). The patient experienced at third week of RT a grade 3 esophagitis requiring a feeding tube and morphinic drugs. Five months after the end of CRT, the patient developed bronchial and esophageal fistulas complicated by mediastinitis and pericarditis. We retrospectively checked all constraints to the esophagus, bronchial tree, and great vessels, which did not exceed recommended values but with a recording of esophagus maximal dose of 76.72 Gy (corresponding to 92.1 Gy EQD2 with α/β ratio of 3). No local recurrence was observed in spite of multiple bronchial/esophageal biopsies and pericardial effusion analysis. We hypothesized that radio-necrosis and rapid shrinkage of the tumor post CRT took away the bronchus and esophagus walls, causing lethal hemorrhage few weeks later. After this adverse event, we modified inclusion criteria to exclude tumors classified as T4 by invasion of mediastinal organs [179, 180]. Therapeutic options for these patients are very limited, and most die eventually from local complications if no curative treatment is given.

Additionally, P4 deceased also from hemoptysis 5 months after CRT. We classified this hemoptysis as a grade 5 toxicity although the event appears rather early after the CRT. This centrally located tumor was classified as cT3 versus cT4N2M0 by suspicious esophagus invasion. At diagnosis, the tumor involved the main left bronchus and the left pulmonary artery involvement was scored as grade 3 (encasement) according to [178]. The prescription to the PTV_{PET} was 75 Gy. Again, all constraints complied with OARs recommendations for esophagus and mediastinum organs. Actually, it is very difficult to make the difference between an adverse event and a local progression. In this regard, the primary tumor showed a net reduced metabolism on FDG-PET

imaging performed 2 months after CRT and it was considered as a stable disease according to RECIST at 4 months on an unplanned CT scan. Incidence of massive hemoptysis is relatively high in central tumor treated by conventional external RT (10%), especially, as in P4, when endobronchial tumor extends into the upper left main bronchus (lying next to left pulmonary artery), encases the left pulmonary artery and when hemoptysis already occurs prior to radiotherapy [38].

Regarding these two patients died from hemoptysis, it is possible that constraints on large vessels, bronchial tree and esophagus should be revised for centrally located tumors encasing or involving some mediastinum organs.

The main limitation is the limited number of patients included in our trial, which was designed as a feasibility study. The main center recruited fewer stage III NSCLC patients than expected, particularly after excluding central T4 tumor with invasion of mediastinum organs. Consequently, another center joined the trial later on to increase the number of patients, but recruitment remained low.

A second limitation of our trial is that we used the conventional ITV approach, according to a planning study demonstrating its safety for TomoTherapy [163]. However, ITV overestimates safety margins, leading to unnecessary irradiation of healthy tissues. In the context of dose escalation especially, the mid-position approach can significantly reduce the PTV and irradiated volumes. Mid-position was proven to be feasible and safe in helical delivery for LA stage NSCLC patients [181], but was not yet available in our center at the time of the trial.

Finally, although the small cohort demonstrates the feasibility concept, we cannot formally generalize our results due to the limited number of recorded events. Randomized studies with more patients, comparing conventional treatment with escalated dose radiation therapy, are still needed, especially after the counterintuitive results of RTOG 0617 [35]. Final results of the randomized PET boost trial are awaited to determine the toxicity of dose escalation and report on tumor control and survival of dose intensification strategy [166]. Especially, they are studying the theoretical concept developed by Niemerko et al. [182, 183] whereby tumor LC depends more on the mean radiation dose to the tumor than on the maximal dose, provided the minimal dose reaches a critical threshold. Patients are randomized accordingly, between a selective (i.e. based on FDG-PET) and a non-selective (i.e. heterogeneous but higher mean dose) dose re-distribution within the tumor [166].

Conclusions

These results suggest that a non-uniform and individualized dose escalation based on FDG-PET in IMRT delivery is feasible. The dose can be further increased for peripheral tumors, compared to central ones. Although acute and late toxicities were comparable to conventional scheme in peripheral tumors, two patients (15%) with centrally located tumors died from fatal hemorrhage. Centrally located tumors with direct invasion of mediastinal organs must thus be treated cautiously to avoid late toxicities.

Chapter 5

Validation of the mid-position concept

Validation of the mid-position strategy for lung tumors in helical TomoTherapy

Marie Wanet, Edmond Sterpin, Guillaume Janssens, Antoine Delor, John Aldo Lee, Xavier Geets

---

Radiotherapy and Oncology 2014; 110 (3): 529-537

Contents

Introduction

Helical TomoTherapy is an appealing irradiation modality to treat unresectable locally advanced stage II-III as well as inoperable stage I non-small cell lung cancer (NSCLC) patients. Indeed, it combines an advanced technique of intensity-modulated radiation therapy (IMRT), leading to highly conformal dose distributions, with an accurate imaging device for patient positioning, based on megavoltage computed tomography (MVCT). These features allow target volumes to be irradiated with sharp dose gradient, and thus help deliver high dose while sparing healthy surrounding tissues.

However, tumor motion caused by breathing may jeopardize treatment quality. In that regard, on-line management of respiratory tumor motion requires dedicated methodologies and techniques, like breath hold, gating [184], or tracking [185], which are not yet available in TomoTherapy systems [163]. Thus, treatment plan robustness against breathing motion still relies on the definition of specific volumes, like an internal target volume (ITV) or the mid-position (MidP), which are expanded with safety margins.

The ITV approach is widely used in clinical practice [44, 116, 186]. The ITV encompasses all tumor positions during the breathing cycle and can be determined from a four-dimensional computed tomography (4D-CT). A planning study with four-dimensional (4D) Monte Carlo (MC) has demonstrated that an expanded ITV can be safely applied in TomoTherapy [163]. In particular, interplay effect between beam and tumor motions did not significantly affect the delivered dose distributions. However, the ITV approach is known to overestimate the safety margins, and thus may lead to unnecessary irradiation of healthy tissues [113, 187].

The MidP, on the other hand, involves a volume that corresponds to the time-weighted mean position of target volumes during the breathing cycle [113]. This approach provides several theoretical advantages over the ITV and partly overcome the issues encountered with the ITV. First, by using a 4D-CT, it eliminates the systematic error that would otherwise occur with a fast 3D CT that is merely a snapshot at some point of the respiratory cycle, possibly polluted by artifacts. In contrast with the ITV approach, the random uncertainty about tumor motion is added in quadrature to the other random geometric uncertainties in the formula for the Planning Target Volume (PTV) margin calculation proposed by Van Herk et al. [42]. As a result, this approach allows the margins to be significantly smaller and therefore comparable to those obtained with gated radiotherapy [113]. Furthermore, the MidP approach allows the treatment planning and delivery workflow to remain the same as in other approaches based on margins.

To our best knowledge, MidP has never been implemented for helical TomoTherapy of moving lung tumors, nor compared to ITV for this treatment modality. In this context, we designed the present study to assess the potential gain of MidP over ITV in terms of margin and PTV reduction. As a second objective, we investigated whether these volumetric changes in the PTV actually lowered the irradiation of the organs at risk using clinically relevant dosimetric parameters. Finally, we also computed motion-corrected dose distributions for both scenarios using a previously validated 4D Monte Carlo (MC) model based on TomoPen [163]. The latter was used to assess the plan quality, especially the potential impact of intra-fraction motion and treatment delivery mechanics on tumor coverage when margins were reduced.

Materials and methods

Figure 5.1 illustrates the complete workflow from image acquisitions to treatment planning.

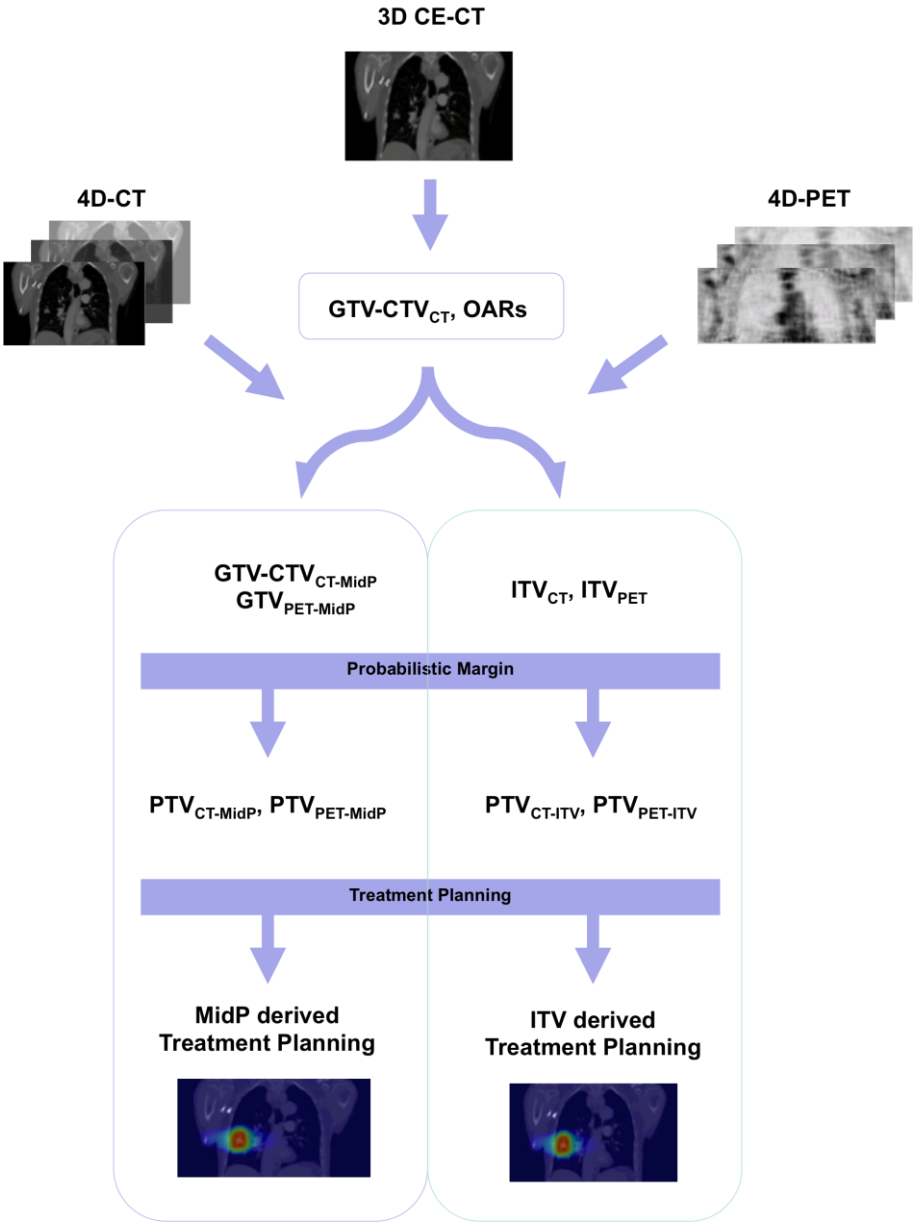

Figure 5.1 *Workflow depicting the definition of target volumes and organs at risk for ITV and mid-position strategies from the image acquisition to the treatment planning.*

1. Patient selection

Fifteen NSCLC patients were retrospectively included in the present study. Among these, 8 patients had stage I NSCLC treated with stereotactic body radiation therapy (SBRT), while the remaining 7 patients had locally-advanced stage II-III NSCLC treated with simultaneous integrated boost (SIB) IMRT in the framework of a dose escalation protocol. The internal review board approved this study and all patients gave their informed consent.

2. Image acquisition

Prior to treatment, all patients underwent a planning imaging session either on a big bore CT scanner (Aquilion LB, Toshiba medical system corporation, Japan) or a combined PET-CT scanner (Gemini TF, Philips Medical system, Cleveland, OH, USA). For all acquisitions, patients were immobilized in a thermoformed plastic mask (CIVCO Medical Solutions, Iowa, USA).

A contrast-enhanced CT (CE-CT) from the entire thoracic region was acquired in free breathing mode for the purpose of delineation, and reconstructed in 2 mm-thick slices. Next, a 4D-CT was acquired and patients were audio-coached to regularize their breathing and thus reduce 4D-CT image artefacts [120, 188]. In this acquisition mode, the CT scanner automatically set the optimal helical pitch according to the patient's breathing period measured from either a pressure belt (Medspira/Mayo Clinic Breath Hold™, Mayo Clinic Medical Devices, USA) or magnetic sensors (Nomics©, Liège, Belgium). The 4D-CT datasets were retrospectively binned into 10 equally distributed temporal phases, for motion management purposes. Finally, an average CT was computed by averaging all 10 phases.

For the SIB group, 4D-FDG-PET images were also acquired 60 to 120 min after injection of an average activity of 8.04 mCi of FDG in patients fasting at least for 6h before examination. The breathing signal was recorded with the same devices as the 4D-CT. After correction for decay, random, scatter, and attenuation, images were reconstructed with the iterative algorithm 3D LOR-OSEM using a window of only 20% of the breathing period and centered on the end of the expiratory phase. The images had a transverse FOV of 180mm (one bed position centered on the region of interest). The attenuation correction was performed using the averaged 4D-CT.

3. Motion estimation

Internal motion due to breathing was estimated with the 4D-CT images. First, the CE-CT and the end-exhale phase of the 4D-CT were non-rigidly registered using a log-domain diffeomorphic Morphon algorithm (see Appendix C for more details). This

method is based on the matching of the local phase (i.e. lines and edges) at different scales and is therefore insensitive to contrast differences between the CE-CT and the 4D-CT. Next, this registration algorithm was run to map the end-exhale phase of the 4D-CT with the other phases, yielding 9 non-rigid transformations [119]. The latter were used in two different ways: first, to compute the deformation between the reference phase and the mean position of the anatomy along the respiratory cycle, which will further be applied to the CE-CT-based target volumes (TVs) to generate their corresponding MidP volumes and, second, to propagate these contours on all other phases of the respiratory cycle, the union of all deformed TVs forming an individual ITV. The deformed contours were visually checked on all phases, to assess registration accuracy. For the SIB group, the combined PET/CT acquisitions allowed MidP PET images to be computed in a straightforward way, just by applying the non-rigid deformations to the PET component.

4. Definition of Target Volumes and Organs at risk

For both the ITV and MidP, Figure 5.1 illustrates the workflow for the definition of the target volumes (TVs) and organs at risk (OARs). It comprises the following steps:

1) OARs, Gross Tumor Volume (GTV_{CT}) and Clinical Target Volume (CTV_{CT}) of primary tumors and lymph nodes were manually delineated on the CE-CT. As there is no CTV extension for the SBRT group (i.e. CTV_{CT} = GTV_{CT}), the GTV will be noted CTV in the rest of the text, for the sake of clarity [189, 190]. Additionally, for the SIB group, a GTV_{PET}, corresponding to the boost region, was automatically segmented on PET images using a previously validated gradient-based method [95, 159].

2) The corresponding ITV_{CT} and ITV_{PET} were generated using non-rigid registration, like previously described.

3) Then, the internal structures were computed in their mid-position, using the transformation vectors from deformable registrations as described earlier. The resulting TVs were noted $GTV_{CT\text{-}MidP}$, $CTV_{CT\text{-}MidP}$ and $GTV_{PET\text{-}MidP}$.

4) The PTV margins were drawn using the formalism proposed by Van Herk et al.

In the last step, the margin thickness formula combines different types of geometric uncertainties and can be written as

$$M_{PTV} = 2.5\sqrt{(\Sigma_{TM}^2 + \Sigma_{BL}^2 + \Sigma_{SETUP}^2 + \Sigma_D^2)} + 1.64\sqrt{(\sigma_{TM}^2 + \sigma_{BL}^2 + \sigma_{SETUP}^2 + \sigma_p^2)} - 1.64\,\sigma_p$$

where Σ and σ denote the standard deviations of the systematic and random errors, respectively. Subscripts *TM*, *BL*, *SETUP*, *D* and *p* refer to tumor motion, baseline shift,

patient setup variability, delineation uncertainty, and penumbra, respectively. The coefficients in the formula ensure that the CTV receives at least 95% of the prescribed dose for 90% of patients. All standard deviations, except Σ_{TM} and σ_{TM}, were set in agreement with the literature, while also taking into account the specificities of TomoTherapy and the handling of operators in our treatment unit [47, 191, 192]. These values were similar for ITV and MidP. In the particular case of penumbra, its width σ_p for helical TomoTherapy was computed as follows. Dose profiles in transverse and longitudinal directions at 5 cm depth for a 5x5 cm^2 field were obtained with TomoPen MC simulations in a 0.33g/cm^3 density phantom. The computed profile was fitted with the sum of two Gaussians according to Witte et al. [121]. The effect of couch motion on dose distributions can be approximated as a convolution of the beam with a square response with width SW width, SW being the slice width. The standard deviation related to the couch motion equals $\frac{SW}{\sqrt{12}}$. The total standard deviation was computed, leading to σ_p adapted for lung density and TomoTherapy delivery. In the end, σ_p equalled 4.6 mm and 4.3 mm in LR and AP directions. For the SI direction, it corresponded to 4.3 mm and 9 mm for the 1 cm or 2.5 cm slice widths, respectively.

Last but not least, standard deviations related to tumor motion were individually estimated, depending on the considered margin strategy:

- For the ITV, the tumor motion uncertainties are implicitly included in the ITV margin, which encompasses the CTV deformed onto the different respiratory phases of the 4D-CT [193]. Both Σ_{TM} and σ_{TM} were therefore set to 0 [113].

- For the MidP, Σ_{TM} was fixed to 0.5 mm, which corresponds to the residual error of deformable registration [113], whereas σ_{TM} was particularized according to the amplitudes of tumor motion measured in the 4D-CT along each axis [113, 192].

Table 5.1 provides volumetric information for the GTVs and CTVs, their motion along each axis, as well as the PTV margins for both ITV and MidP approaches. It is noteworthy that primary tumor and lymph nodes move differently but, for the sake of clarity, Table 5.1 does not report this information.

Table 5.1 *GTV and CTV with their corresponding motion amplitudes and PTV margins for both ITV and MidP approaches. Patients 1-8 correspond to the SBRT group (i.e. GTV=CTV) and patients 9-15 correspond to the SIB treatment group.*

Pat. no	CTV $_{T\text{-}CT}$ (cc)	CTV $_{N\text{-}CT}$ (cc)	GTV $_{PET}$ (cc)	LR motion (mm)	AP motion (mm)	SI motion (mm)	PTV_{MidP} LR margins (mm)	PTV_{MidP} AP margins (mm)	PTV_{MidP} SI margins (mm)	PTV_{ITV} LR margins (mm)	PTV_{ITV} AP margins (mm)	PTV_{ITV} SI margins (mm)
1	2.8	-	-	1.7	7.5	8.0	5.7	10.2	10.0	5.5	8.7	8.5
2	4.8	-	-	5.3	8.1	8.5	6.3	10.0	9.9	5.5	8.7	8.5
3	12.2	-	-	0.8	0.6	2.0	5.7	8.8	8.7	5.5	8.7	8.5
4	2.5	-	-	3.2	3.3	10.8	6.2	9.5	9.6	5.5	8.7	8.5
5	10.5	-	-	5.2	11.8	30.0	6.3	11.0	20.9	5.5	8.7	8.5
6	5.2	-	-	2.1	7.5	10.3	5.8	9.8	10.9	5.5	8.7	8.5
7	10.9	-	-	1.4	2.4	7.5	5.7	8.9	9.1	5.5	8.7	8.5
8	3.5	-	-	2.2	3.8	24.6	5.8	9.1	18.3	5.5	8.7	8.5
9	183.8	-	88.7	1.3	1.5	2.1	5.7	8.8	8.4	5.5	8.7	8.2
10	122.1	66.8	61.0	0.4	2.3	2.0	5.7	8.9	8.4	5.5	8.7	8.2
11	29.3	34.1	8.9	1.0	3.7	4.2	5.7	9.1	8.6	5.5	8.7	8.2
12	212.0	38.4	57.3	0.3	1.7	0.7	5.7	8.8	8.3	5.5	8.7	8.2
13	319.9	24.5	187.5	0.4	1.3	5.9	5.5	8.7	8.7	5.5	8.7	8.2
14	99.0	29.5	39.6	1.2	2.4	5.4	5.7	8.9	8.7	5.5	8.7	8.2
15	137.6	-	63.6	1.0	4.3	12.0	5.7	9.2	10.1	5.5	8.7	8.2

Abbreviations: $CTV_{T\text{-}CT}$ and $CTV_{N\text{-}CT}$, Clinical Target Volume of the primary tumor and the lymph nodes on CT images, respectively; GTV_{PET}, Gross Tumor Volume of the primary tumor on PET images; LR, left-right; AP, anterior-posterior; SI, superior-inferior; PTV_{MidP} and PTV_{ITV} margin, Planning Target Volume margins derived from the mid-position and the Internal Target Volume approaches, respectively.

5. Treatment planning

For each patient, two treatments were planned, either with an ITV or a MidP.

For the SBRT group, a dose of 54Gy in 3 fractions to the PTV was prescribed, except for two patients who received 60Gy and 48Gy in 4 fractions due to the proximity between their tumor and critical mediastinal structures. For the SIB group, a dose of 62.5Gy was prescribed to the PTV of the primary tumor defined on CT images ($PTV_{T\text{-}CT}$) and the PTV of the lymph nodes defined on CT images ($PTV_{N\text{-}CT}$), and delivered in 25 fractions of 2.5Gy. Simultaneously, a higher dose was individually prescribed to the PTV_{PET} based on the maximal tolerance of each organ at risk [13]. These doses were prescribed to 95% and 50% of the PTV for SBRT and SIB treatment groups respectively, according to RTOG 0236 and 0618 trials and ICRU83 recommendations [18, 189, 194-196].

Treatment plans were performed on a research version of the TomoTherapy Treatment Planning System (TPS). Its new dose engine, performing computations on a general-purpose graphical processing unit, showed excellent agreement with former versions running on conventional central processors, and was previously validated for heterogeneous media on phantoms and patient cases [197, 198]. For SBRT patients, treatment plans were generated using a fine dose grid, a 1 cm field width, a pitch ranging from 0.172 to 0.215, and a planned modulation factor (ranging from 1.2 to 1.5) adapted in order to obtain a gantry period below 60 sec (required by the TPS) and a treatment time short enough to keep the patient setup variability as low as possible. For SIB treatment patients, all plans were generated using a 2.5 cm field width, a pitch of 0.287 and a planned modulation factor of 2.0.

Treatment planning was performed on the average CT. Although the CE-CT acquired in free breathing offers the optimal contrast for delineation purpose, it only represents a snapshot of the patient's anatomy at a given time point, and may suffer from motion-related artefacts. On the contrary, the average CT represents a voxel-wise average of the ten 4D-CT phases and therefore adequately renders the mean geometry and density of the patient [199-201].

The evaluation of treatment plan quality relied on constraints to TVs and OARs. In the SBRT group, constraints on the PTV were set as follows in an overlapping mode: D_{95} equals the prescription dose; D_{99} above 90% of the prescribed dose; D_2 within a range of 110-140% of the prescribed dose according to RTOG recommendations [196, 202, 203]. Constraints to the OARs were also set according to these trials [196, 202, 203]. In the SIB group, the acceptability criteria for TVs, in an overlapping mode, were: D_{50} equals prescribed dose for both the PTV_{CT} and PTV_{PET}, a D_{95} above 95% of the prescribed dose, a D_{99} above 90% of the prescribed dose and a D_2 below 105% of the prescribed dose for the PTV_{PET}. The physical dose constraints for the OARs, taken from the literature [15, 20, 22, 24, 29, 34, 153, 164-167], were normalized for the prescribed dose (i.e. 62.5Gy given in 25 fractions) and equivalent doses in 2Gy per fraction (EQD2) using the appropriate α / β values were calculated with the LQ-model for each parameter.

6. MC simulations with TomoPen

In the case of dynamic IMRT delivery, patient and beam motions may interfere, potentially resulting in a distortion of the dose distributions, i.e. the so-called interplay effect [204]. Dose distributions were computed using a previously validated 4D MC model based on TomoPen, in order to assess the impact of intra-fraction tumor

motion on tumor coverage, with and without the interplay effect [205-208]. TomoPen was used to:

1) Recompute the 3D dose distributions, comparable to the planned dose generated with TomoTherapy's TPS and denoted 3D MC planned doses hereafter.
2) Compute 4D dose distributions for every 4D-CT data set, with or without beamlet-phase correlation, that is, with interplay simulation (4D MC IS) or no interplay (4D MC NI) [163, 209].

The 4D MC model was previously described in [163]. The simulated dose maps with and without interplay were compared with MC dose distributions computed on the average CT used for planning.

It is noteworthy that the 4D MC doses include the effect of motion, in contrast to the 3D MC planned dose. As a consequence, 4D MC doses must be assessed with smaller volumes whose margins account for all uncertainties but tumor motion. In other words, GTVs and CTVs are expanded differently, isotropically and with $\Sigma_{TM} = 0$ and $\sigma_{TM} = 0$, into volumes called GTV_{PET}^{exp} and CTV_{CT}^{exp}, to be compared to the PTVs in the 3D MC doses.

Finally, the impact of tumor motion and interplay on tumor dose coverage was quantified by comparing the different dose-volume histogram (DVH) metrics obtained for the 3D MC planned dose and the 4D MC doses with and without interplay. Firstly, D_{mean}, D_{99}, D_{95}, and D_2 were computed for the 3D MC planned dose distribution in the PTVs. Secondly, these metrics were computed for 4D MC dose distributions with and without interplay on the modified GTV and CTV volumes (GTV_{PET}^{exp} and CTV_{CT}^{exp}). Basically, the various DVH metrics in the PTV for the 3D MC planned dose distributions were compared to the same metrics in the GTV_{PET}^{exp} and CTV_{CT}^{exp} drawn on the 4D MC dose distributions with and without interplay. Afterwards, DVH metrics for 4D MC doses with or without interplay were compared to single out the potential interplay effect alone.

7. Statistical evaluation

PTVs expanded from the MidP and ITV were compared in terms of volumes. Dosimetric parameters (mean +/- standard deviation) for TVs and OARs were computed and compared between the MidP and ITV treatment plans. Likewise, plan conformity indexes were calculated and compared between plans. The Paddick conformity index is defined as $CI_{Paddick} = \frac{TV_{PI}^2}{TV\ x\ PI}$ where TV_{PI} is the target volume (TV) within the prescribed isodose volume (PI). Dice's similarity index is defined as $DSI = \frac{2xTV_{PI}}{(TV+PI)}$. A perfect plan would have TV_{PI} = PI = TV and therefore $CI_{Paddick}$ = 1 and DSI = 1 [210-212].

All the statistical calculations were performed with NCSS software 2004© (Number Cruncher Statistical System, Kaysville, UT, USA), p-values lower than 0.05 were considered statistically significant and all tests were two-sided. Doses and volumes were pairwise compared between ITV and MidP using either Student t-tests when data were normally distributed, or Wilcoxon signed rank tests for non-Gaussian distributions.

Results

1. Volumetric analysis

The PTVs expressed in cc are reported in Table 5.2. The PTVs expanded from the ITV were on average 1.2 times larger than those obtained with the MidP. This difference was statistically significant for both the SBRT and the SIB groups (t-test, $p<0.001$ and $p=0.027$, respectively).

Table 5.2 *PTV corresponding to the primary tumors, lymph nodes and PET-based boost expressed in cc for mid-position and ITV plans for all patients. The ratios between ITV and MidP derived PTV are also presented.*

Patient no		$PTV_{T\text{-}CT}$ (cc)			$PTV_{N\text{-}CT}$ (cc)			PTV_{PET} (cc)		
		MidP	ITV	ratio	MidP	ITV	ratio	MidP	ITV	ratio
SBRT	1	24.6	33.3	1.36	-	-	-	-	-	-
	2	33.9	48.2	1.42	-	-	-	-	-	-
	3	52.8	57.9	1.10	-	-	-	-	-	-
	4	20.3	31.7	1.56	-	-	-	-	-	-
	5	84.5	95.1	1.13	-	-	-	-	-	-
	6	38.6	50.5	1.31	-	-	-	-		-
	7	48.2	63.2	1.31	-	-	-	-	-	-
	8	36.5	46.2	1.26	-	-	-	-	-	-
	mean	42.4	53.3	1.31	-	-	-	-	-	-
	SD	20.2	20.1	0.15	-	-	-	-	-	-
SIB	9	396.6	443.7	1.12	-	-	-	212.7	214.5	1.01
	10	270.4	295.6	1.09	210.0	251.7	1.20	120.7	128.3	1.06
	11	90.6	109.1	1.20	140.6	184.3	1.31	29.0	37.8	1.30
	12	533.9	627.8	1.18	153.3	194.6	1.27	72.3	72.8	1.01
	13	591.0	668.5	1.13	97.7	122.2	1.25	312.2	337.3	1.08
	14	259.4	313.7	1.21	118.5	147.4	1.24	66.5	74.1	1.11
	15	358.9	459.4	1.28	-	-	-	105.0	126.9	1.21
	mean	357.3	416.8	1.17	144.0	180.0	1.25	131.2	141.7	1.11
	SD	171.1	196.0	0.06	42.6	49.4	0.04	98.6	103.4	0.11

Abbreviations: MidP: mid-position; ITV: Internal Target Volume; SD: standard deviation

2. Dosimetric analysis for OARs

Smaller PTVs allowed MidP to outperform the ITV by delivering less dose to each OAR (see Table 5.3). In the SBRT group, the differences were statistically significant for the mean lung dose (MLD) and V_{20Gy}, D_2 for the spinal cord, D_2 and V_{30Gy} for the thoracic wall, and finally D_2 for the esophagus. In the SIB group, the differences were statistically significant for V_{20Gy} for the lungs-GTV, V_{25Gy} for the heart, D_{mean} for the esophagus, and D_2 for the main bronchi.

Table 5.3 *Comparison of dosimetric metrics for the OARs (mean ± SD) between treatment plans with MidP and ITV.*

			SIB				SBRT			
OARs	Parameters		MidP (mean±SD)	ITV (mean±SD)	Δ (mean±SD)	p-value	MidP (mean±SD)	ITV (mean±SD)	Δ (mean±SD)	p-value
Lungs-GTV	MLD	(Gy)	15.86±1.48	16.57±1.43	0.72±0.87	0.072	3.70±1.24	4.00±1.24	0.30±0.23	0.008
	Bio MLD	(Gy)	14.57±1.74	15.33±1.43	0.76±0.74	0,035	-	-	-	-
	V_{20Gy}	(%)	25.29±2.97	27.00±3.47	1.71±1.69	0.028	5.04±2.33	5.55±2.27	0.51±0.22	<0.001
Spinal cord	D_2	(Gy)	28.77±5.73	33.07±7.41	4.30±8.48	0.23	7.20±3.33	7.89±3.42	0.70±0.70	0.025
Heart	D_2	(Gy)	-	-	-	-	7.02±7.75	7.83±8.48	0.80±1.01	0.06
	V_{25Gy}	(%)	11.62±8.36	14.92±11.07	3.31±2.87	0.023	-	-	-	-
Esophagus	D_2	(Gy)	-	-	-	-	40.70±14.92	42.52±15.15	1.82±1.24	0.018
	D_{mean}	(Gy)	24.47±9.32	26.33±9.47	1.86±0.63	<0.001	-	-	-	-
	D_{max}	(Gy)	68.26±14.08	70.11±10.98	1.85±4.35	0.31	-	-	-	-
Rib cage	D_2	(Gy)	-	-	-	-	14.29±10.41	17.14±10.42	2.85±2.42	0.004
	V_{30Gy}	(cc)	-	-	-	-	10.91±5.58	12.14±6.16	1.22±1.12	0.013
Vessels	D_2	(Gy)	70.65±9.25	71.59±8.22	0.94±1.42	0.12	-	-	-	-
Bronchus	D_2	(Gy)	75.51±9.25	76.48±9.35	0.75±0.45	0.005	-	-	-	-

Abbreviations: OARs, organs at risk; SIB, Simultaneous Integrated Boost; SBRT, Stereotactic Body Radiation Therapy; MidP, mid-position; ITV, Internal Target Volume; Δ, difference between ITV and MidP values; MLD, mean lung dose; V_xGy, volume of the OAR receiving x Gy; D_x, dose received by x percent of the OAR volume

3. Dosimetric analysis for TVs

The MidP and ITV plans significantly differed for TVs parameters, with p-values ranging between 0.04 and 0.006 for D_{mean}, D_{99}, D_{95} and D_2 to the PTV. However, these differences were inferior to 1%, except for D_{95} in the SIB group, where it is inferior to 4% due to the higher dose in the boosted sub-volume of the PTV; this higher difference was not clinically relevant. Notwithstanding, the mean conformity indexes

computed for the MidP and ITV plans were similar in the SBRT group (Paddick of 0.84±0.05 with p=0.92, DSI of 0.92±0.03 with p=0.91), and did not significantly differ in the SIB group, with Paddick of 0.67±0.23 and 0.62±0.23 (p=0.20), and DSI of 0.80±0.18 and 0.76±0.18 (p=0.24), for MidP and ITV plans respectively. This showed that both the ITV and MidP plans were similar enough in terms of PTV coverage to be further compared.

4. MC simulations

Figure 5.2 reports for each patient the relative difference (in percent) for D_{95} between the 3D MC planned dose distributions and the "interplay simulated" or "no interplay" dose distributions for the primary TVs (note that nodes and boost volumes are not illustrated) used to assess the plans quality. A table compiling all the different metrics, i.e. D_{mean}, D_{99}, D_{95} and D_2 for primary tumors, nodes and boost volumes, is included in the Appendix C.

For all SBRT patients, D_{mean}, D_{99}, D_{95}, and D_2 of the 4D MC dose in CTV_{CT}^{exp} complied with the planning recommendations when using the ITV approach. In particular, tumor motion and interplay effect did not degrade the plan quality.

In contrast, MidP failed to adequately cover CTV_{CT}^{exp} in 3 patients. For patient 5, the simulated interplay effect decreased D_{99} and D_{95} in CTV_{CT}^{exp} by 7.20% and 4.35%, respectively, compared to the planned dose distributions (Figure 5.3a). Although the interplay effect did not affect the two other patients, MC simulations demonstrated significant underdosages of CTV_{CT}^{exp}, compared to the planned doses, with D_{mean}, D_{99}, and D_{95} reduced by 1.90%, 2.16%, and 2.61% for patient 4 and by 2.52%, 1.36%, and 2.16% for patient 8, respectively (Figure 5.3b).

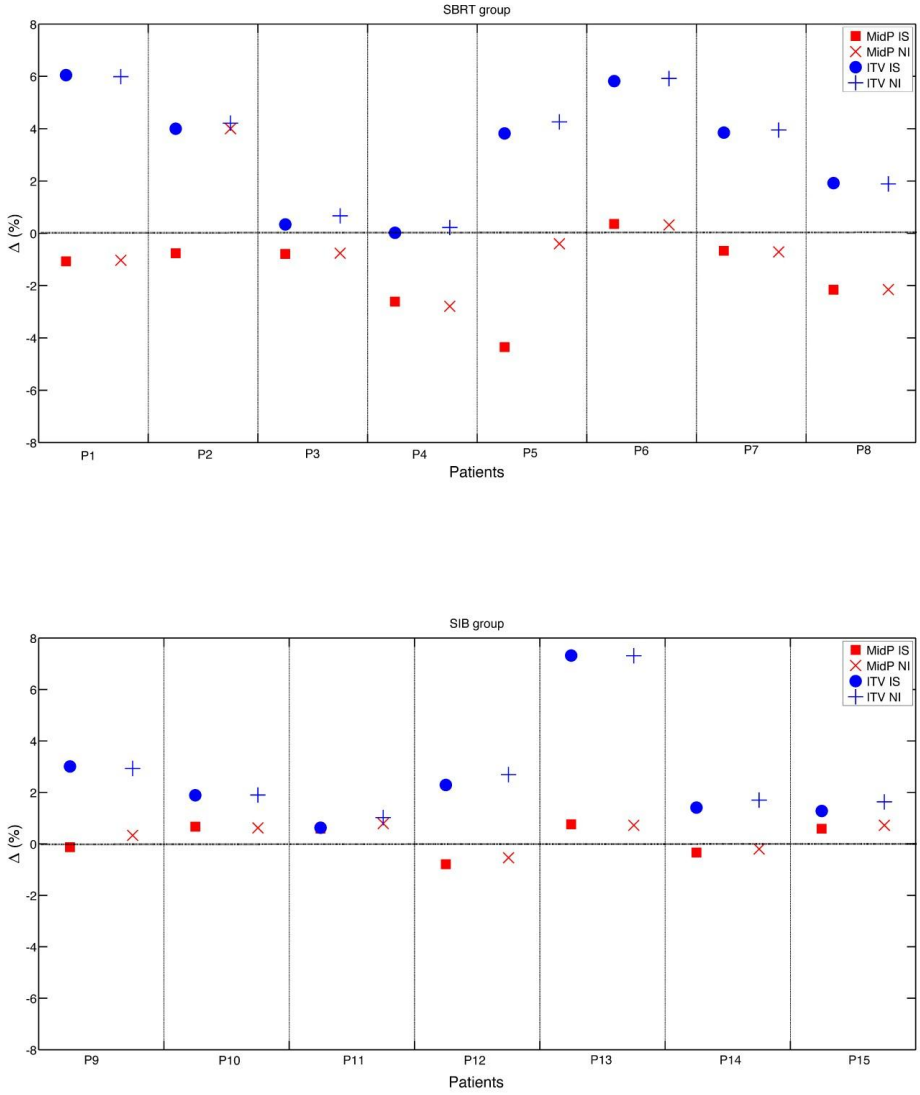

Figure 5.2 *Relative difference (Δ) for D_{95} to the CT based primary target volume (CTV_{CT}^{exp}) between the 3D Monte Carlo (MC) planned dose distributions and Interplay Simulated (IS) or No Interplay (NI) dose distributions calculated using a 4D MC model for mid-position and ITV strategies for SBRT (a) and SIB group (b). In the former case, it is important to note that ITV approach ensures adequate tumor coverage for all patients. In contrast, MidP strategy do not guarantee sufficient dose coverage to the CTV_{CT}^{exp} in 3 patients. For P5, the reduction of dose coverage to the CTV_{CT}^{exp} is due to the interplay effect. For P4 and P8, the significant underdosage to the CTV_{CT}^{exp} arises from the breathing motion alone. For the SIB group, both strategies ensure adequate tumor coverage for all patients. Neither tumor motion nor the interplay effect degrades the plan quality.*

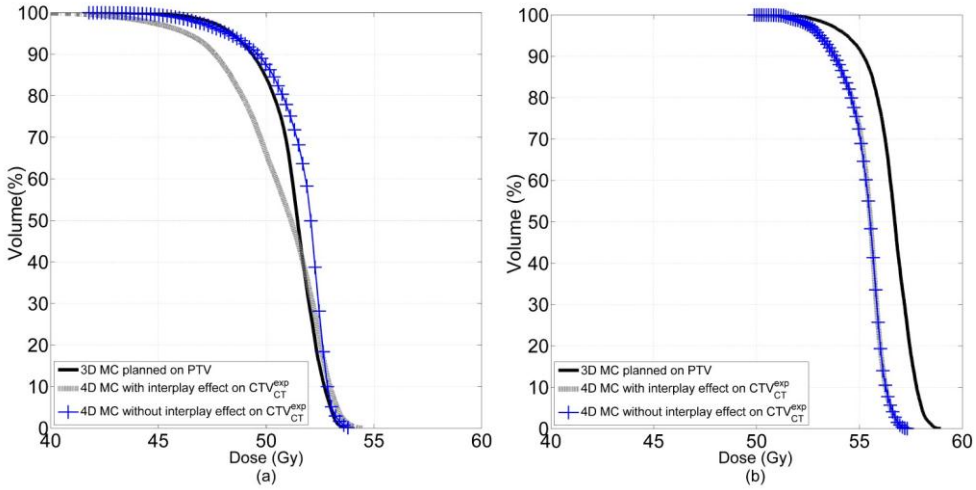

Figure 5.3 *Dose-volume histograms (DVHs) representing the planned dose on the Planning Target Volume (PTV) and the actual delivered doses calculated with and without the interplay effect on the expanded Gross Tumor Volume (CTV_{CT}^{exp}) for patient 5 (a) and patient 8 (b).*

For all SIB patients, D_{mean}, D_{99}, D_{95} and D_2 to the CTV_{CT}^{exp} and GTV_{PET}^{exp} computed from 4D MC dose distributions complied with the planning recommendations when using both approaches. In particular, it is important to note that neither the tumor motion nor the interplay effect affect the plan quality. On the other hand, a significant tumor coverage improvement to the CTV_{CT}^{exp} was observed in 4D MC computed plans compared to the 3D planned MC ones when ITV approach was used in both SIB and SBRT groups (see Figure 5.2).

Discussion

Our study confirmed that the MidP leads to significantly smaller PTVs than the ITV, which also translated into lower doses delivered to the OARs. Although the dose reduction may seem modest at first sight, it matters in the context of hypo-fractionated RT schemes with high biologically equivalent doses. As all plans were made in a similar way by the same person and showed comparable dose conformities to the PTV, the differences in dose distributions to OARs are believed to faithfully reflect volumetric changes.

Based on these observations, the MidP appears as an appealing option for motion management in lung cancer treatment with TomoTherapy. A MidP volume can be derived for any moving structure, such as the primary tumor, lymph nodes, or even tumor sub-volumes. Moreover, MidP is easy to implement in clinical routine because it affects only the target volumes definition, and leaves all other aspects of planning unchanged; MidP does not require neither any additional equipment in the treatment room, nor complex 4D features in the TPS. It only entails the computation of the target volumes in their time-weighted average position, using a 4D-CT scan whose phases are non-rigidly registered. Unfortunately, no commercial implementation of MidP exists at the moment, which hinders adoption in clinical routine.

The most innovative aspect of our study was the MC verification of the dose distributions in the target volumes for both the ITV and MidP. In agreement with our previous study [163], the 4D MC simulations confirmed that the ITV ensured adequate dose coverage to CTV_{CT}^{exp} in all cases. Overdosage in CTV_{CT}^{exp} observed in 4D MC plans was mainly attributable to the intrinsic overestimation of motion in the calculation of the PTV margin with the ITV. This improved D_{95} compared to the PTV without motion. For the CTV_{CT}^{exp} in the SIB group, additional overdosage may also stem from the use of two prescription levels on a moving target, with a substantial portion of the CTV entering the high dose region defined by the PTV_{PET}, especially for P11, P13 and P15 with SI motion as large as 12 mm.

In contrast, 4D MC simulations indicated that the MidP strategy did not guarantee sufficient dose coverage to the CTV_{CT}^{exp} in 3 out of 15 cases, all in the SBRT group. In the first case (P5), underdosage resulted from the interplay effect, which is specific to TomoTherapy and manifests in the form of undesired hot and cold spots within the TVs, comparable to constructive and destructive interferences. It results from a delivering fluence different from the planned fluence when respiratory intra-fraction motion and couch progression take place in TomoTherapy delivery. Kissick et al.

showed that these hot and cold spots are minimized when the jaw width is large and scanning velocity is small relatively to the breathing amplitude and frequency [213, 214]. For this patient, we used the smallest jaw width (1.0 cm) and a couch pitch of 0.215. Moreover, the patient breathing period was 6 s, and tumor motion was particularly large, with displacements of 5.16, 11.81 and 29.97 mm in LR, AP and SI directions, respectively. Finally, our MC simulations calculated only one fraction of the treatment, which maximizes the interplay effect. Previous studies showed that interplay effect tends to average out after multiple fractions [213, 215]. However, the small number of fractions, only 4 here, limits this advantageous effect.

In both other cases (P4 and P8), the significant agreement between 4D MC dose distributions with and without interplay suggested that breathing motion alone was responsible for the degradation of the DVHs. Possible reasons are simplifications introduced in the PTV margin formula:

1) Spherical GTVs were assumed while most tumors deviate from this shape. Moreover, the formula ignores the GTV size and shape as long as it is large compared to random errors (σ) [42]. However, in these two cases, the tumor volumes were very small with GTV of about 3 cc and 1.5 cm diameter in both cases, thus questioning the applicability of the model.

2) Rotations and shape variations of the tumor have been disregarded in the model. Nonetheless, in these cases, we could expect that rotational errors be most likely of minor clinical importance given the limited size and quite regular shape of the considered tumors [216-218].

3) The margin formula assumes Gaussian distributions for all geometric errors, on the basis of the central limit theorem [42]. If this theorem applies, convolving the dose with a Gaussian distribution can simulate the global effect of geometric uncertainties on dose distributions. However, breathing motion may easily depart from normality and hence invalidate the whole formula if the contribution of tumor motion is large compared to other source of uncertainties.

The first and third hypotheses are not met in P4 and P8. Indeed, P4 and P8 had very small tumors (2.48 and 3.49 cc) combined with large tumor motion (10.84 and 24.63 mm of displacement in the SI directions, see also Table 5.1). In comparison, the penumbras for SBRT patients were 4.6, 4.6, and 4.3 mm in the LR, AP, and SI directions, thus undermining the applicability of the central limit theorem for those patients. In this context, P4 and P8 deviate from the formalism of Van Herk et al. and one might expect the MidP to underestimate the presence of the tumor at both ends of its trajectory, thereby jeopardizing coverage.

From a pragmatic point of view, simple rules based on tumor size and motion amplitude could be applied to choose between both margin strategies: the MidP should be privileged against the ITV since it allows for significant TV and dose reduction, except in tumors showing simultaneously small size (i.e. below 1.5 cm) and large motion amplitude (i.e. above 1 cm). In this scenario, the benefit of margin reduction should be weighted against the risk of tumor underdosage, and ITV should be considered as a safer option in these specific conditions.

In conclusion, compared to the conventional ITV, the MidP strategy significantly reduced the PTV and the irradiated volumes in all patients, with potential room for dose escalation protocols. Furthermore, MidP proved to be feasible and safe in helical delivery for a representative set of patients commonly treated by radiation therapy and with lung tumors whose stage ranged from early to locally advanced. However, patients having very small tumors with large amplitude motions must be treated cautiously; the conventional ITV remains safer in this particular case.

Chapter 6

Summary and perspectives

Contents

Summary

The first study has shown that FDG-PET outperforms CT for the delineation of primary tumor volumes in NSCLC, as previously observed in HNSCC patients. We have also confirmed the superiority of the gradient-based segmentation, compared to usual threshold-based delineation both in terms of accuracy and robustness. However, the added value of FDG-PET is more pronounced in cases of tumors surrounded by densifications of the lung parenchyma. For well-defined and peripherally located tumors, the CT with mediastinal windowing remains a clinically acceptable alternative to FDG-PET. Therefore, we suggest using the gradient-based method as the reference segmentation tool in the field of PET-driven delineation of lung tumors, surely when they are poorly identifiable on conventional CT.

The second study demonstrated the feasibility of a non-uniform and individualized dose escalation based on FDG-PET in IMRT delivery for LA NSCLC patients. The dose can be further increased for peripheral tumors, compared to central ones. Our study suggests an appreciable local tumor control whereas distant recurrence remains an important issue. Nonetheless, randomized and larger patient cohorts are required to confirm our results. Although acute and late toxicities were comparable to conventional scheme in peripheral tumors, two patients with centrally located tumors died from fatal hemorrhage. Centrally located tumors with direct invasion of mediastinal organs must thus be treated with extreme caution to avoid late toxicities.

Our third study confirmed that the MidP leads to significantly smaller PTVs than the ITV and also translates into lower doses delivered to the OARs. Furthermore, MidP proved to be feasible and safe in helical delivery for a representative set of patients commonly treated by radiation therapy and with lung tumors whose stage ranged from early to locally advanced. However, patients having very small tumors (<5cc) with large amplitude motions (>10mm) must be treated cautiously; the conventional ITV remains safer in this particular case.

Perspectives

Locally advanced stage NSCLC comprises a very heterogeneous group of patients with respect to histology, tumor extent, prognosis, molecular pathology, patient characteristics, comorbidities, and treatment options. Up to now, all patients have been treated in the same way, according to conventional treatments. However, novel therapeutic options are investigated as part of the multimodality approach, including new RT strategies, optimal combination of chemotherapeutic drugs and new biological agents. Advances in technology and imaging might lead to a better prediction and selection of those patients most likely to benefit from a particular therapy.

LA stage NSCLC can be considered as a model containing local and regional compartments in the chest and a distant compartment harboring potential micro-metastases. Cancer cells death in each compartment is required to cure the patient.

Since several years, many efforts have been assigned to improve the tumor local control and overall survival. Unfortunately, the disease tends to relapse quite frequently as distant metastasis or in non-irradiated lymph nodes. The survival of LA stage NSCLC patients seems to be related not only to the primary tumor control but also to the micro-metastatic disease. Consequently, we have to act on all possible fronts. In that regard, dose escalation combined with dose painting, adaptive RT and optimal motion management, as well as the use of particle therapy might improve the local tumor control, while development of novel therapies acting against micro-metastases, including new chemotherapeutic agents, targeted therapy and immunotherapy might reduce regional and distant recurrences. Finally, decreasing toxicities by using robust OARs dosimetric parameters, accurate biomarkers able to predict toxicities, highly conformal RT and pharmacological normal tissue protection is of utmost importance.

1. Improving the local control: the cornerstone of radiotherapy

1.1. Dose painting

Although radiation therapy is a key element in the multidisciplinary treatment of NSCLC and participates in improvement of local control, it is currently far from optimal.

Nowadays, the conventional radiation therapy delivers a standard, homogeneous and static dose to the TVs along the treatment. However, from a biological point of view, a tumor is all except homogeneous and furthermore, it changes in shape, size and

metabolism during the treatment. Therefore, a heterogeneous dose distribution based on functional imaging might increase the tumor control probability. PET imaging has the potential to reveal various tumor molecular pathways, including metabolism, proliferation, hypoxia, and receptor or gene expressions, depending on the tracer used. A few years ago appeared the innovative concept of biology-guided radiotherapy, also called dose painting. In this concept, the tumor is considered as a complex cells model in which aggressiveness and sensitivity to radiotherapy can considerably vary. Dose painting by contours, addressed in Chapter 4, makes use of sub-volumes that are generated using an automated segmentation method and creates two or more discrete dose levels. The dose painting by numbers (DPBN), in contrast, considers a continuously increasing relationship between the voxel intensity of the image and the risk of local recurrence in that voxel. As a result, the dose is prescribed on a voxel-by-voxel basis as a function of the signal intensity [219, 220].

Nonetheless, the main issues of PET-guided dose painting remain the poor spatial resolution, the low signal to noise ratio, especially when tracers other than FDG are used, and the integration of geometrical uncertainties (e.g. tumor motion). Although DPBN appears as an attractive approach, the PET image only represents a snapshot of a dynamic biological system. This raises the question of the ability of DPBN to produce dose distributions that really match the underlying tumor biology, as illustrated in Figure 6.1 [221].

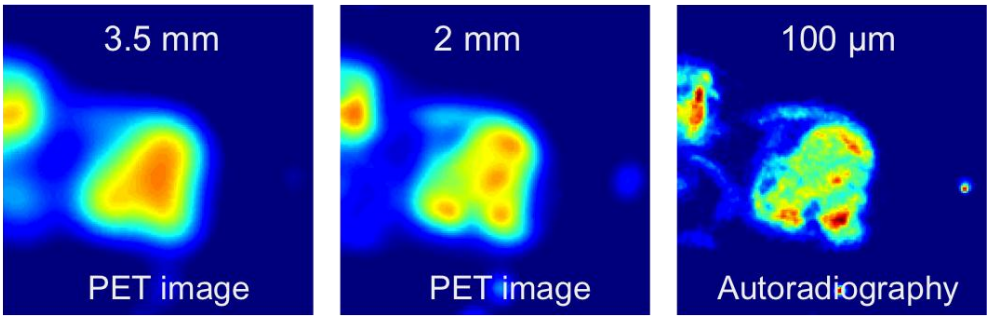

Figure 6.1 *Discrepancies are found between in vivo PET images (3.5 mm and 2 mm spatial resolution) of small animal and the microscopic reality, illustrated by autoradiography (100 µm spatial resolution). From Christian et al. Radiother Oncol, 2009.*

In addition to the biological relevance of heterogeneous prescription and the technical feasibility of matching the prescription with an actual dose distribution, the issue of patient-related geometrical uncertainties integration into DPBN process remains to be solved. These are subjects of intensive research in our laboratory.

Although several preclinical and clinical studies have already confirmed the feasibility of dose painting approaches [222-225], additional advances in imaging techniques are required before it can be used in practice. Afterwards, further studies will be needed to accurately define radio-resistant areas [225], to validate the concept in different anatomical sites, to assess the impact of dose escalation on these sub-areas considered as radio-resistant and to select the patient sub-groups that would beneficiate from this technique.

Eventually, other imaging modalities could potentially be considered for dose painting. Image quality of MRI surpasses the other currently available imaging modalities. Besides the accurate anatomical representation, MRI provides functional and biological images required for dose painting purpose. Although some technical characteristics seem challenging compared to CT, MRI-guided dose painting might be another topic of promising research.

1.2. Adaptive radiation therapy

As previously discussed, a tumor is highly heterogeneous, and submitted to anatomical and biological changes over time. In that context, a single treatment plan based on the initial imaging session, performed prior to treatment, might lead to suboptimal treatment. The planning CT is hardly representative of the patient's anatomy in all its complexity, as it does not display complex geometrical errors such as tumor motion, baseline shift or anatomical and tumor changes along the treatment course.

It is essential to decrease these uncertainties to target tumor volumes with tighter margins, enabling potential dose escalation and local control improvement. IGRT is one of the most important advances in this field, ensuring online position correction through a couch shift. However, although image guidance allows repositioning of the patient using rigid image registration between the planning CT and the daily imaging, it cannot modify the initial plan for non-rigid changes, such as rotations, shape and size changes or the baseline shift differential between primary tumor and lymph nodes. This is precisely the role of adaptive radiation therapy (ART), which uses rigid and non-rigid registration to adapt the initial plan to the new patient and tumor status. Nonetheless, a particular attention has to be paid when using ART in case of tumor response [226]. Indeed, a decreased GTV size on the CT images or a reduced metabolic activity on PET images does not necessarily correlate with shrinkage of the CTV or with cell death within the tumor. A careful analysis of tumor regression patterns is required before the implementation of tumor response adaptive management in clinical daily use.

Currently, ART is at a very early stage and relies mostly on planning data. Typically, an off-line plan modification is applied only when significant anatomical changes (e.g. atelectasis disappearance, drastic weight loss or mediastinal shift after significant tumor shrinkage) are observed on daily imaging, usually once or twice during the entire treatment course. In the near future, it is expected that weekly adaptations or even online daily re-planning will be performed. Such treatment will require online automated adaptive protocols, including deformable registration tools based on image information from current and previous fractions, aiming to account for both inter- and intra-fraction variations.

Therefore, ART is a considerable progress towards truly personalized radiation medicine with a potential for tumor dose escalation and/or reduced patient toxicity.

1.3. Tumor motion management

Tumor motion is a key issue in thoracic radiotherapy. As described in Chapter 1, several approaches can be used to integrate it into the treatment planning. We demonstrated in Chapter 5 that MidP concept outperforms the ITV in terms of irradiated volumes. Moreover, we showed its feasibility and safe applicability in helical TomoTherapy as long as motion amplitude was less than 10 mm for tumor diameter of 15 mm or less. Indeed, in this strategy, the tumor motion is considered as a random uncertainty as systematic error due to 3D sampling and hysteresis are eliminated. As the contribution of random errors on margin computation is much smaller than the systematic errors, tumor motion has actually little impact on the resulting PTV margin when MidP is considered. It was also demonstrated that margins applied for an idealized gating treatment and MidP method were similar for the majority of patients [113]. In addition, compared to respiratory synchronized techniques such as gating or tracking, margin-based MidP strategy is much easier to implement, and do not require any dedicated 4D planning strategy. Noteworthy, gating and tracking techniques suffers from a wide range of uncertainties (i.e. accurate determination of the tumor position, correct relationship between the target and its surrogate) potentially resulting in considerable and additional safety margins. Moreover, they involve advance equipment, education and training in the use of complex technology, and the implementation of a dedicated quality assurance program. Due to the inherent limitations of these approaches, their clinical gain in photon therapy appears very limited, compared to MidP strategy.

1.4. What about the clinical target volume?

Even though local relapse usually occurs into the GTV, some loco-regional recurrences might be attributed, at least partially, to a lack of microscopic disease coverage. This

hypothesis has been suggested in a study, in which patients at high risk of microscopic disease extension were more subject to develop loco-regional relapse than distant metastasis after stereotactic body radiation therapy (SBRT), especially if the dose surrounding the GTV was low [227]. It would be interesting to confirm these data in order to identify tumors at high risk of microscopic extension and to appraise the impact of adding a CTV margin for the treatment of selected early stage NSCLC patients.

However, as for LA stage NSCLC patients, the next question will be the most appropriate CTV margin value. In the setting of LA stage NSCLC, an extension from GTV to CTV of 5 mm both for primary tumor and involved lymph nodes is currently applied. In agreement with our first study results (see Chapter 3), several authors conclude that CT images using lung window lead to a large overestimation of the true tumor volume [87, 88, 149, 228]. It could be hypothesized that defining the tumor on this image (i.e. overestimating the GTV) covers a part of the microscopic tumor extension, offsetting the lack of CTV margin.

Hence, an accurate assessment of the CTV margin is crucial, in particular in the era of dose escalation and adaptive radiotherapy, where the GTV tends to be thoroughly defined and geometric uncertainties are minimized. Actually, a PET-based GTV definition and reduced PTV margin could lead to miss part of the target if CTV margin is not adequately estimated.

Nonetheless, this estimation is a challenging task, as the CTV correlation has to be performed between some imaging and the true microscopic tumor volume on pathology. Previous analyses reporting the evaluation of microscopic tumor extension in NSCLC were methodologically heterogeneous with resulting CTV margin values from 5 to up to 22.5 mm [87, 149, 228-230]. Additional assessment of microscopic disease extension should be investigated with a robust and reliable method.

Finally, an appealing approach would be to image the tumor cell density in order to differentiate the macroscopic area from the microscopic extension. This decisive information combined with the integration of TCP-NTCP model parameters and geometric uncertainties directly into the optimization process, might lead to probabilistic models of 3D dose distribution and progressively replace GTV, CTV and PTV concepts, according to the tumor cell density.

1.5. Particle therapy

In recent years, particle therapy (PT) has gained increasing attention. Indeed, it demonstrates better dose distribution and physical properties compared to photon therapy together with superior biological properties (for carbons). Theoretically, PT

could lead to an increased therapeutic index, either escalating the dose to TVs while keeping isotoxic doses to OARs or decreasing toxicities while using conventional doses. However, the dose distribution obtained with PT is very sensitive to moving target and anatomical change in tumor and surrounding tissues. It is thus essential to properly include tumor motion, range and set-up uncertainties in treatment planning.

The availability of 4D imaging and motion compensation techniques might be even more critical for PT than for photon therapy, especially in pencil beam scanning (PBS) delivery, where interference between dynamic beam delivery and motion of TVs and OARs can cause complex patterns of over and under dosage within the target. This interplay effect can be mitigated by using fractionated treatment and multiple treatment fields. Additional techniques, such as rescanning, gating or larger spot size scanning could also optimize the dose distribution, especially in hypo-fractionation treatment [231]. For moderate tumor motion, homogeneous dose distribution can be obtained when using conventional fractionation and rescanning, while for large tumor motion (>20 mm), only gating techniques combined with large spot scanning might be effective to reduce the breathing motion effect [231]. Although the gating approach requires an onboard imaging device and seems technically challenging, like in photon therapy, this strategy might become feasible for clinical use in the near future. By contrast, in addition to be technically very demanding, the tracking approach would not necessarily reduce the interplay effect and is not suitable for LA stages NSCLC, as primary tumor and positive lymph nodes can move differently.

Eventually, besides the technical difficulties in PT, the cost effectiveness of the technique is questioned. Although numerous planning studies have shown the dosimetric benefits of protons over photons, randomized controlled trials comparing photons and PT are largely lacking, especially in NSCLC [232, 233]. In early stage lung cancer, clinical data tend to demonstrate that SBRT is comparable to protons in terms of survival outcome even though the latter present a highly favorable toxicity profile. In contrast, for LA stages NSCLC, PT might appear in the near future as a new tool to improve local control, at least in a subset of patients, provided that related technical issues will be adequately managed and well-designed and prospective trials with regards to current photon radiation treatments will be conducted.

2. Improving the regional control: a multi-modality challenge

In our dose escalation study, we observed a high rate of regional recurrence, as discussed in Chapter 4. Actually, 5 patients (38.5%) developed out of field recurrences while 1 patient (7.7%) experienced an in field recurrence.

NSCLC is characterized by a high risk of occult lymph node metastasis, even for early stages [234]. In the past, elective nodal irradiation (ENI), i.e. clinically or radiologically uninvolved lymph nodes, was recommended to cover the potential microscopic tumor invasion. Nonetheless, since the use of PET/CT for initial NSCLC staging, it is commonly accepted that only involved lymph nodes have to be included in the radiation field, given the quite low risk of out of field lymph node recurrence. Some consider this risk, estimated at 5-10%, as relatively low, whereas others estimate it as meaningful. Surprisingly, in a recent systematic review, Kepka et al. showed that the rate of out of field regional recurrence was substantially similar after stereotactic treatment for early stages NSCLC and conventional treatment for LA stages NSCLC [235]. Likewise, a recent study of Grills et al. demonstrated that T2 lung tumors (>3 cm) treated by SBRT have the same LC than T1 tumors (<3 cm) but a poorer OS, related to a higher rate of regional recurrences [236]. These findings together with our trial results might lead to two observations. First, the dose gradient delivered with new radiation techniques, such as IMRT or even worse with proton therapy, is steeper than with 2D or 3D-CRT. Consequently, incidental doses to radiologically uninvolved (but potentially invaded by microscopic tumor cells) mediastinal, contralateral or sub-clavicular lymph nodes are by far less than 40-50 Gy, which were doses classically delivered in ENI. However, it seems inconceivable to go back to this old practice because ENI increases toxicity and hampers delivering a high dose to the primary tumor, which remains the first site of relapse. Second, the initial mediastinal staging of the disease has to be optimal, notably using PET/CT imaging, EBUS/EUS or mediastinoscopy. In case of definitive radiotherapy, it appears crucial to keep the time-interval between the PET/CT imaging and the start of RT as short as possible to avoid false negative results. In that context, it might be interesting to perform a new planning PET/CT, as presented in our study, covering the whole LN stations, from 1 to 2 weeks before the start of radiotherapy, as part of the simulation step. However, PET/CT imaging is not able to identify microscopic tumor extension and its sensibility decreases from 91% for enlarged LN to 75% for LN of <1cm in short axis on CT images [237]. It is thus important not to be overconfident on imaging and the final decision to selectively irradiate a PET negative lymph node suspicious on CT imaging remains at the radiation oncologist evaluation. Eventually, the question of a more aggressive mediastinal staging arises. Would it be more appropriate to perform a mediastinoscopy or even thoracoscopy (for station 5 or 6) with sampling of whole accessible nodal stations before each radical RT for early stage or CRT for LA stage NSCLC?

Despite the current precautions, it is likely that regional relapse will appear in a few cases with the development of extremely conformal delivery radiation treatment. It

might be valuable to pursue research on additional molecules acting against micro-metastasis either concomitantly or in adjuvant therapy after definitive CRT. It would be also interesting to identify biomarkers, predictive and prognosis indicators to select those patients that will most likely benefit from these molecules, including targeted therapy, immunotherapy or new chemotherapy agents, among others. This topic will be developed in the next paragraph.

3. Improving the distant control: a key issue for the future

Distant progression remains an issue in the treatment of NSCLC, as illustrated in our study (Chapter 4) and in many other trials. The local, the regional as well as the distant tumor control might affect overall survival. In that regard, novel radiosensitizing systemic cytotoxic agents and drugs targeting specific molecular pathways, combined with technologic progresses in RT, might decrease both loco-regional and distant risk of relapse, thus improving the outcome of these patients.

Since last decade, considerable investigations have been conducted in the field of molecular biology leading to the development of several molecular targeted therapy agents for NSCLC patients. Given the good results of agents directed against epidermal growth factor receptor (EGFR), vascular endothelial growth factor (VEGF) receptors, tyrosine kinase inhibitors (TKI) or anti-VEGF antibodies in advanced metastatic disease, it might be expected that they would also prove some efficiency in combined modality treatment for LA advanced stage NSCLC [238]. Nevertheless, it must be admitted that, so far, these drugs have failed to demonstrate a gain when associated with concurrent chemo-radiotherapy [239, 240]. However, these disappointing results might stem from the lack of patient selection for the target or from a negative interaction in some patients when chemotherapy and EGFR TKI were prescribed concomitantly. These results highlight once again the importance of improving our knowledge on lung cancer biology. Ongoing research will precise the value of these new agents as part of the curative intent multi-modality treatment.

Future areas of research encompass immunotherapy that offers exciting prospects for the treatment of lung cancer. Currently, ongoing studies are assessing the opportunities of antigen-dependent immunotherapy, including vaccines and antigen-independent immunotherapy, targeting immune checkpoints.

In addition to novel therapies development, the abscopal effect of radiotherapy gains increasing interest [241-244]. Although biological and cellular mechanisms are still not well understood, this immunologically mediated phenomenon reduces or inhibits tumor growth outside the irradiation field by stimulating the immune response, notably by an increased tumor antigen presentation due to the radiation-induced

inflammation. Consequently, it appears promising to study, among others, the combination of anti cytotoxic T-lymphocytes-associated protein 4 (CTLA 4), programmed cell death 1 (PD-1) and programmed death-ligand 1 (PD-L1) inhibitor agents and radiotherapy for potentiating the anti-tumor immune response [245-248]. It is assumed that efficacy will be based on the association of several drugs but the optimal combination and sequence of chemotherapy, radiotherapy and immunotherapy to ensure maximum synergy remains to be determined.

In the foreseeable future, one might expect the generalization of sequencing the whole genome and transcriptome. This might help to identify and study all specific oncogenic alterations, which would accelerate the development of agents with highly specific activity.

4. Decreasing toxicities: an ambitious daily concern

As already mentioned in Chapter 1, the first step in toxicity assessment is probably the standardization of OARs contours, dosimetric constraints definition and classification of adverse effects.

Then, the use of highly conformal radiation delivery techniques, including IMRT, SBRT and PT, represents an opportunity to improve dose distribution and reduce potential radio-induced early and late effects.

Nonetheless, several patients with centrally located lung tumors present, at diagnosis, a mediastinal involvement that precludes dose escalation, even with novel radiation technique, since the probability of adverse effects remains extremely high. For these patients, therapeutic prospects are very limited and combining RT with innovative systemic therapeutic agents, as discussed above, might increase tumor local control. In these particular cases, the choice of a sequential CRT approach with a highly effective drug would potentially be of interest. In selected patients with good response on the primary site, a dose escalation RT could be re-considered.

Moreover, it seems crucial to develop accurate biomarkers able to predict the risk of early and late toxicities. In this way, it would be easier to select patients for more aggressive treatment, e.g. safe and isotoxic dose escalation.

Eventually, pharmacological normal tissue protection might be another attractive field of research. In that regard, investigation focused on the pathogenesis of radio-induced pneumonitis, esophagitis and mediastinal organ damages will be required to identify appropriate targets for preventive therapy. Using such molecules would allow to increase local tumor control, especially when OARs are dose-limiting.

5. Perspectives conclusion

Survival of LA NSCLC patients depends primarily on local tumor control but also on the control of micro-metastases located regionally or distantly. Therefore, it is crucial to act at every level to improve patient's outcome.

Refinement of anatomical and functional imaging together with an optimal management of geometric uncertainties should allow the generalization of clinical daily use of innovative radiation techniques that are essential to ensure a better local tumor control.

Additionally, combination of multiple treatments, including novel therapeutic agents, is a promising and active field of research, which is of particular importance to act in synergy on microscopic tumor cells.

More than ever, a better understanding of lung cancer biology is a challenging but mandatory step towards personalized management and improved outcome of NSCLC patients.

Chapter 7

Appendices

Appendix A

TNM classification for non-small cell lung cancer (7th edition AJCC)

Table 1. TNM classification for non-small cell lung cancer.

Primary tumor (T)	
TX	Primary tumor cannot be assessed, or the tumor is proven by the presence of malignant cells in sputum or bronchial washing but is not visualized by imaging or bronchoscopy
T0	No evidence of primary tumor
Tis	Carcinoma in situ
T1	Tumor ≤3 cm in greatest dimension, surrounded by lung or visceral pleura, no bronchoscopic evidence of invasion more proximal than the lobar bronchus (not in the main bronchus); Superficial spreading of tumor in the central airways (confined to the bronchial wall)
T1a	Tumor ≤2 cm in the greatest dimension
T1b	Tumor >2 cm but ≤3 cm in the greatest dimension
T	Tumor >3 cm but ≤7 cm or tumor with any of the following: ❖ Invades visceral pleura; ❖ Involves the main bronchus ≥2 cm distal to the carina; ❖ Associated with atelectasis/obstructive pneumonitis extending to hilar region but not involving the entire lung
T2a	Tumor >3 cm but ≤5 cm in the greatest dimension
T2b	Tumor >5 cm but ≤7 cm in the greatest dimension
T3	Tumor >7 cm or one that directly invades any of the following: ❖ Chest wall (including superior sulcus tumors), diaphragm, phrenic nerve, mediastinal pleura, or parietal pericardium; ❖ Or tumor in the main bronchus <2 cm distal to the carina but without involvement of the carina; ❖ Or associated atelectasis/obstructive pneumonitis of the entire lung or separate tumor nodule(s) in the same lobe
T4	Tumor of any size that invades any of the following: mediastinum, heart, great vessels, trachea, recurrent laryngeal nerve, esophagus, vertebral body, or carina; or separate tumor nodule(s) in a different ipsilateral lobe
Regional lymph nodes (N)	
NX	Regional lymph nodes cannot be assessed
N0	No regional node metastasis
N1	Metastasis in ipsilateral peribronchial and/or ipsilateral hilar lymph nodes and intrapulmonary nodes, including involvement by direct extension
N2	Metastasis in the ipsilateral mediastinal and/or subcarinal lymph node(s)
N3	Metastasis in the contralateral mediastinal, contralateral hilar, ipsilateral or contralateral scalene, or supraclavicular lymph nodes
Distant metastasis (M)	
MX	Distant metastasis cannot be assessed
M0	No distant metastasis
M1	Distant metastasis
M1a	Separate tumor nodule(s) in a contralateral lobe; tumor with pleural nodules or malignant pleural (or pericardial) effusion
M1b	Distant metastasis

Appendix B: Supplementary data for the dose escalation study (Chapter 4)

Table 1. *Measurement of SUL_{peak} (PERCIST), SUV_{max} (EORTC) and longest diameter (RECIST 1.1) of the primary tumor for all patients*

	PERCIST SUL_{peak}					EORTC SUV_{max}					RECIST 1.1 (mm)				
	t_0	t_1	t_2	t_3	t_4	t_0	t_1	t_2	t_3	t_4	t_0	t_1	t_2	t_3	t_4
P1	9.8	2.5	5.1	10.6	-	16.4	3.9	9.2	18.5	-	55	51	NM	NM	-
P2	11.1	2.6	3.4	2.8	3.4	16.0	4.4	5.1	4.0	2.9	58	46	42	35	35
P3	3.9	1.6	1.9	-	-	6.2	2.3	2.7	-	-	34	34	29	-	-
P4	8.4	2.6	-	-	-	12.8	4.2	-	-	-	50	37	-	-	-
P5	5.5	3.0	1.9	1.9	2.0	10.0	5.2	2.6	2.8	2.5	46	37	29	26	31
P6	9.6	3.5	2.9	4.0	-	16.1	5.9	4.7	6.6	-	68	54	44	42	-
P7	4.3	1.5	1.5	1.2	0.8	12.7	4.2	5.0	4.1	4.2	57	54	44	42	NM
P8	7.4	9.6	7.2	-	-	10.5	13.1	10.4	-	-	81	64	54	-	-
P9	5.1	4.3	1.8	1.3	1.4	10.3	6.2	2.8	0.7	0.7	30	30	27	21	17
P10	10.1	1.9	2.3	2.0	-	19.4	3.1	3.3	3.3	-	49	31	31	NM	-
P11	9.9	1.2	0.8	0.8	1.3	17.2	1.8	1.1	1.3	1.4	27	14	12	9	7
P12	3.2	1.8	1.3	0.4	0.6	7.5	2.8	6.5	1.1	1.1	35	29	26	NM	NM
P13	7.4	3.5	1.4	2.3	1.6	18.8	7.6	5.1	5.5	3.4	47	25	NM	26	26

Abbreviation: t_0, baseline; t_1, 2 months post-treatment; t_2, 6 months post-treatment; t_3, 1 year post-treatment; t_4, 2 years post-treatment; NM, non-measurable.

Table 2. *Overall survival*

OVERALL SURVIVAL		
Characteristics		*Total N=13*
Survie	Number of patients alive	7 (53.8%)
	Number of patients deceased	6 (46.2%)
Kaplan Meier estimate of OS (months)	median	NE
	CI95	(13.85 - NE)
	minimum	4.9
	maximum	46.3
OS rate at	6 months	92.3%
	12 months	84.6%
	18 months	61.5%
	24 months	52.8%
	36 months	52.8%

Note: NE = Not Estimable due to insufficient events.

Table 3. *Overall progression free survival*

OVERALL PROGRESSION FREE SURVIVAL		
Characteristics		*Total N=13*
Overall progression	Number of patients with overall progression	7 (53.8%)
	Number of patients without any progression	6 (46.2%)
Kaplan Meier estimate of Overall PFS (months)	median	18.78
	CI95	(4.31 - NE)
	minimum	2.6
	maximum	40.6
Overall PFS rate at	6 months	76.9%
	12 months	53.9%
	18 months	53.9%
	24 months	46.2%
	36 months	34.6%

Note: NE = Not Estimable due to insufficient events.

Table 4. *Local progression free survival*

LOCAL PROGRESSION FREE SURVIVAL		
Characteristics		*Total N=13*
Local progression	Number of patients with local progression	2 (15.4%)
	Number of patients without any local progression	11 (84.6%)
Kaplan Meier estimate of local PFS (months)	median	NE
	CI95	(9.18 - NE)
	minimum	4.9
	maximum	46.3
Local PFS rate at	6 months	92.3%
	12 months	76.9%
	18 months	61.5%
	24 months	52.8%
	36 months	52.8%

Note: NE = Not Estimable due to insufficient events.

Table 5. *Regional progression free survival*

REGIONAL PROGRESSION FREE SURVIVAL		
Characteristics		*Total N=13*
Regional progression	Number of patients with regional progression	6 (46.2%)
	Number of patients without any regional progression	7 (53.8%)
Kaplan Meier estimate of Regional PFS (months)	median	25.13
	CI95	(7.20 - NE)
	minimum	4.3
	maximum	40.6
Regional PFS rate at	6 months	92.3%
	12 months	61.5%
	18 months	52.8%
	24 months	52.8%
	36 months	31.7%

Note: NE = Not Estimable due to insufficient events.

Table 6. *Distant progression free survival*

DISTANT PROGRESSION FREE SURVIVAL		
Characteristics		*Total N=13*
Distant progression	Number of patients with distant progression	6 (46.2%)
	Number of patients without any distant progression	7 (53.8%)
Kaplan Meier estimate of Distant PFS (months)	median	18.78
	CI95	(4.90-NE)
	minimum	2.6
	maximum	40.6
Distant PFS rate at	6 months	76.9%
	12 months	61.5%
	18 months	53.9%
	24 months	46.2%
	36 months	34.6%

Note: NE = Not Estimable due to insufficient events.

Table 7. *Primary tumor response rates for PERCIST and RECIST 1.1. methods.*

FU interval	2 months		6 months		12 months		24 months	
	PERCIST	RECIST	PERCIST	RECIST	PERCIST	RECIST	PERCIST	RECIST
Number of patients alive	13	13	12	12	10	10	7	7
Number of evaluable patients	11	13	11	10	10	7	7	5
CR	8	0	9	0	8	0	7	0
PR	2	3	0	7	0	7	0	4
SD	1	10	1	5	0	0	0	0
PD	0	0	1	0	2	0	0	1

Abbreviations: FU, follow-up; CR, complete response; PR, partial response; SD, stable disease; PD, progressive disease.
Some lesions were not evaluable on PET imaging due to radio-induced lung inflammation and on CT imaging due to non-measurable target lesions according to RECIST 1.1.

Figure 1. *Evolution of the primary tumor SUL_{peak} at each time point, with median values of 7.40, 2.62, 1.93, 1.92 and 1.41 at baseline, 2, 6, 12 and 24 months post-treatment, respectively. SUL_{peak} decreases dramatically at 2 months after CRT and remains at the background level as seen in SBRT series. P1 and P6 recurred locally at 6 and 12 months, respectively. P3, P4 and P8 died before 1-year follow-up, while P1, P6 and P10 died before 2-year follow-up.*

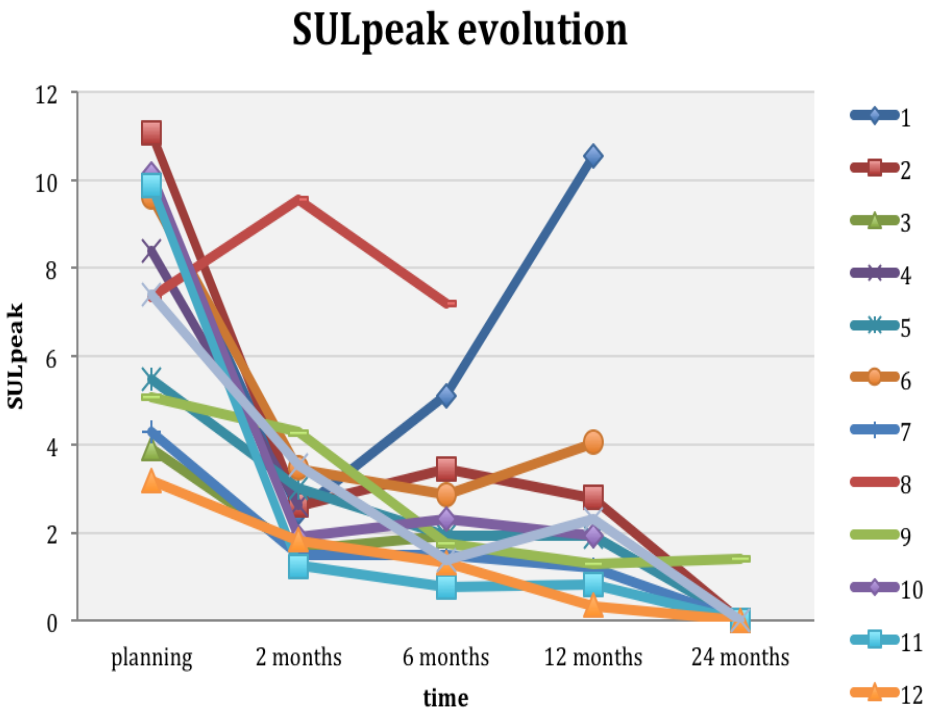

Figure 2. a *Kaplan-Meir curves of overall survival*

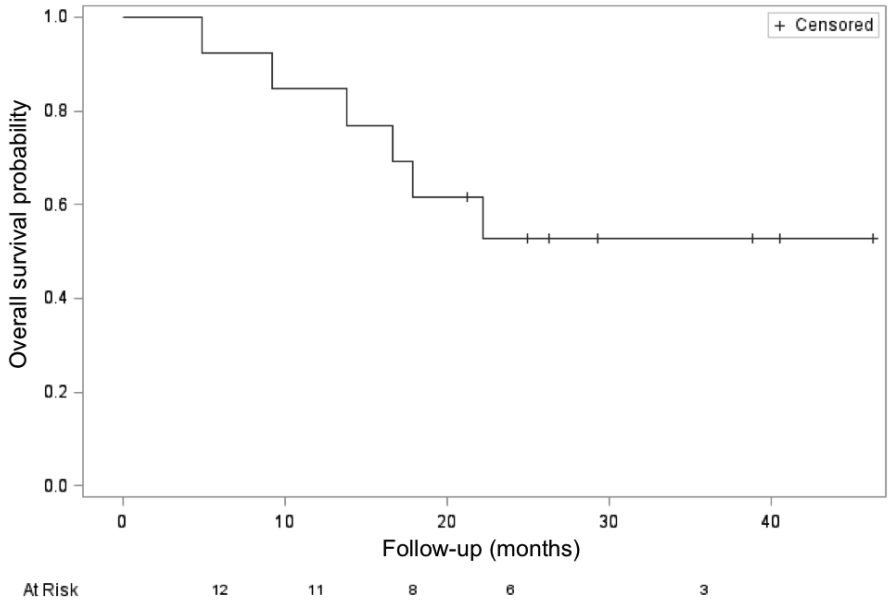

Figure 2. b *Kaplan-Meir curves of overall progression free survival*

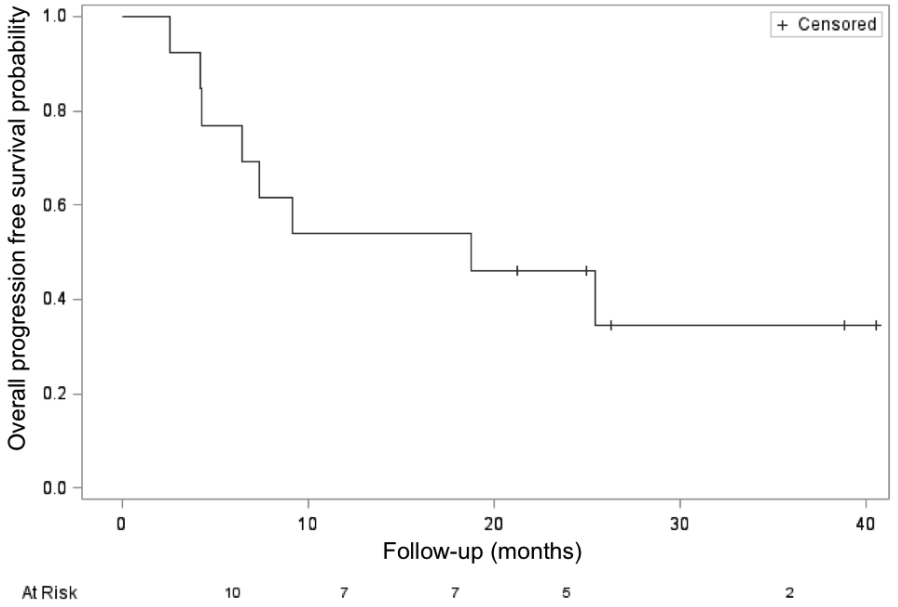

Figure 2. c *Kaplan-Meir curves of local progression free survival*

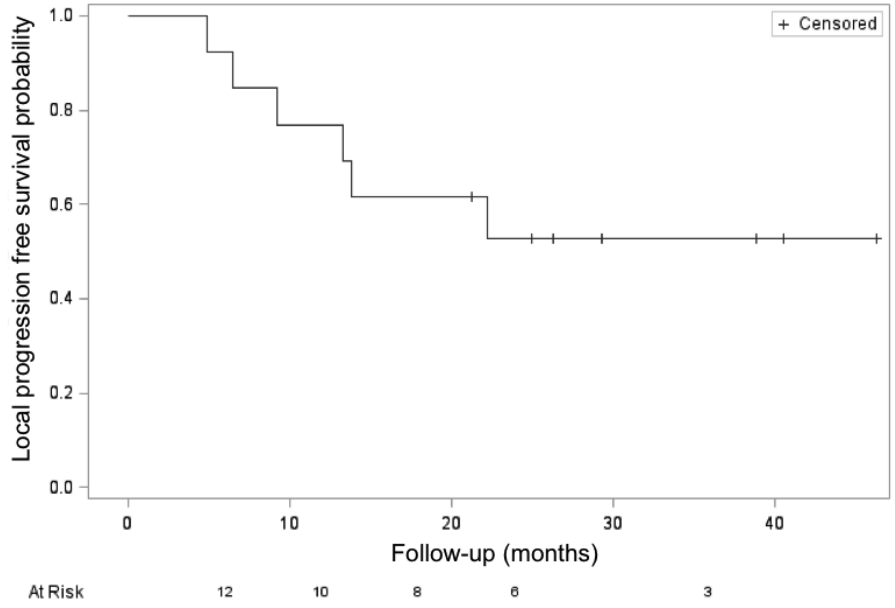

Figure 2. d *Kaplan-Meir curves of regional progression free survival*

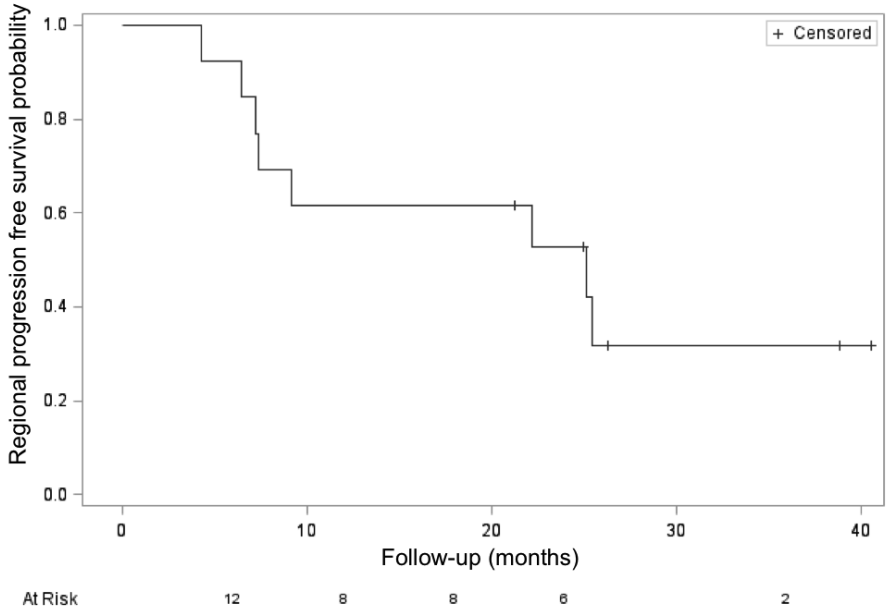

Figure 2. e *Kaplan-Meir curves of distant progression free survival*

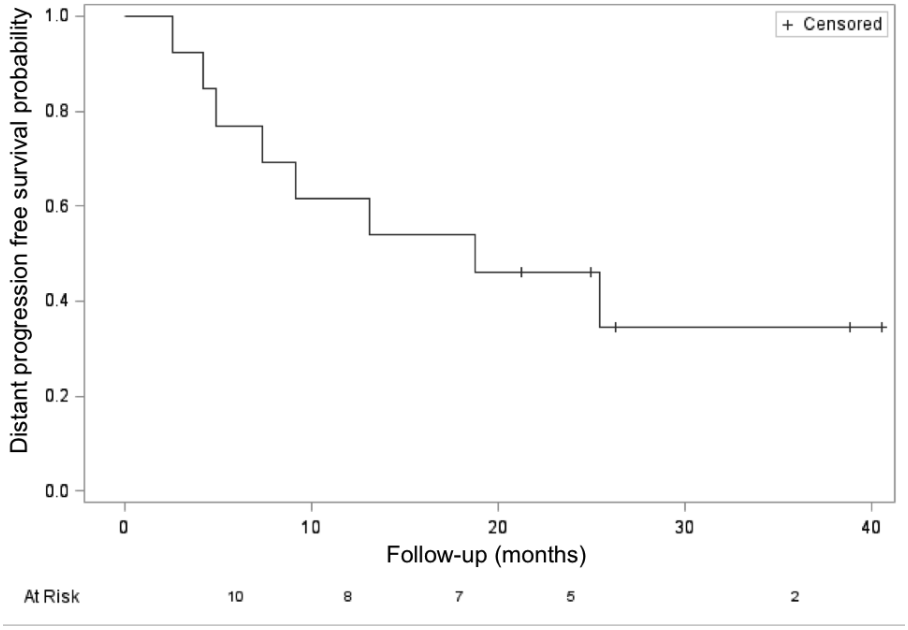

Figure 3. *Diagram of quality of life (QoL) for all patients before, during and after chemo-radiation. QoL is presented as mean ± 1 standard deviation. As expected, it degrades during the treatment but improved 2 months after. The decreasing QoL at 2 years after chemo-radiation relies on tumor recurrences for 7 patients, who received salvage chemotherapy.*

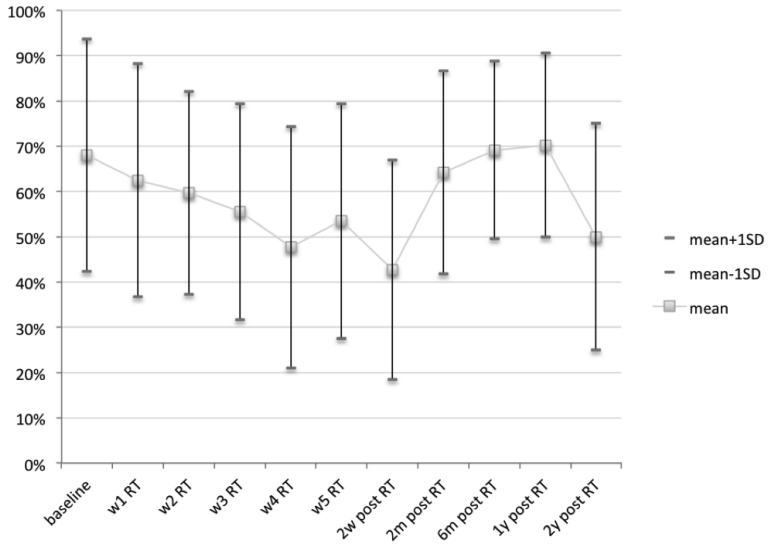

Appendix C : Supplementary data for the mid-position study (Chapter 5)

1. Motion estimation

1.1. Registration of the 4D CT phases

Non-rigid registration was performed between a reference CT phase (maximum exhale phase in this study, as it corresponds to the trigger for both CT and PET reconstruction) and all other phases of the 4D-CT in order to estimate the internal deformations in the thorax. The registration method used in this study was a non-parametric registration which combines the phase-based displacement field estimation of the Morphon algorithm with a diffeomorphic field accumulation [119]. The diffeomorphic accumulation allows us to define the displacement as the transformation resulting from a time-invariant velocity field. The operation that converts velocity into displacement is the field exponential, denoted Φ in the following, and the velocity can then be recovered using the field logarithm. The interest of using the velocity, i.e. working in the "log-domain", is that it becomes possible to perform Euclidean operations on the vector field, which are not consistent when dealing with displacement fields. For instance, the averaging of two velocity fields can be achieved using the mean of vector components, while this does not make sense for displacement fields, as illustrated in Fig. 4 in the case of two diffeomorphic fields D1 and D2 representing equal rotations but in opposite directions. One can clearly see that the mean of the two displacement fields does not reflect the ``average'' transformation but leads to a global ``shrinking''. In the contrary, the mean of corresponding velocity fields V1 and V2 leads to the identity transformation, which reflects the ``average'' transformation.

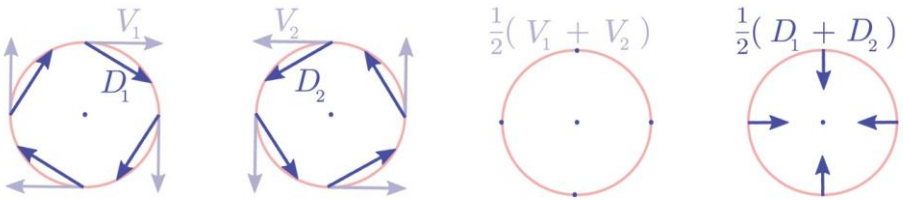

Figure 4. *Computing the average of two invertible displacement fields D1 and D2 using a simple Euclidean operation (mean vector computation) on their time-invariant velocity fields V1=Φ(D1) and V2=Φ(D2).*

1.2. Constrained registration of the 4D PET phases

Once the anatomical deformations have been estimated based on the 4D-CT images, these deformations were used to estimate the motion between PET images by limiting the possible solutions. However, as the binning is different in 4D-PET and 4D CT acquisition, the estimated deformations of the 4D CT may not directly applied on a PET phase. Under the assumption that the breathing is sufficiently reproducible along several cycles, the possible respiratory motions are limited to the trajectory defined by all possible interpolations between 2 successive displacement fields resulting from CT registrations. This interpolation is computed in the log-domain in order to preserve diffeomorphism.

Limiting the motion to the CT-based trajectory reduces the number of optimization variables from 3 times the number of voxels to only 1 variable, which is the temporal position on the trajectory. The registration of PET images then becomes a simple optimization of a metric (sum of square differences was chosen in this study) according to one single variable, which is the position on the trajectory.

Let us denote V(i) the velocity field resulting from the registration between the CT phase i and the reference. The corresponding displacement field is given by D(i) = Φ(V(i)). For each PET phase j, the objective function of the registration process is then given by:

$$\underset{t}{\operatorname{argmin}} \quad \mathcal{M}(p_{ref}, p_j \diamond D(t)),$$

where t is the optimization variable and $p_j \diamond D(t)$ denotes the deformation of the PET phase pj by the displacement field D(t). This field is computed using linear interpolation between velocity fields:

$$D(t) = \Phi\big((\overline{t} - t)V(\underline{t}) + (t - \underline{t})V(\overline{t})\big),$$

where underscore denotes the rounding to the closest lower integer and overscore denotes the rounding to the closest higher integer.

This makes the PET registration very fast, robust and physically meaningful in spite of the lack of reliable information in 4D PET images.

1.3. Mid-position 3D PET reconstruction

The time-weighted average of all inter-CT deformations, which is computed in the log-domain for the reason explained previously, gives the displacement from the reference phase to the average anatomical position (i.e. mid-position). Then the difference between this average deformation and each inter-PET deformation was computed in the log-domain, resulting in a transformation from each PET phase to the mid-position.

The PET phases were deformed accordingly and summed to produce a mid-position 3D PET image.

2. Monte Carlo (MC) simulations: detailed results

2.1. MC results for primary tumor volumes defined on CT image

Table reporting, for each patient, the relative difference for various dose-volume histograms (DVH) metrics between the 3D MC planned dose distributions and Interplay Simulated (IS) or No Interplay (NI) dose distributions calculated using a 4D MC model for both concepts, i.e. mid-position and ITV.

	Patient no	Parameters	PTV_{CT} P	CTV_{CT}^{exp} IS	Δ	CTV_{CT}^{exp} NI	Δ	PTV_{CT} P	CTV_{CT}^{exp} IS	Δ	CTV_{CT}^{exp} NI	Δ
			MidP (Gy)	MidP (Gy)	MidP (%)	MidP (Gy)	MidP (%)	ITV (Gy)	ITV (Gy)	ITV (%)	ITV (Gy)	ITV (%)
SBRT	1	D_{mean}	56.13	56.16	0.06	56.24	0.22	58.58	59.69	2.05	59.70	2.07
		D_{99}	51.31	52.01	1.29	52.01	1.29	51.54	56.16	8.55	56.09	8.43
		D_{95}	54.11	53.53	-1.07	53.55	-1.03	54.30	57.57	6.05	57.54	5.99
		D_2	58.14	58.39	0.46	58.40	0.48	61.07	61.84	1.43	61.75	1.27
	2	D_{mean}	55.89	55.42	-0.87	55.48	-0.76	57.78	57.94	0.29	58.04	0.48
		D_{99}	53.03	52.57	-0.85	52.68	-0.66	52.60	55.88	6.09	55.98	6.26
		D_{95}	54.08	53.67	-0.76	53.81	-0.50	54.45	56.61	4.00	56.72	4.21
		D_2	58.49	57.45	-1.94	57.31	-2.19	60.56	59.72	-1.55	59.91	-1.20
	3	D_{mean}	63.53	62.98	-0.91	63.04	-0.83	64.03	63.72	-0.52	63.81	-0.36
		D_{99}	56.93	56.36	-0.95	56.42	-0.84	57.01	57.43	0.69	57.69	1.12
		D_{95}	60.25	59.78	-0.79	59.80	-0.76	60.37	60.58	0.34	60.77	0.67
		D_2	66.40	65.70	-1.17	65.72	-1.13	67.01	66.40	-1.02	66.48	-0.88
	4	D_{mean}	55.87	54.84	-1.90	54.67	-2.23	56.48	55.73	-1.39	55.87	-1.13
		D_{99}	52.98	51.81	-2.16	51.88	-2.02	53.00	53.70	1.31	53.78	1.45
		D_{95}	54.20	52.79	-2.61	52.70	-2.79	54.29	54.30	0.02	54.41	0.22
		D_2	57.58	57.14	-0.80	56.70	-1.62	58.37	57.37	-1.85	57.32	-1.93
	5	D_{mean}	51.21	50.61	-1.26	51.57	0.75	51.84	52.63	1.64	52.75	1.89
		D_{99}	46.47	43.01	-7.20	45.71	-1.59	46.27	49.06	5.82	49.20	6.10
		D_{95}	48.41	46.32	-4.35	48.22	-0.40	48.58	50.41	3.82	50.63	4.26
		D_2	53.19	53.61	0.86	53.34	0.31	54.04	54.42	0.80	54.39	0.73
	6	D_{mean}	55.96	55.93	-0.06	55.99	0.04	58.57	59.36	1.47	59.42	1.57
		D_{99}	53.26	52.98	-0.51	53.11	-0.28	51.79	56.06	7.91	56.05	7.89
		D_{95}	54.17	54.36	0.36	54.34	0.32	54.51	57.65	5.82	57.71	5.92
		D_2	57.85	57.47	-0.71	57.60	-0.47	61.07	60.70	-0.70	60.80	-0.50
	7	D_{mean}	57.50	56.85	-1.21	56.88	-1.15	58.56	58.55	-0.02	58.60	0.08
		D_{99}	52.16	52.41	0.46	52.38	0.40	52.24	55.02	5.14	55.05	5.20
		D_{95}	54.25	53.89	-0.67	53.87	-0.71	54.33	56.41	3.85	56.46	3.95
		D_2	60.08	59.06	-1.88	59.22	-1.58	61.56	60.79	-1.43	60.79	-1.43
	8	D_{mean}	56.63	55.27	-2.52	55.27	-2.52	56.91	57.14	0.41	57.14	0.41
		D_{99}	52.49	51.76	-1.36	51.76	-1.36	52.39	54.32	3.57	54.17	3.29
		D_{95}	54.24	53.07	-2.16	53.08	-2.15	54.25	55.29	1.92	55.27	1.89
		D_2	58.43	56.80	-3.01	56.80	-3.01	59.03	58.72	-0.58	58.67	-0.67

SIB	9	D_{mean}	77.62	77.60	-0.03	77.75	0.21	76.89	78.18	2.08	78.23	2.14
		D_{99}	60.87	60.66	-0.33	61.05	0.30	59.92	61.62	2.72	61.67	2.80
		D_{95}	63.51	63.43	-0.13	63.71	0.33	62.58	64.46	3.01	64.41	2.93
		D_2	87.11	86.70	-0.66	86.83	-0.46	87.60	87.33	-0.44	87.37	-0.38
	10	D_{mean}	78.48	78.51	0.05	78.55	0.11	77.97	79.14	1.87	79.16	1.90
		D_{99}	60.23	60.61	0.62	60.49	0.42	58.89	61.21	3.72	61.12	3.58
		D_{95}	62.81	63.23	0.67	63.20	0.62	61.62	62.80	1.89	62.81	1.90
		D_2	88.67	88.42	-0.39	88.47	-0.31	87.80	87.64	-0.24	87.58	-0.34
	11	D_{mean}	110.51	110.19	-0.51	110.34	-0.28	92.07	94.29	3.56	94.43	3.77
		D_{99}	68.24	69.52	2.04	69.42	1.89	54.58	59.35	7.63	59.34	7.62
		D_{95}	86.62	87.09	0.76	87.07	0.72	69.89	74.47	7.32	74.46	7.31
		D_2	124.64	123.93	-1.13	124.15	-0.77	106.50	106.22	-0.45	106.28	-0.35
	12	D_{mean}	65.88	66.15	0.45	66.23	0.56	64.57	65.36	1.25	65.43	1.37
		D_{99}	54.69	55.57	1.40	55.56	1.39	52.67	55.88	5.13	56.06	5.43
		D_{95}	61.44	61.81	0.59	61.94	0.79	60.18	60.57	0.63	60.82	1.02
		D_2	76.50	76.65	0.23	76.65	0.23	75.58	75.92	0.55	75.91	0.53
	13	D_{mean}	66.29	66.05	-0.39	66.12	-0.27	66.94	67.22	0.44	67.25	0.49
		D_{99}	58.35	57.61	-1.18	57.62	-1.16	58.66	62.07	5.47	62.12	5.54
		D_{95}	61.79	61.30	-0.79	61.45	-0.54	62.61	64.04	2.29	64.29	2.69
		D_2	71.99	71.81	-0.29	71.51	-0.78	71.41	71.50	0.14	70.91	-0.81
	14	D_{mean}	73.01	72.70	-0.49	72.73	-0.44	70.66	71.79	1.81	72.09	2.29
		D_{99}	59.66	59.46	-0.33	59.63	-0.05	58.03	60.22	3.51	60.40	3.79
		D_{95}	62.20	61.99	-0.34	62.08	-0.20	60.51	61.39	1.41	61.57	1.70
		D_2	84.82	84.03	-1.26	84.13	-1.11	85.96	85.96	-1.37	85.56	-0.64
	15	Dmean	70.76	70.92	0.25	70.98	0.35	70.59	72.60	3.21	72.68	3.34
		D99	56.64	58.28	2.61	58.30	2.64	56.60	60.18	5.72	60.15	5.67
		D95	60.81	61.18	0.59	61.26	0.72	60.57	61.37	1.28	61.59	1.63
		D2	83.14	82.37	-1.23	82.47	-1.07	83.64	83.05	-0.94	83.06	-0.92

Abbreviations: Patient no, PTV_{CT}, Planning Target Volume defined on CT images; $^{CTV_{CT}^{exp}}$, modified CTV volumes expanded by all geometric uncertainties except the tumor motion; Δ, the relative difference for various DVH metrics between the 3D MC planned (P) dose distributions and Interplay Simulated (IS) or No Interplay (NI) dose distributions; SBRT, Stereotactic Body Radiation Therapy; SIB, Simultaneous Integrated Boost; MidP, mid-position; ITV, Internal Target Volume.

2.2. MC results for primary tumor volumes defined on PET images

Table reporting, for each patient, the relative difference for various dose-volume histograms (DVH) metrics between the 3D MC planned dose distributions and Interplay Simulated (IS) or No Interplay (NI) dose distributions calculated using a 4D MC model for both concepts, i.e. mid-position and ITV.

	Patient no	Parameters	PTV_{PET} P MidP (Gy)	GTV_{PET}^{exp} IS MidP (Gy)	Δ MidP (%)	GTV_{PET}^{exp} NI MidP (Gy)	Δ MidP (%)	PTV_{PET} P ITV (Gy)	GTV_{PET}^{exp} IS ITV (Gy)	Δ ITV (%)	GTV_{PET}^{exp} NI ITV (Gy)	Δ ITV (%)
SIB	9	D_{mean}	83.70	83.67	-0.04	83.81	0.13	83.84	83.93	0.11	84.02	0.21
		D_{99}	77.52	77.49	-0.03	77.64	0.15	77.71	78.07	0.44	78.07	0.44
		D_{95}	79.53	79.68	0.19	79.78	0.30	79.53	79.92	0.47	79.96	0.52
		D_2	88.12	87.72	-0.49	87.82	-0.37	88.59	88.14	-0.55	88.24	-0.44
	10	D_{mean}	86.19	86.06	-0.16	86.19	0.00	89.58	89.68	0.11	89.67	0.10
		D_{99}	79.59	79.76	0.21	79.92	0.40	83.31	83.79	0.57	83.69	0.45
		D_{95}	82.17	82.01	-0.19	82.25	0.10	85.52	85.88	0.43	85.86	0.40
		D_2	90.01	89.88	-0.16	89.79	-0.27	92.67	92.51	-0.19	92.42	-0.29
	11	D_{mean}	119.79	119.26	-0.44	119.41	-0.31	123.91	124.89	0.82	125.04	0.94
		D_{99}	113.95	113.19	-0.64	113.37	-0.48	111.98	118.34	5.31	118.77	5.66
		D_{95}	115.57	115.15	-0.35	115.31	-0.22	117.19	120.51	2.76	120.74	2.96
		D_2	124.55	123.73	-0.69	123.93	-0.52	130.23	129.78	-0.37	129.89	-0.28
	12	D_{mean}	75.49	75.71	0.29	75.76	0.36	74.67	74.95	0.38	74.99	0.43
		D_{99}	71.82	72.27	0.61	72.45	0.84	70.99	71.50	0.68	71.59	0.79
		D_{95}	72.76	73.08	0.43	73.23	0.62	71.91	72.28	0.50	72.36	0.60
		D_2	78.09	77.95	-0.19	78.07	-0.03	77.99	78.15	0.21	78.19	0.26
	13	D_{mean}	67.89	67.67	-0.34	67.77	-0.19	67.81	67.75	-0.09	67.80	-0.02
		D_{99}	63.57	63.57	0.00	63.98	0.60	63.26	63.53	0.40	64.13	1.30
		D_{95}	64.73	64.66	-0.11	64.91	0.26	64.74	64.60	-0.20	65.05	0.47
		D_2	72.09	71.91	-0.28	71.51	-0.87	71.35	71.40	0.08	70.73	-0.91
	14	D_{mean}	83.24	82.75	-0.60	82.81	-0.52	83.17	82.73	-0.53	83.15	-0.03
		D_{99}	77.80	77.93	0.15	78.02	0.26	77.69	78.43	0.90	78.98	1.57
		D_{95}	80.60	80.44	-0.20	80.41	-0.24	79.32	79.67	0.42	80.16	1.02
		D_2	85.74	84.87	-1.06	85.00	-0.89	87.00	86.00	-1.21	86.51	-0.59
	15	Dmean	80.74	80.48	-0.32	80.57	-0.22	80.90	80.70	-0.24	80.79	-0.14
		D99	75.50	76.00	0.63	75.84	0.43	76.71	77.34	0.78	77.51	0.99
		D95	76.94	77.50	0.70	77.52	0.72	78.00	78.38	0.48	78.42	0.53
		D2	84.30	83.34	-1.21	83.43	-1.09	84.61	83.67	-1.18	83.70	-1.14

Abbreviations: Patient no, PTV_{PET}, Planning Target Volume defined on PET images; GTV_{PET}^{exp}, modified GTV volumes expanded by all geometric uncertainties except the tumor motion; Δ, the relative difference for various DVH metrics between the 3D MC planned (P) dose distributions and Interplay Simulated (IS) or No Interplay (NI) dose distributions; SIB, Simultaneous Integrated Boost; MidP, mid-position; ITV, Internal Target Volume

2.3. MC results for lymph node volumes defined on CT images

Table reporting, for each patient, the relative difference for various dose-volume histograms (DVH) metrics between the 3D MC planned dose distributions and Interplay Simulated (IS) or No Interplay (NI) dose distributions calculated using a 4D MC model for both concepts, i.e. mid-position and ITV.

	Patient no	Parameters	PTV_{CT} P	CTV_{CT}^{exp} IS	Δ	CTV_{CT}^{exp} NI	Δ	PTV_{CT} P	CTV_{CT}^{exp} IS	Δ	CTV_{CT}^{exp} NI	Δ
			MidP (Gy)	MidP (Gy)	MidP (%)	MidP (Gy)	MidP (%)	ITV (Gy)	ITV (Gy)	ITV (%)	ITV (Gy)	ITV (%)
SIB	9	D_{mean}	-	-	-	-	-	-	-	-	-	-
		D_{99}	-	-	-	-	-	-	-	-	-	-
		D_{95}	-	-	-	-	-	-	-	-	-	-
		D_2	-	-	-	-	-	-	-	-	-	-
	10	D_{mean}	63.79	63.63	-0.26	63.67	-0.20	63.23	63.33	0.16	63.42	0.29
		D_{99}	58.66	57.27	-2.23	57.87	-1.27	57.02	60.37	5.36	60.54	5.63
		D_{95}	60.88	60.34	-0.86	60.71	-0.28	60.29	61.14	1.36	61.35	1.69
		D_2	74.79	73.13	-2.65	72.92	-3.00	76.63	73.99	-4.22	74.18	-3.91
	11	D_{mean}	62.28	62.29	0.02	62.21	-0.11	63.78	64.05	0.44	64.01	0.37
		D_{99}	58.44	58.66	0.36	58.66	0.36	55.29	60.39	8.15	60.35	8.09
		D_{95}	59.63	59.75	0.20	59.70	0.11	59.57	61.48	3.05	61.43	2.97
		D_2	73.92	74.36	0.70	74.10	0.29	79.51	76.48	-4.85	76.33	-5.10
	12	D_{mean}	63.22	63.32	0.16	63.38	0.26	61.57	61.77	0.33	61.84	0.43
		D_{99}	59.41	59.58	0.28	59.47	0.10	58.51	59.45	1.51	59.77	2.02
		D_{95}	61.18	61.21	0.05	61.50	0.51	59.69	60.13	0.71	60.44	1.20
		D_2	65.98	65.80	-0.30	65.82	-0.26	64.91	64.56	-0.56	64.45	-0.72
	13	D_{mean}	62.85	62.72	-0.22	62.85	0.00	64.12	64.11	-0.02	64.20	0.13
		D_{99}	59.33	59.16	-0.27	59.26	-0.10	59.91	61.35	2.31	61.67	2.82
		D_{95}	60.96	60.96	0.00	61.12	0.25	62.01	62.57	0.89	62.73	1.15
		D_2	65.22	65.12	-0.17	65.17	-0.08	66.88	66.39	-0.79	66.26	-1.01
	14	D_{mean}	65.13	64.58	-0.88	64.63	-0.80	64.46	63.68	-1.25	63.77	-1.10
		D_{99}	60.17	60.03	-0.23	60.19	0.03	59.62	60.35	1.17	60.51	1.43
		D_{95}	61.43	61.24	-0.31	61.29	-0.23	60.95	60.97	0.03	61.04	0.15
		D_2	81.75	80.89	-1.38	80.86	-1.43	83.14	79.80	-5.34	79.93	-5.14
	15	Dmean	-	-	-	-	-	-	-	-	-	-
		D99	-	-	-	-	-	-	-	-	-	-
		D95	-	-	-	-	-	-	-	-	-	-
		D2	-	-	-	-	-	-	-	-	-	-

Abbreviations: Patient no, PTV_{CT}, Planning Target Volume defined on CT images; CTV_{CT}^{exp}, modified GTV volumes expanded by all geometric uncertainties except the tumor motion; Δ, the relative difference for various DVH metrics between the 3D MC planned (P) dose distributions and Interplay Simulated (IS) or No Interplay (NI) dose distributions; SIB, Simultaneous Integrated Boost; MidP, mid-position; ITV, Internal Target Volume

Chapter 8

Bibliography

[1] Belgian Cancer Registry. Cancer survival in Belgium 2004-2008. 2012;Brussels.
[2] Wauters I RJ, Verleye L, Holdt Henningsen K, Hulstaert F, Berghmans T, De Wever W, Lievens Y, Pauwels P, Stroobants S, Van Houtte P, Van Meerbeeck J, Van Schil P, Weynand B, De Grève J. Small Cell and Non-Small Cell Lung Cancer: Diagnosis, Treatment and Follow-up. Good Clinical Practice (GCP). Brussels: Belgian Health Care Knowledge Centre (KCE) KCE Reports 206. 2013.
[3] Delaney G, Jacob S, Featherstone C, Barton M. The role of radiotherapy in cancer treatment: estimating optimal utilization from a review of evidence-based clinical guidelines. Cancer. 2005;104:1129-37.
[4] Zatloukal P, Petruzelka L, Zemanova M, et al. Concurrent versus sequential chemoradiotherapy with cisplatin and vinorelbine in locally advanced non-small cell lung cancer: a randomized study. Lung cancer. 2004;46:87-98.
[5] Fournel P, Robinet G, Thomas P, et al. Randomized phase III trial of sequential chemoradiotherapy compared with concurrent chemoradiotherapy in locally advanced non-small-cell lung cancer: Groupe Lyon-Saint-Etienne d'Oncologie Thoracique-Groupe Francais de Pneumo-Cancerologie NPC 95-01 Study. Journal of clinical oncology : official journal of the American Society of Clinical Oncology. 2005;23:5910-7.
[6] Furuse K, Fukuoka M, Kawahara M, et al. Phase III study of concurrent versus sequential thoracic radiotherapy in combination with mitomycin, vindesine, and cisplatin in unresectable stage III non-small-cell lung cancer. Journal of clinical oncology : official journal of the American Society of Clinical Oncology. 1999;17:2692-9.
[7] Auperin A, Le Pechoux C, Rolland E, et al. Meta-analysis of concomitant versus sequential radiochemotherapy in locally advanced non-small-cell lung cancer. Journal of clinical oncology : official journal of the American Society of Clinical Oncology. 2010;28:2181-90.
[8] Auperin A, Le Pechoux C, Pignon JP, et al. Concomitant radio-chemotherapy based on platin compounds in patients with locally advanced non-small cell lung cancer (NSCLC): a meta-analysis of individual data from 1764 patients. Annals of oncology : official journal of the European Society for Medical Oncology / ESMO. 2006;17:473-83.

[9] Martel MK, Ten Haken RK, Hazuka MB, et al. Estimation of tumor control probability model parameters from 3-D dose distributions of non-small cell lung cancer patients. Lung cancer. 1999;24:31-7.
[10] Machtay M, Hsu C, Komaki R, et al. Effect of overall treatment time on outcomes after concurrent chemoradiation for locally advanced non-small-cell lung carcinoma: analysis of the Radiation Therapy Oncology Group (RTOG) experience. International journal of radiation oncology, biology, physics. 2005;63:667-71.
[11] Fowler JF, Chappell R. Non-small cell lung tumors repopulate rapidly during radiation therapy. International journal of radiation oncology, biology, physics. 2000;46:516-7.
[12] Saunders M, Dische S, Barrett A, et al. Continuous, hyperfractionated, accelerated radiotherapy (CHART) versus conventional radiotherapy in non-small cell lung cancer: mature data from the randomised multicentre trial. CHART Steering committee. Radiotherapy and oncology : journal of the European Society for Therapeutic Radiology and Oncology. 1999;52:137-48.
[13] van Baardwijk A, Bosmans G, Bentzen SM, et al. Radiation dose prescription for non-small-cell lung cancer according to normal tissue dose constraints: an in silico clinical trial. International journal of radiation oncology, biology, physics. 2008;71:1103-10.
[14] Aerts HJ, Bosmans G, van Baardwijk AA, et al. Stability of 18F-deoxyglucose uptake locations within tumor during radiotherapy for NSCLC: a prospective study. International journal of radiation oncology, biology, physics. 2008;71:1402-7.
[15] van Baardwijk A, Wanders S, Boersma L, et al. Mature results of an individualized radiation dose prescription study based on normal tissue constraints in stages I to III non-small-cell lung cancer. Journal of clinical oncology : official journal of the American Society of Clinical Oncology. 2010;28:1380-6.
[16] van Baardwijk A, Reymen B, Wanders S, et al. Mature results of a phase II trial on individualised accelerated radiotherapy based on normal tissue constraints in concurrent chemo-radiation for stage III non-small cell lung cancer. European journal of cancer. 2012;48:2339-46.
[17] De Ruysscher D, van Baardwijk A, Steevens J, et al. Individualised isotoxic accelerated radiotherapy and chemotherapy are associated with improved long-term survival of patients with stage III NSCLC: a prospective population-based study. Radiotherapy and oncology :

journal of the European Society for Therapeutic Radiology and Oncology. 2012;102:228-33.
[18] Prescribing, Recording, and Reporting Photon-Beam Intensity-Modulated Radiation Therapy (IMRT): Contents. Journal of the ICRU. 2010;10:NP.
[19] Rodrigues G, Lock M, D'Souza D, Yu E, Van Dyk J. Prediction of radiation pneumonitis by dose - volume histogram parameters in lung cancer--a systematic review. Radiotherapy and oncology : journal of the European Society for Therapeutic Radiology and Oncology. 2004;71:127-38.
[20] Marks LB, Bentzen SM, Deasy JO, et al. Radiation dose-volume effects in the lung. International journal of radiation oncology, biology, physics. 2010;76:S70-6.
[21] Yom SS, Liao Z, Liu HH, et al. Initial evaluation of treatment-related pneumonitis in advanced-stage non-small-cell lung cancer patients treated with concurrent chemotherapy and intensity-modulated radiotherapy. International journal of radiation oncology, biology, physics. 2007;68:94-102.
[22] Song CH, Pyo H, Moon SH, et al. Treatment-related pneumonitis and acute esophagitis in non-small-cell lung cancer patients treated with chemotherapy and helical tomotherapy. International journal of radiation oncology, biology, physics. 2010;78:651-8.
[23] Vinogradskiy Y, Tucker SL, Liao Z, Martel MK. Balancing radiation pneumonitis versus locoregional tumor control in non-small-cell lung cancer. Journal of thoracic oncology : official publication of the International Association for the Study of Lung Cancer. 2013;8:e47-8.
[24] Shi A, Zhu G, Wu H, et al. Analysis of clinical and dosimetric factors associated with severe acute radiation pneumonitis in patients with locally advanced non-small cell lung cancer treated with concurrent chemotherapy and intensity-modulated radiotherapy. Radiation oncology. 2010;5:35.
[25] Schallenkamp JM, Miller RC, Brinkmann DH, Foote T, Garces YI. Incidence of radiation pneumonitis after thoracic irradiation: Dose-volume correlates. International journal of radiation oncology, biology, physics. 2007;67:410-6.
[26] Kwa SL, Lebesque JV, Theuws JC, et al. Radiation pneumonitis as a function of mean lung dose: an analysis of pooled data of 540 patients. International journal of radiation oncology, biology, physics. 1998;42:1-9.

[27] De Ruysscher D, Faivre-Finn C, Nestle U, et al. European Organisation for Research and Treatment of Cancer recommendations for planning and delivery of high-dose, high-precision radiotherapy for lung cancer. Journal of clinical oncology : official journal of the American Society of Clinical Oncology. 2010;28:5301-10.
[28] Kirkpatrick JP, van der Kogel AJ, Schultheiss TE. Radiation dose-volume effects in the spinal cord. International journal of radiation oncology, biology, physics. 2010;76:S42-9.
[29] Werner-Wasik M, Yorke E, Deasy J, Nam J, Marks LB. Radiation dose-volume effects in the esophagus. International journal of radiation oncology, biology, physics. 2010;76:S86-93.
[30] De Ruysscher D, Dehing C, Bremer RH, et al. Maximal neutropenia during chemotherapy and radiotherapy is significantly associated with the development of acute radiation-induced dysphagia in lung cancer patients. Annals of oncology : official journal of the European Society for Medical Oncology / ESMO. 2007;18:909-16.
[31] Belderbos J, Heemsbergen W, Hoogeman M, et al. Acute esophageal toxicity in non-small cell lung cancer patients after high dose conformal radiotherapy. Radiotherapy and oncology : journal of the European Society for Therapeutic Radiology and Oncology. 2005;75:157-64.
[32] Gayed IW, Liu HH, Yusuf SW, et al. The prevalence of myocardial ischemia after concurrent chemoradiation therapy as detected by gated myocardial perfusion imaging in patients with esophageal cancer. Journal of nuclear medicine : official publication, Society of Nuclear Medicine. 2006;47:1756-62.
[33] Syed WY SS, Iyad ND. Radiation-induced heart disease: A clinical update. Cardiology Research and Practice. 2011.
[34] Gagliardi G, Constine LS, Moiseenko V, et al. Radiation dose-volume effects in the heart. International journal of radiation oncology, biology, physics. 2010;76:S77-85.
[35] Bradley JD, Paulus R, Komaki R, et al. Standard-dose versus high-dose conformal radiotherapy with concurrent and consolidation carboplatin plus paclitaxel with or without cetuximab for patients with stage IIIA or IIIB non-small-cell lung cancer (RTOG 0617): a randomised, two-by-two factorial phase 3 study. The Lancet Oncology. 2015;16:187-99.
[36] Vivekanandan S. Dose-escalated radiotherapy for NSCLC: Heart doses versus survival in IDEAL-CRT (ID 454). MINI3302 IASLC, Denver. 2015.

[37] Kelsey CR, Kahn D, Hollis DR, et al. Radiation-induced narrowing of the tracheobronchial tree: an in-depth analysis. Lung cancer. 2006;52:111-6.
[38] Langendijk JA, Tjwa MK, de Jong JM, ten Velde GP, Wouters EF. Massive haemoptysis after radiotherapy in inoperable non-small cell lung carcinoma: is endobronchial brachytherapy really a risk factor? Radiotherapy and oncology : journal of the European Society for Therapeutic Radiology and Oncology. 1998;49:175-83.
[39] Miller KL, Shafman TD, Anscher MS, et al. Bronchial stenosis: an underreported complication of high-dose external beam radiotherapy for lung cancer? International journal of radiation oncology, biology, physics. 2005;61:64-9.
[40] Emami B, Lyman J, Brown A, et al. Tolerance of normal tissue to therapeutic irradiation. International journal of radiation oncology, biology, physics. 1991;21:109-22.
[41] Hall WH, Guiou M, Lee NY, et al. Development and validation of a standardized method for contouring the brachial plexus: preliminary dosimetric analysis among patients treated with IMRT for head-and-neck cancer. International journal of radiation oncology, biology, physics. 2008;72:1362-7.
[42] van Herk M, Remeijer P, Rasch C, Lebesque JV. The probability of correct target dosage: dose-population histograms for deriving treatment margins in radiotherapy. International journal of radiation oncology, biology, physics. 2000;47:1121-35.
[43] Seppenwoolde Y, Shirato H, Kitamura K, et al. Precise and real-time measurement of 3D tumor motion in lung due to breathing and heartbeat, measured during radiotherapy. Int J Radiat Oncol Biol Phys. 2002;53:822-34.
[44] Liu HH, Balter P, Tutt T, et al. Assessing respiration-induced tumor motion and internal target volume using four-dimensional computed tomography for radiotherapy of lung cancer. International journal of radiation oncology, biology, physics. 2007;68:531-40.
[45] Rietzel E, Chen GTY. 4D Imaging and Treatment Planning. New Technologies in Radiation Oncology: Springer Berlin Heidelberg; 2006. p. PP 81-97.
[46] Bouilhol G. Uncertainties and motion management in lung radiotherapy:

from photons to ions. Thesis. 2013.

[47] Sonke JJ, Lebesque J, van Herk M. Variability of four-dimensional computed tomography patient models. International journal of radiation oncology, biology, physics. 2008;70:590-8.
[48] Bowden P, Fisher R, Mac Manus M, et al. Measurement of lung tumor volumes using three-dimensional computer planning software. Int J Radiat Oncol Biol Phys. 2002;53:566-73.
[49] Caldwell CB, Mah K, Ung YC, et al. Observer variation in contouring gross tumor volume in patients with poorly defined non-small-cell lung tumors on CT: the impact of 18FDG-hybrid PET fusion. International journal of radiation oncology, biology, physics. 2001;51:923-31.
[50] Giraud P, Elles S, Helfre S, et al. Conformal radiotherapy for lung cancer: different delineation of the gross tumor volume (GTV) by radiologists and radiation oncologists. Radiother Oncol. 2002;62:27-36.
[51] Macpherson RE, Higgins GS, Murchison JT, et al. Non-small-cell lung cancer dimensions: CT-pathological correlation and interobserver variation. Br J Radiol. 2009;82:421-5.
[52] Senan S, van Sornsen de Koste J, Samson M, et al. Evaluation of a target contouring protocol for 3D conformal radiotherapy in non-small cell lung cancer. Radiotherapy and oncology : journal of the European Society for Therapeutic Radiology and Oncology. 1999;53:247-55.
[53] Steenbakkers RJ, Duppen JC, Fitton I, et al. Observer variation in target volume delineation of lung cancer related to radiation oncologist-computer interaction: a 'Big Brother' evaluation. Radiother Oncol. 2005;77:182-90.
[54] Van de Steene J, Linthout N, de Mey J, et al. Definition of gross tumor volume in lung cancer: inter-observer variability. Radiother Oncol. 2002;62:37-49.
[55] Vorwerk H, Beckmann G, Bremer M, et al. The delineation of target volumes for radiotherapy of lung cancer patients. Radiother Oncol. 2009;91:455-60.
[56] Khan FM. The physics of radiation therapy. 2003;3rd ed.
[57] van Herk M, Remeijer P, Lebesque JV. Inclusion of geometric uncertainties in treatment plan evaluation. International journal of radiation oncology, biology, physics. 2002;52:1407-22.
[58] Witte MG, van der Geer J, Schneider C, et al. IMRT optimization including random and systematic geometric errors based on the expectation of TCP and NTCP. Medical physics. 2007;34:3544-55.

[59] Boellaard R, Delgado-Bolton R, Oyen WJ, et al. FDG PET/CT: EANM procedure guidelines for tumour imaging: version 2.0. European journal of nuclear medicine and molecular imaging. 2015;42:328-54.
[60] James W, Waterlow J. U.K. Department of Health and Social Security/Medical Research Council Group on Obesity Research. Research on obesity: A report of DSHH/MRC Group. London, England: H.M.S.O. 1976.
[61] Young H, Baum R, Cremerius U, et al. Measurement of clinical and subclinical tumour response using [18F]-fluorodeoxyglucose and positron emission tomography: review and 1999 EORTC recommendations. European Organization for Research and Treatment of Cancer (EORTC) PET Study Group. European journal of cancer. 1999;35:1773-82.
[62] Wahl RL, Jacene H, Kasamon Y, Lodge MA. From RECIST to PERCIST: Evolving Considerations for PET response criteria in solid tumors. Journal of nuclear medicine : official publication, Society of Nuclear Medicine. 2009;50 Suppl 1:122S-50S.
[63] Borst GR, Belderbos JS, Boellaard R, et al. Standardised FDG uptake: a prognostic factor for inoperable non-small cell lung cancer. European journal of cancer. 2005;41:1533-41.
[64] van Baardwijk A, Bosmans G, Dekker A, et al. Time trends in the maximal uptake of FDG on PET scan during thoracic radiotherapy. A prospective study in locally advanced non-small cell lung cancer (NSCLC) patients. Radiotherapy and oncology : journal of the European Society for Therapeutic Radiology and Oncology. 2007;82:145-52.
[65] Mac Manus MP, Hicks RJ, Matthews JP, et al. Metabolic (FDG-PET) response after radical radiotherapy/chemoradiotherapy for non-small cell lung cancer correlates with patterns of failure. Lung Cancer. 2005;49:95-108.
[66] Vera P, Mezzani-Saillard S, Edet-Sanson A, et al. FDG PET during radiochemotherapy is predictive of outcome at 1 year in non-small-cell lung cancer patients: a prospective multicentre study (RTEP2). European journal of nuclear medicine and molecular imaging. 2014;41:1057-65.
[67] Aerts HJ, Bussink J, Oyen WJ, et al. Identification of residual metabolic-active areas within NSCLC tumours using a pre-radiotherapy FDG-PET-CT scan: a prospective validation. Lung cancer. 2012;75:73-6.
[68] Aerts HJ, van Baardwijk AA, Petit SF, et al. Identification of residual metabolic-active areas within individual NSCLC tumours using a pre-

radiotherapy (18)Fluorodeoxyglucose-PET-CT scan. Radiother Oncol. 2009;91:386-92.
[69] Petit SF, Aerts HJ, van Loon JG, et al. Metabolic control probability in tumour subvolumes or how to guide tumour dose redistribution in non-small cell lung cancer (NSCLC): an exploratory clinical study. Radiotherapy and oncology : journal of the European Society for Therapeutic Radiology and Oncology. 2009;91:393-8.
[70] Nestle U, Walter K, Schmidt S, et al. 18F-deoxyglucose positron emission tomography (FDG-PET) for the planning of radiotherapy in lung cancer: high impact in patients with atelectasis. Int J Radiat Oncol Biol Phys. 1999;44:593-7.
[71] Hanna GG, Carson KJ, Lynch T, et al. 18F-fluorodeoxyglucose positron emission tomography/computed tomography-based radiotherapy target volume definition in non-small-cell lung cancer: delineation by radiation oncologists vs. joint outlining with a PET radiologist? International journal of radiation oncology, biology, physics. 2010;78:1040-51.
[72] Steenbakkers RJ, Duppen JC, Fitton I, et al. Reduction of observer variation using matched CT-PET for lung cancer delineation: a three-dimensional analysis. International journal of radiation oncology, biology, physics. 2006;64:435-48.
[73] Ashamalla H, Rafla S, Parikh K, et al. The contribution of integrated PET/CT to the evolving definition of treatment volumes in radiation treatment planning in lung cancer. Int J Radiat Oncol Biol Phys. 2005;63:1016-23.
[74] Schinagl DA, Vogel WV, Hoffmann AL, et al. Comparison of five segmentation tools for 18F-fluoro-deoxy-glucose-positron emission tomography-based target volume definition in head and neck cancer. Int J Radiat Oncol Biol Phys. 2007;69:1282-9.
[75] Nestle U, Kremp S, Schaefer-Schuler A, et al. Comparison of different methods for delineation of 18F-FDG PET-positive tissue for target volume definition in radiotherapy of patients with non-Small cell lung cancer. J Nucl Med. 2005;46:1342-8.
[76] Grills IS, Yan D, Black QC, et al. Clinical implications of defining the gross tumor volume with combination of CT and 18FDG-positron emission tomography in non-small-cell lung cancer. Int J Radiat Oncol Biol Phys. 2007;67:709-19.
[77] Deniaud-Alexandre E, Touboul E, Lerouge D, et al. Impact of computed tomography and 18F-deoxyglucose coincidence detection

emission tomography image fusion for optimization of conformal radiotherapy in non-small-cell lung cancer. Int J Radiat Oncol Biol Phys. 2005;63:1432-41.
[78] Brianzoni E, Rossi G, Ancidei S, et al. Radiotherapy planning: PET/CT scanner performances in the definition of gross tumour volume and clinical target volume. Eur J Nucl Med Mol Imaging. 2005;32:1392-9.
[79] Giraud P, Grahek D, Montravers F, et al. CT and (18)F-deoxyglucose (FDG) image fusion for optimization of conformal radiotherapy of lung cancers. International journal of radiation oncology, biology, physics. 2001;49:1249-57.
[80] Erdi YE, Rosenzweig K, Erdi AK, et al. Radiotherapy treatment planning for patients with non-small cell lung cancer using positron emission tomography (PET). Radiother Oncol. 2002;62:51-60.
[81] Ciernik IF, Dizendorf E, Baumert BG, et al. Radiation treatment planning with an integrated positron emission and computer tomography (PET/CT): a feasibility study. Int J Radiat Oncol Biol Phys. 2003;57:853-63.
[82] Fox JL, Rengan R, O'Meara W, et al. Does registration of PET and planning CT images decrease interobserver and intraobserver variation in delineating tumor volumes for non-small-cell lung cancer? Int J Radiat Oncol Biol Phys. 2005;62:70-5.
[83] Daisne JF, Sibomana M, Bol A, et al. Tri-dimensional automatic segmentation of PET volumes based on measured source-to-background ratios: influence of reconstruction algorithms. Radiother Oncol. 2003;69:247-50.
[84] Hong R, Halama J, Bova D, Sethi A, Emami B. Correlation of PET standard uptake value and CT window-level thresholds for target delineation in CT-based radiation treatment planning. Int J Radiat Oncol Biol Phys. 2007;67:720-6.
[85] Wu K, Ung YC, Hornby J, et al. PET CT thresholds for radiotherapy target definition in non-small-cell lung cancer: how close are we to the pathologic findings? Int J Radiat Oncol Biol Phys. 2010;77:699-706.
[86] Daisne JF, Duprez T, Weynand B, et al. Tumor volume in pharyngolaryngeal squamous cell carcinoma: comparison at CT, MR imaging, and FDG PET and validation with surgical specimen. Radiology. 2004;233:93-100.

[87] Stroom J, Blaauwgeers H, van Baardwijk A, et al. Feasibility of pathology-correlated lung imaging for accurate target definition of lung tumors. Int J Radiat Oncol Biol Phys. 2007;69:267-75.
[88] Yu HM, Liu YF, Hou M, et al. Evaluation of gross tumor size using CT, 18F-FDG PET, integrated 18F-FDG PET/CT and pathological analysis in non-small cell lung cancer. Eur J Radiol. 2009;72:104-13.
[89] Yu J, Li X, Xing L, et al. Comparison of tumor volumes as determined by pathologic examination and FDG-PET/CT images of non-small-cell lung cancer: a pilot study. International journal of radiation oncology, biology, physics. 2009;75:1468-74.
[90] van Baardwijk A, Bosmans G, Boersma L, et al. PET-CT-based auto-contouring in non-small-cell lung cancer correlates with pathology and reduces interobserver variability in the delineation of the primary tumor and involved nodal volumes. Int J Radiat Oncol Biol Phys. 2007;68:771-8.
[91] Biehl KJ, Kong FM, Dehdashti F, et al. 18F-FDG PET definition of gross tumor volume for radiotherapy of non-small cell lung cancer: is a single standardized uptake value threshold approach appropriate? J Nucl Med. 2006;47:1808-12.
[92] Erdi YE, Mawlawi O, Larson SM, et al. Segmentation of lung lesion volume by adaptive positron emission tomography image thresholding. Cancer. 1997;80:2505-9.
[93] Black QC, Grills IS, Kestin LL, et al. Defining a radiotherapy target with positron emission tomography. Int J Radiat Oncol Biol Phys. 2004;60:1272-82.
[94] Schaefer A, Kremp S, Hellwig D, et al. A contrast-oriented algorithm for FDG-PET-based delineation of tumour volumes for the radiotherapy of lung cancer: derivation from phantom measurements and validation in patient data. Eur J Nucl Med Mol Imaging. 2008;35:1989-99.
[95] Geets X, Lee JA, Bol A, Lonneux M, Gregoire V. A gradient-based method for segmenting FDG-PET images: methodology and validation. European journal of nuclear medicine and molecular imaging. 2007;34:1427-38.
[96] Hoffmann AL, Troost EG, Huizenga H, Kaanders JH, Bussink J. Individualized dose prescription for hypofractionation in advanced non-small-cell lung cancer radiotherapy: an in silico trial. International journal of radiation oncology, biology, physics. 2012;83:1596-602.
[97] Dehing-Oberije C, De Ruysscher D, Petit S, et al. Development, external validation and clinical usefulness of a practical prediction

model for radiation-induced dysphagia in lung cancer patients. Radiotherapy and oncology : journal of the European Society for Therapeutic Radiology and Oncology. 2010;97:455-61.
[98] Dehing-Oberije C, De Ruysscher D, van Baardwijk A, et al. The importance of patient characteristics for the prediction of radiation-induced lung toxicity. Radiotherapy and oncology : journal of the European Society for Therapeutic Radiology and Oncology. 2009;91:421-6.
[99] Kong FM, Ritter T, Quint DJ, et al. Consideration of dose limits for organs at risk of thoracic radiotherapy: atlas for lung, proximal bronchial tree, esophagus, spinal cord, ribs, and brachial plexus. International journal of radiation oncology, biology, physics. 2011;81:1442-57.
[100] Lievens Y, Nulens A, Gaber MA, et al. Intensity-modulated radiotherapy for locally advanced non-small-cell lung cancer: a dose-escalation planning study. International journal of radiation oncology, biology, physics. 2011;80:306-13.
[101] Veldeman L, Madani I, Hulstaert F, et al. Evidence behind use of intensity-modulated radiotherapy: a systematic review of comparative clinical studies. The Lancet Oncology. 2008;9:367-75.
[102] Sura S, Gupta V, Yorke E, et al. Intensity-modulated radiation therapy (IMRT) for inoperable non-small cell lung cancer: the Memorial Sloan-Kettering Cancer Center (MSKCC) experience. Radiotherapy and oncology : journal of the European Society for Therapeutic Radiology and Oncology. 2008;87:17-23.
[103] Holloway CL, Robinson D, Murray B, et al. Results of a phase I study to dose escalate using intensity modulated radiotherapy guided by combined PET/CT imaging with induction chemotherapy for patients with non-small cell lung cancer. Radiotherapy and oncology : journal of the European Society for Therapeutic Radiology and Oncology. 2004;73:285-7.
[104] Liao ZX, Komaki RR, Thames HD, Jr., et al. Influence of technologic advances on outcomes in patients with unresectable, locally advanced non-small-cell lung cancer receiving concomitant chemoradiotherapy. International journal of radiation oncology, biology, physics. 2010;76:775-81.
[105] Grills IS, Yan D, Martinez AA, et al. Potential for reduced toxicity and dose escalation in the treatment of inoperable non-small-cell lung cancer: a comparison of intensity-modulated radiation therapy (IMRT),

3D conformal radiation, and elective nodal irradiation. International journal of radiation oncology, biology, physics. 2003;57:875-90.
[106] Murshed H, Liu HH, Liao Z, et al. Dose and volume reduction for normal lung using intensity-modulated radiotherapy for advanced-stage non-small-cell lung cancer. International journal of radiation oncology, biology, physics. 2004;58:1258-67.
[107] Ayadi M, Zahra N, Thariat J, et al. [Intensity-modulated radiation therapy in non-small cell lung cancers]. Cancer radiotherapie : journal de la Societe francaise de radiotherapie oncologique. 2014;18:406-13.
[108] Goossens S, Senny F, Lee JA, Janssens G, Geets X. Assessment of tumor motion reproducibility with audio-visual coaching through successive 4D CT sessions. Journal of applied clinical medical physics / American College of Medical Physics. 2014;15:4332.
[109] Goossens S, Descampe A, Orban de Xivry J, et al. Impact of motion induced artifacts on automatic registration of lung tumors in Tomotherapy. Physica medica : PM : an international journal devoted to the applications of physics to medicine and biology : official journal of the Italian Association of Biomedical Physics. 2015.
[110] Mageras GS, Yorke E. Deep inspiration breath hold and respiratory gating strategies for reducing organ motion in radiation treatment. Seminars in radiation oncology. 2004;14:65-75.
[111] Cole AJ, Hanna GG, Jain S, O'Sullivan JM. Motion management for radical radiotherapy in non-small cell lung cancer. Clinical oncology. 2014;26:67-80.
[112] Bouilhol G, Ayadi M, Rit S, et al. Is abdominal compression useful in lung stereotactic body radiation therapy? A 4DCT and dosimetric lobe-dependent study. Physica medica : PM : an international journal devoted to the applications of physics to medicine and biology : official journal of the Italian Association of Biomedical Physics. 2013;29:333-40.
[113] Wolthaus JW, Sonke JJ, van Herk M, et al. Comparison of different strategies to use four-dimensional computed tomography in treatment planning for lung cancer patients. International journal of radiation oncology, biology, physics. 2008;70:1229-38.
[114] Linthout N, Bral S, Van de Vondel I, et al. Treatment delivery time optimization of respiratory gated radiation therapy by application of audio-visual feedback. Radiotherapy and oncology : journal of the European Society for Therapeutic Radiology and Oncology. 2009;91:330-5.

[115] Verellen D, Depuydt T, Gevaert T, et al. Gating and tracking, 4D in thoracic tumours. Cancer radiotherapie : journal de la Societe francaise de radiotherapie oncologique. 2010;14:446-54.
[116] Keall PJ, Mageras GS, Balter JM, et al. The management of respiratory motion in radiation oncology report of AAPM Task Group 76. Medical physics. 2006;33:3874-900.
[117] Depuydt T, Verellen D, Haas O, et al. Geometric accuracy of a novel gimbals based radiation therapy tumor tracking system. Radiotherapy and oncology : journal of the European Society for Therapeutic Radiology and Oncology. 2011;98:365-72.
[118] Sawant A, Venkat R, Srivastava V, et al. Management of three-dimensional intrafraction motion through real-time DMLC tracking. Medical physics. 2008;35:2050-61.
[119] Janssens G, Jacques L, Orban de Xivry J, Geets X, Macq B. Diffeomorphic registration of images with variable contrast enhancement. International journal of biomedical imaging. 2011;2011:891585.
[120] Wolthaus JW, Sonke JJ, van Herk M, Damen EM. Reconstruction of a time-averaged midposition CT scan for radiotherapy planning of lung cancer patients using deformable registration. Medical physics. 2008;35:3998-4011.
[121] Witte MG, van der Geer J, Schneider C, Lebesque JV, van Herk M. The effects of target size and tissue density on the minimum margin required for random errors. Medical physics. 2004;31:3068-79.
[122] Engelsman M, Damen EM, De Jaeger K, van Ingen KM, Mijnheer BJ. The effect of breathing and set-up errors on the cumulative dose to a lung tumor. Radiotherapy and oncology : journal of the European Society for Therapeutic Radiology and Oncology. 2001;60:95-105.
[123] Adkison JB, Khuntia D, Bentzen SM, et al. Dose escalated, hypofractionated radiotherapy using helical tomotherapy for inoperable non-small cell lung cancer: preliminary results of a risk-stratified phase I dose escalation study. Technology in cancer research & treatment. 2008;7:441-7.
[124] De Ruysscher D, Dehing C, Bentzen SM, et al. Can we optimize chemo-radiation and surgery in locally advanced stage III non-small cell lung cancer based on evidence from randomized clinical trials? A hypothesis-generating study. Radiotherapy and oncology : journal of the European Society for Therapeutic Radiology and Oncology. 2009;93:389-95.

[125] van Baardwijk A, Bosmans G, Boersma L, et al. Individualized radical radiotherapy of non-small-cell lung cancer based on normal tissue dose constraints: a feasibility study. International journal of radiation oncology, biology, physics. 2008;71:1394-401.
[126] Gambhir SS, Czernin J, Schwimmer J, et al. A tabulated summary of the FDG PET literature. J Nucl Med. 2001;42:1S-93S.
[127] Mah K, Caldwell CB, Ung YC, et al. The impact of (18)FDG-PET on target and critical organs in CT-based treatment planning of patients with poorly defined non-small-cell lung carcinoma: a prospective study. Int J Radiat Oncol Biol Phys. 2002;52:339-50.
[128] van Der Wel A, Nijsten S, Hochstenbag M, et al. Increased therapeutic ratio by 18FDG-PET CT planning in patients with clinical CT stage N2-N3M0 non-small-cell lung cancer: a modeling study. Int J Radiat Oncol Biol Phys. 2005;61:649-55.
[129] Chiti A, Kirienko M, Gregoire V. Clinical use of PET-CT data for radiotherapy planning: what are we looking for? Radiother Oncol. 2010;96:277-9.
[130] Hanna GG, Carson KJ, Lynch T, et al. (18)F-Fluorodeoxyglucose Positron Emission Tomography/Computed Tomography-based Radiotherapy Target Volume Definition in Non-small-cell Lung Cancer: Delineation by Radiation Oncologists vs. Joint Outlining with a PET Radiologist? Int J Radiat Oncol Biol Phys. 2010.
[131] De Ruysscher D, Kirsch CM. PET scans in radiotherapy planning of lung cancer. Radiother Oncol. 2010;96:335-8.
[132] Abramyuk A, Tokalov S, Zophel K, et al. Is pre-therapeutical FDG-PET/CT capable to detect high risk tumor subvolumes responsible for local failure in non-small cell lung cancer? Radiother Oncol. 2009;91:399-404.
[133] Thorwarth D, Geets X, Paiusco M. Physical radiotherapy treatment planning based on functional PET/CT data. Radiother Oncol. 2010;96:317-24.
[134] Klopp AH, Chang JY, Tucker SL, et al. Intrathoracic patterns of failure for non-small-cell lung cancer with positron-emission tomography/computed tomography-defined target delineation. Int J Radiat Oncol Biol Phys. 2007;69:1409-16.
[135] Lee JA. Segmentation of positron emission tomography images: some recommendations for target delineation in radiation oncology. Radiother Oncol. 2010;96:302-7.

[136] Yu J, Li X, Xing L, et al. Comparison of tumor volumes as determined by pathologic examination and FDG-PET/CT images of non-small-cell lung cancer: a pilot study. Int J Radiat Oncol Biol Phys. 2009;75:1468-74.
[137] Dahele M, Hwang D, Peressotti C, et al. Developing a methodology for three-dimensional correlation of PET-CT images and whole-mount histopathology in non-small-cell lung cancer. Curr Oncol. 2008;15:62-9.
[138] Faria SL, Menard S, Devic S, et al. Impact of FDG-PET/CT on radiotherapy volume delineation in non-small-cell lung cancer and correlation of imaging stage with pathologic findings. Int J Radiat Oncol Biol Phys. 2008;70:1035-8.
[139] Caldwell CB, Mah K, Skinner M, Danjoux CE. Can PET provide the 3D extent of tumor motion for individualized internal target volumes? A phantom study of the limitations of CT and the promise of PET. Int J Radiat Oncol Biol Phys. 2003;55:1381-93.
[140] Chi PC, Mawlawi O, Luo D, et al. Effects of respiration-averaged computed tomography on positron emission tomography/computed tomography quantification and its potential impact on gross tumor volume delineation. Int J Radiat Oncol Biol Phys. 2008;71:890-9.
[141] Bettinardi V, Picchio M, Di Muzio N, et al. Detection and compensation of organ/lesion motion using 4D-PET/CT respiratory gated acquisition techniques. Radiother Oncol. 2010;96:311-6.
[142] Beddar AS, Kainz K, Briere TM, et al. Correlation between internal fiducial tumor motion and external marker motion for liver tumors imaged with 4D-CT. Int J Radiat Oncol Biol Phys. 2007;67:630-8.
[143] Shirato H, Suzuki K, Sharp GC, et al. Speed and amplitude of lung tumor motion precisely detected in four-dimensional setup and in real-time tumor-tracking radiotherapy. Int J Radiat Oncol Biol Phys. 2006;64:1229-36.
[144] Juhler Nottrup T, Korreman SS, Pedersen AN, et al. Intra- and interfraction breathing variations during curative radiotherapy for lung cancer. Radiother Oncol. 2007;84:40-8.
[145] Gregoire V, Daisne JF, Geets X. Comparison of CT- and FDG-PET-defined GT: in regard to Paulino et al. (Int J Radiat Oncol Biol Phys 2005;61:1385-1392). Int J Radiat Oncol Biol Phys. 2005;63:308-9; author reply 9.
[146] Senan S, De Ruysscher D, Giraud P, et al. Literature-based recommendations for treatment planning and execution in high-dose radiotherapy for lung cancer. Radiotherapy and oncology : journal of

the European Society for Therapeutic Radiology and Oncology. 2004;71:139-46.
[147] Giraud P. Influence of CT images visualization parameters for target volume delineation in lung cancer. Proceeding of 19th ESTRO Istanbul, 2000. Radiat Oncol. 2000;S39.
[148] Harris KM, Adams H, Lloyd DC, Harvey DJ. The effect on apparent size of simulated pulmonary nodules of using three standard CT window settings. Clin Radiol. 1993;47:241-4.
[149] Grills IS, Fitch DL, Goldstein NS, et al. Clinicopathologic analysis of microscopic extension in lung adenocarcinoma: defining clinical target volume for radiotherapy. Int J Radiat Oncol Biol Phys. 2007;69:334-41.
[150] Siedschlag C, van Loon J, van Baardwijk A, et al. Analysis of the relative deformation of lung lobes before and after surgery in patients with NSCLC. Phys Med Biol. 2009;54:5483-92.
[151] Soret M, Bacharach SL, Buvat I. Partial-volume effect in PET tumor imaging. J Nucl Med. 2007;48:932-45.
[152] Palma D, Visser O, Lagerwaard FJ, et al. Impact of introducing stereotactic lung radiotherapy for elderly patients with stage I non-small-cell lung cancer: a population-based time-trend analysis. Journal of clinical oncology : official journal of the American Society of Clinical Oncology. 2010;28:5153-9.
[153] Kong FM, Ten Haken RK, Schipper MJ, et al. High-dose radiation improved local tumor control and overall survival in patients with inoperable/unresectable non-small-cell lung cancer: long-term results of a radiation dose escalation study. International journal of radiation oncology, biology, physics. 2005;63:324-33.
[154] Belderbos JS, Heemsbergen WD, De Jaeger K, Baas P, Lebesque JV. Final results of a Phase I/II dose escalation trial in non-small-cell lung cancer using three-dimensional conformal radiotherapy. International journal of radiation oncology, biology, physics. 2006;66:126-34.
[155] Bentzen SM, Saunders MI, Dische S. From CHART to CHARTWEL in non-small cell lung cancer: clinical radiobiological modelling of the expected change in outcome. Clinical oncology. 2002;14:372-81.
[156] Saunders MI, Rojas A, Lyn BE, Wilson E, Phillips H. Dose-escalation with CHARTWEL (continuous hyperfractionated accelerated radiotherapy week-end less) combined with neo-adjuvant chemotherapy in the treatment of locally advanced non-small cell lung cancer. Clinical oncology. 2002;14:352-60.

[157] Machtay M, Bae K, Movsas B, et al. Higher biologically effective dose of radiotherapy is associated with improved outcomes for locally advanced non-small cell lung carcinoma treated with chemoradiation: an analysis of the Radiation Therapy Oncology Group. International journal of radiation oncology, biology, physics. 2012;82:425-34.
[158] Cox JD. Are the results of RTOG 0617 mysterious? International journal of radiation oncology, biology, physics. 2012;82:1042-4.
[159] Wanet M, Lee JA, Weynand B, et al. Gradient-based delineation of the primary GTV on FDG-PET in non-small cell lung cancer: a comparison with threshold-based approaches, CT and surgical specimens. Radiotherapy and oncology : journal of the European Society for Therapeutic Radiology and Oncology. 2011;98:117-25.
[160] Velazquez ER, Aerts HJ, Oberije C, De Ruysscher D, Lambin P. Prediction of residual metabolic activity after treatment in NSCLC patients. Acta oncologica. 2010;49:1033-9.
[161] Mehta M, Scrimger R, Mackie R, et al. A new approach to dose escalation in non-small-cell lung cancer. International journal of radiation oncology, biology, physics. 2001;49:23-33.
[162] Schwarz M, Alber M, Lebesque JV, Mijnheer BJ, Damen EM. Dose heterogeneity in the target volume and intensity-modulated radiotherapy to escalate the dose in the treatment of non-small-cell lung cancer. International journal of radiation oncology, biology, physics. 2005;62:561-70.
[163] Sterpin E, Janssens G, Orban de Xivry J, et al. Helical tomotherapy for SIB and hypo-fractionated treatments in lung carcinomas: a 4D Monte Carlo treatment planning study. Radiother Oncol. 2012;104:173-80.
[164] Bradley J, Graham MV, Winter K, et al. Toxicity and outcome results of RTOG 9311: a phase I-II dose-escalation study using three-dimensional conformal radiotherapy in patients with inoperable non-small-cell lung carcinoma. International journal of radiation oncology, biology, physics. 2005;61:318-28.
[165] Bradley JD, Moughan J, Graham MV, et al. A phase I/II radiation dose escalation study with concurrent chemotherapy for patients with inoperable stages I to III non-small-cell lung cancer: phase I results of RTOG 0117. International journal of radiation oncology, biology, physics. 2010;77:367-72.
[166] van Elmpt W, De Ruysscher D, van der Salm A, et al. The PET-boost randomised phase II dose-escalation trial in non-small cell lung

cancer. Radiotherapy and oncology : journal of the European Society for Therapeutic Radiology and Oncology. 2012;104:67-71.
[167] Socinski MA, Morris DE, Halle JS, et al. Induction and concurrent chemotherapy with high-dose thoracic conformal radiation therapy in unresectable stage IIIA and IIIB non-small-cell lung cancer: a dose-escalation phase I trial. Journal of clinical oncology : official journal of the American Society of Clinical Oncology. 2004;22:4341-50.
[168] Skougaard K, Nielsen D, Jensen BV, Hendel HW. Comparison of EORTC criteria and PERCIST for PET/CT response evaluation of patients with metastatic colorectal cancer treated with irinotecan and cetuximab. Journal of nuclear medicine : official publication, Society of Nuclear Medicine. 2013;54:1026-31.
[169] Eisenhauer EA, Therasse P, Bogaerts J, et al. New response evaluation criteria in solid tumours: revised RECIST guideline (version 1.1). European journal of cancer. 2009;45:228-47.
[170] De Ruysscher D, Wanders S, van Haren E, et al. Selective mediastinal node irradiation based on FDG-PET scan data in patients with non-small-cell lung cancer: a prospective clinical study. International journal of radiation oncology, biology, physics. 2005;62:988-94.
[171] Rosenzweig KE, Sim SE, Mychalczak B, et al. Elective nodal irradiation in the treatment of non-small-cell lung cancer with three-dimensional conformal radiation therapy. International journal of radiation oncology, biology, physics. 2001;50:681-5.
[172] Senan S, Burgers S, Samson MJ, et al. Can elective nodal irradiation be omitted in stage III non-small-cell lung cancer? Analysis of recurrences in a phase II study of induction chemotherapy and involved-field radiotherapy. International journal of radiation oncology, biology, physics. 2002;54:999-1006.
[173] Emami B, Mirkovic N, Scott C, et al. The impact of regional nodal radiotherapy (dose/volume) on regional progression and survival in unresectable non-small cell lung cancer: an analysis of RTOG data. Lung cancer. 2003;41:207-14.
[174] Bradley JD, Wahab S, Lockett MA, Perez CA, Purdy JA. Elective nodal failures are uncommon in medically inoperable patients with Stage I non-small-cell lung carcinoma treated with limited radiotherapy fields. International journal of radiation oncology, biology, physics. 2003;56:342-7.

[175] Garg S, Gielda BT, Turian JV, et al. Patterns of regional failure in stage III non-small cell lung cancer treated with neoadjuvant chemoradiation therapy and resection. Practical radiation oncology. 2013;3:287-93.
[176] Provencio M, Sanchez A, Garrido P, Valcarcel F. New molecular targeted therapies integrated with radiation therapy in lung cancer. Clinical lung cancer. 2010;11:91-7.
[177] Zhuang H, Zhao X, Zhao L, Chang JY, Wang P. Progress of clinical research on targeted therapy combined with thoracic radiotherapy for non-small-cell lung cancer. Drug design, development and therapy. 2014;8:667-75.
[178] Han CB, Wang WL, Quint L, et al. Pulmonary artery invasion, high-dose radiation, and overall survival in patients with non-small cell lung cancer. International journal of radiation oncology, biology, physics. 2014;89:313-21.
[179] Timmerman R, McGarry R, Yiannoutsos C, et al. Excessive toxicity when treating central tumors in a phase II study of stereotactic body radiation therapy for medically inoperable early-stage lung cancer. Journal of clinical oncology : official journal of the American Society of Clinical Oncology. 2006;24:4833-9.
[180] Cannon DM, Mehta MP, Adkison JB, et al. Dose-limiting toxicity after hypofractionated dose-escalated radiotherapy in non-small-cell lung cancer. Journal of clinical oncology : official journal of the American Society of Clinical Oncology. 2013;31:4343-8.
[181] Wanet M, Sterpin E, Janssens G, et al. Validation of the mid-position strategy for lung tumors in helical TomoTherapy. Radiotherapy and oncology : journal of the European Society for Therapeutic Radiology and Oncology. 2014.
[182] Niemierko A, Goitein M. Implementation of a model for estimating tumor control probability for an inhomogeneously irradiated tumor. Radiotherapy and oncology : journal of the European Society for Therapeutic Radiology and Oncology. 1993;29:140-7.
[183] Niemierko A. Reporting and analyzing dose distributions: a concept of equivalent uniform dose. Medical physics. 1997;24:103-10.
[184] Guckenberger M, Kavanagh A, Webb S, Brada M. A novel respiratory motion compensation strategy combining gated beam delivery and mean target position concept --a compromise between small safety margins and long duty cycles. Radiother Oncol. 2011;98:317-22.

[185] van der Voort van Zyp NC, Prevost JB, Hoogeman MS, et al. Stereotactic radiotherapy with real-time tumor tracking for non-small cell lung cancer: clinical outcome. Radiother Oncol. 2009;91:296-300.
[186] Ekberg L, Holmberg O, Wittgren L, Bjelkengren G, Landberg T. What margins should be added to the clinical target volume in radiotherapy treatment planning for lung cancer? Radiotherapy and oncology : journal of the European Society for Therapeutic Radiology and Oncology. 1998;48:71-7.
[187] Mutaf YD, Brinkmann DH. Optimization of internal margin to account for dosimetric effects of respiratory motion. International journal of radiation oncology, biology, physics. 2008;70:1561-70.
[188] Kruis MF, van de Kamer JB, Sonke JJ, Jansen EP, van Herk M. Registration accuracy and image quality of time averaged mid-position CT scans for liver SBRT. Radiother Oncol. 2013.
[189] Hurkmans CW, Cuijpers JP, Lagerwaard FJ, et al. Recommendations for implementing stereotactic radiotherapy in peripheral stage IA non-small cell lung cancer: report from the Quality Assurance Working Party of the randomised phase III ROSEL study. Radiation oncology. 2009;4:1.
[190] Potters L, Kavanagh B, Galvin JM, et al. American Society for Therapeutic Radiology and Oncology (ASTRO) and American College of Radiology (ACR) practice guideline for the performance of stereotactic body radiation therapy. International journal of radiation oncology, biology, physics. 2010;76:326-32.
[191] Bissonnette JP, Franks KN, Purdie TG, et al. Quantifying interfraction and intrafraction tumor motion in lung stereotactic body radiotherapy using respiration-correlated cone beam computed tomography. International journal of radiation oncology, biology, physics. 2009;75:688-95.
[192] Wolthaus JW, Schneider C, Sonke JJ, et al. Mid-ventilation CT scan construction from four-dimensional respiration-correlated CT scans for radiotherapy planning of lung cancer patients. International journal of radiation oncology, biology, physics. 2006;65:1560-71.
[193] Orban de Xivry J, Janssens G, Bosmans G, et al. Tumour delineation and cumulative dose computation in radiotherapy based on deformable registration of respiratory correlated CT images of lung cancer patients. Radiotherapy and oncology : journal of the European Society for Therapeutic Radiology and Oncology. 2007;85:232-8.

[194] Timmerman R, Galvin J. RTOG 0236: a phase II trial of stereotactic body radiation therapy (hypo-fractionated) in the treatment of patients with medically inoperable stage I/II non-small cell lung cancer. RTOG. 2007.
[195] Timmerman R, Gore E, Pass H, Edelman M, Kong F. RTOG 0618 a phase II trial of stereotactic body radiation therapy (hypo-fractionated) in the treatment of patients with operable stage I/II non-small cell lung cancer. RTOG. 2007.
[196] Xiao Y, Papiez L, Paulus R, et al. Dosimetric evaluation of heterogeneity corrections for RTOG 0236: stereotactic body radiotherapy of inoperable stage I-II non-small-cell lung cancer. International journal of radiation oncology, biology, physics. 2009;73:1235-42.
[197] Ardu V, Broggi S, Cattaneo GM, Mangili P, Calandrino R. Dosimetric accuracy of tomotherapy dose calculation in thorax lesions. Radiation oncology. 2011;6:14.
[198] Chen Q, Lu W, Chen Y, et al. Validation of GPU based TomoTherapy dose calculation engine. Medical physics. 2012;39:1877-86.
[199] Admiraal MA, Schuring D, Hurkmans CW. Dose calculations accounting for breathing motion in stereotactic lung radiotherapy based on 4D-CT and the internal target volume. Radiotherapy and oncology : journal of the European Society for Therapeutic Radiology and Oncology. 2008;86:55-60.
[200] Guckenberger M, Wilbert J, Krieger T, et al. Four-dimensional treatment planning for stereotactic body radiotherapy. International journal of radiation oncology, biology, physics. 2007;69:276-85.
[201] Han K, Basran PS, Cheung P. Comparison of helical and average computed tomography for stereotactic body radiation treatment planning and normal tissue contouring in lung cancer. Clinical oncology. 2010;22:862-7.
[202] Timmerman RD GJ, Gore E, Pass H, Edelman MJ, Kong FP. RTOG 0618 a phase II trial of stereotactic body radiation therapy (hypo-fractionated) in the treatment of patients with operable stage I/II non-small cell lung cancer. RTOG. 2007.
[203] Timmerman RD MJ, Galvin J, et al. RTOG 0236: a phase II trial of stereotactic body radiation therapy (hypo-fractionated) in the treatment of patients with medically inoperable stage I/II non-small cell lung cancer. RTOG. 2007.

[204] Bortfeld T, Jokivarsi K, Goitein M, Kung J, Jiang SB. Effects of intra-fraction motion on IMRT dose delivery: statistical analysis and simulation. Physics in medicine and biology. 2002;47:2203-20.
[205] Sterpin E, Hundertmark BT, Mackie TR, et al. Monte Carlo-based analytical model for small and variable fields delivered by TomoTherapy. Radiother Oncol. 2010;94:229-34.
[206] Sterpin E, Salvat F, Olivera G, Vynckier S. Monte Carlo evaluation of the convolution/superposition algorithm of Hi-Art tomotherapy in heterogeneous phantoms and clinical cases. Medical physics. 2009;36:1566-75.
[207] Sterpin E, Salvat F, Cravens R, et al. Monte Carlo simulation of helical tomotherapy with PENELOPE. Physics in medicine and biology. 2008;53:2161-80.
[208] Sterpin E TM, Cravens R, et al. Monte Carlo simulation of the Tomotherapy treatment unit in the static mode using MC HAMMER a Monte Carlo tool dedicated to Tomotherapy. J Phys: Confer Ser. 2007;74:021019.
[209] Zhao YL, Mackenzie M, Kirkby C, Fallone BG. Monte Carlo evaluation of a treatment planning system for helical tomotherapy in an anthropomorphic heterogeneous phantom and for clinical treatment plans. Medical physics. 2008;35:5366-74.
[210] Paddick I. A simple scoring ratio to index the conformity of radiosurgical treatment plans. Technical note. Journal of neurosurgery. 2000;93 Suppl 3:219-22.
[211] Wu QR, Wessels BW, Einstein DB, et al. Quality of coverage: conformity measures for stereotactic radiosurgery. Journal of applied clinical medical physics / American College of Medical Physics. 2003;4:374-81.
[212] Dice LR. Measures of the amount of ecologic association between species. Ecology. 1945;26:297-302.
[213] Kissick MW, Flynn RT, Westerly DC, et al. On the impact of longitudinal breathing motion randomness for tomotherapy delivery. Physics in medicine and biology. 2008;53:4855-73.
[214] Yang JN, Mackie TR, Reckwerdt P, Deasy JO, Thomadsen BR. An investigation of tomotherapy beam delivery. Medical physics. 1997;24:425-36.
[215] Kissick MW, Boswell SA, Jeraj R, Mackie TR. Confirmation, refinement, and extension of a study in intrafraction motion interplay with sliding jaw motion. Medical physics. 2005;32:2346-50.

[216] Cao M, Lasley FD, Das IJ, et al. Evaluation of rotational errors in treatment setup of stereotactic body radiation therapy of liver cancer. International journal of radiation oncology, biology, physics. 2012;84:e435-40.
[217] Guckenberger M, Meyer J, Vordermark D, et al. Magnitude and clinical relevance of translational and rotational patient setup errors: a cone-beam CT study. International journal of radiation oncology, biology, physics. 2006;65:934-42.
[218] Schubert LK, Westerly DC, Tome WA, et al. A comprehensive assessment by tumor site of patient setup using daily MVCT imaging from more than 3,800 helical tomotherapy treatments. International journal of radiation oncology, biology, physics. 2009;73:1260-9.
[219] Bentzen SM, Gregoire V. Molecular imaging-based dose painting: a novel paradigm for radiation therapy prescription. Seminars in radiation oncology. 2011;21:101-10.
[220] Meijer G, Steenhuijsen J, Bal M, et al. Dose painting by contours versus dose painting by numbers for stage II/III lung cancer: practical implications of using a broad or sharp brush. Radiotherapy and oncology : journal of the European Society for Therapeutic Radiology and Oncology. 2011;100:396-401.
[221] Christian N, Lee JA, Bol A, et al. The limitation of PET imaging for biological adaptive-IMRT assessed in animal models. Radiotherapy and oncology : journal of the European Society for Therapeutic Radiology and Oncology. 2009;91:101-6.
[222] Duprez F, De Neve W, De Gersem W, Coghe M, Madani I. Adaptive dose painting by numbers for head-and-neck cancer. International journal of radiation oncology, biology, physics. 2011;80:1045-55.
[223] Madani I, Duprez F, Boterberg T, et al. Maximum tolerated dose in a phase I trial on adaptive dose painting by numbers for head and neck cancer. Radiotherapy and oncology : journal of the European Society for Therapeutic Radiology and Oncology. 2011;101:351-5.
[224] Trani D, Reniers B, Persoon L, et al. What level of accuracy is achievable for preclinical dose painting studies on a clinical irradiation platform? Radiation research. 2015;183:501-10.
[225] Trani D, Yaromina A, Dubois LJ, et al. Preclinical assessment of efficacy of radiation dose painting based on intratumoral FDG-PET uptake. Clinical cancer research : an official journal of the American Association for Cancer Research. 2015.

[226] Kwint M, Conijn S, Schaake E, et al. Intra thoracic anatomical changes in lung cancer patients during the course of radiotherapy. Radiotherapy and oncology : journal of the European Society for Therapeutic Radiology and Oncology. 2014;113:392-7.
[227] Salguero FJ, Belderbos JS, Rossi MM, et al. Microscopic disease extensions as a risk factor for loco-regional recurrence of NSCLC after SBRT. Radiotherapy and oncology : journal of the European Society for Therapeutic Radiology and Oncology. 2013;109:26-31.
[228] van Loon J, Siedschlag C, Stroom J, et al. Microscopic disease extension in three dimensions for non-small-cell lung cancer: development of a prediction model using pathology-validated positron emission tomography and computed tomography features. International journal of radiation oncology, biology, physics. 2012;82:448-56.
[229] Giraud P, Antoine M, Larrouy A, et al. Evaluation of microscopic tumor extension in non-small-cell lung cancer for three-dimensional conformal radiotherapy planning. International journal of radiation oncology, biology, physics. 2000;48:1015-24.
[230] Li WL, Yu JM, Liu GH, et al. [A comparative study on radiology and pathology target volume in non-small-cell lung cancer]. Zhonghua zhong liu za zhi [Chinese journal of oncology]. 2003;25:566-8.
[231] Grassberger C. Four-dimensional monte carlo simulations of lung cancer treatments with scanned proton beams. Thesis, ETH Zurich, Switzerland. 2014.
[232] Grutters JP, Kessels AG, Pijls-Johannesma M, et al. Comparison of the effectiveness of radiotherapy with photons, protons and carbon-ions for non-small cell lung cancer: a meta-analysis. Radiotherapy and oncology : journal of the European Society for Therapeutic Radiology and Oncology. 2010;95:32-40.
[233] Roelofs E, Engelsman M, Rasch C, et al. Results of a multicentric in silico clinical trial (ROCOCO): comparing radiotherapy with photons and protons for non-small cell lung cancer. Journal of thoracic oncology : official publication of the International Association for the Study of Lung Cancer. 2012;7:165-76.
[234] Wu J, Ohta Y, Minato H, et al. Nodal occult metastasis in patients with peripheral lung adenocarcinoma of 2.0 cm or less in diameter. The Annals of thoracic surgery. 2001;71:1772-7; discussion 7-8.
[235] Kepka L, Socha J. PET-CT use and the occurrence of elective nodal failure in involved field radiotherapy for non-small cell lung cancer: A

systematic review. Radiotherapy and oncology : journal of the European Society for Therapeutic Radiology and Oncology. 2015;115:151-6.
[236] Grills IS, Belderbos J, Hope A, et a. Higher risk of failure and death after stereotactic lung radiotherapy for T2 lung cancer. IASLC. 2015.
[237] Gould MK, Kuschner WG, Rydzak CE, et al. Test performance of positron emission tomography and computed tomography for mediastinal staging in patients with non-small-cell lung cancer: a meta-analysis. Annals of internal medicine. 2003;139:879-92.
[238] Mendez M, Custodio A, Provencio M. New molecular targeted therapies for advanced non-small-cell lung cancer. Journal of thoracic disease. 2011;3:30-56.
[239] Huber RM, Reck M, Thomas M. Current status of and future strategies for multimodality treatment of unresectable stage III nonsmall cell lung cancer. The European respiratory journal. 2013;42:1119-33.
[240] Mery B, Guy JB, Swalduz A, et al. The evolving locally-advanced non-small cell lung cancer landscape: Building on past evidence and experience. Critical reviews in oncology/hematology. 2015;96:319-27.
[241] Deutsch E, Levy A, Chargari C. [Radiation therapy and immunomodulation: Focus on experimental data]. Cancer radiotherapie : journal de la Societe francaise de radiotherapie oncologique. 2015;19:515-8.
[242] Finkelstein SE, Timmerman R, McBride WH, et al. The confluence of stereotactic ablative radiotherapy and tumor immunology. Clinical & developmental immunology. 2011;2011:439752.
[243] Reynders K, Illidge T, Siva S, Chang JY, De Ruysscher D. The abscopal effect of local radiotherapy: using immunotherapy to make a rare event clinically relevant. Cancer treatment reviews. 2015;41:503-10.
[244] Sun R, Sbai A, Ganem G, et al. [Non-targeted effects (bystander, abscopal) of external beam radiation therapy: an overview for the clinician]. Cancer radiotherapie : journal de la Societe francaise de radiotherapie oncologique. 2014;18:770-8.
[245] Apetoh L, Ladoire S, Coukos G, Ghiringhelli F. Combining immunotherapy and anticancer agents: the right path to achieve cancer cure? Annals of oncology : official journal of the European Society for Medical Oncology / ESMO. 2015;26:1813-23.

[246] Domagala-Kulawik J. The role of the immune system in non-small cell lung carcinoma and potential for therapeutic intervention. Translational lung cancer research. 2015;4:177-90.
[247] Freeman-Keller M, Goldman J, Gray J. Vaccine immunotherapy in lung cancer: Clinical experience and future directions. Pharmacology & therapeutics. 2015;153:1-9.
[248] Teng F, Kong L, Meng X, Yang J, Yu J. Radiotherapy combined with immune checkpoint blockade immunotherapy: Achievements and challenges. Cancer letters. 2015;365:23-9.